Structural Analysis and Design of Adaptive Lightweight Mirrors

by

Celia H. Liu

B.S. in Aeronautics and Astronautics
Massachusetts Institute of Technology (1992)

Submitted to the Department of Aeronautics and Astronautics
in Partial Fulfillment of the Requirements for the Degree of

Master of Science
at the

Massachusetts Institute of Technology

June 1993

Signature of Author _____
Department of Aeronautics and Astronautics
May 21, 1993

Certified by _____
Professor Nesbitt W. Hagood IV, Thesis Supervisor
Department of Aeronautics and Astronautics

Certified by _____
Dr. Eric Hall II, EIP Company Thesis Advisor
The Aerospace Corporation

Certified by _____
Dr. Mohan Aswani, EIP Company Supervisor
The Aerospace Corporation

Accepted by _____
Professor Harold Wachman, Chairman
Departmental Graduate Committee

Structural Analysis and Design of Adaptive Lightweight Mirrors

by

Celia H. Liu

Submitted to the Department of Aeronautics and Astronautics
in Partial Fulfillment of the Requirements for the degree of
Master of Science in Aeronautics and Astronautics

Abstract

Stringent weight limitations for advanced spacecraft and large apertures in ground based telescopes demand optical instruments that have high mechanical and thermal stability, but minimum weight. Current lightweight mirror designs utilize a cellular configuration to offer significant weight savings while providing adequate stiffness and a high quality surface. The complexity of such designs, however, makes analyzing and optimizing these mirrors to meet specified requirements a difficult process. This thesis contributes a methodology for improving the lightweight mirror design process while improving mirror performance. An efficient and practical methodology for evaluating mirror designs is developed to ease the process for conducting design trade-offs, and the feasibility of an adaptive lightweight mirror that utilizes piezoceramic actuators for correcting self-weight and thermal deformations is explored.

A methodology based on finite element modeling and analysis was developed, and an automatic lightweight mirror model generation program called AMMAP was coded to improve modeling efficiency. This methodology was used in parametric studies to arrive at an adaptive lightweight mirror design which met specified requirements. After verifying the process for modeling equivalent thermal strains to represent piezo-actuation strains, the adaptive mirror was analyzed and actuation profiles were obtained. These profiles were compiled into a matrix format, and least squares solutions were obtained for deflection corrections. Using a cost factor to limit the value of the applied field for piezoceramics, it was found that deflection corrections of an order of magnitude can be easily accomplished with low actuation voltages. Then, a successive placement optimization algorithm was used to evaluate the appropriate placement of a discrete number of piezoceramics. The results indicate that it is feasible to significantly correct deflections by utilizing a small number of piezoelectric actuators.

Thesis Supervisor: Dr. Nesbitt W. Hagood IV
Assistant Professor of Aeronautics and Astronautics
Massachusetts Institute of Technology

Thesis Advisor: Dr. Eric K. Hall II
Member of the Technical Staff
The Aerospace Corporation

Acknowledgments

I am grateful to The Aerospace Corporation for providing the environment and funding for my thesis research. I am especially indebted to my company thesis advisor, Dr. Eric Hall II, who made substantial contributions to every aspect of my education here at Aerospace and graciously gave his time and technical expertise to help direct my research and writing. Sincere appreciation also goes to my faculty thesis advisor, Professor Nesbitt Hagood, whose insights and guidance were highly valuable.

I would like to acknowledge my company supervisor Dr. Mohan Aswani, and Aerospace colleagues Kiet Luu, Harvey Shew, Mike Stallard, and Brett Coulter. All unselfishly provided their time for my numerous questions. Thanks also go to all the people who kept me sane during this period: Beau Lintereur, Nancy Cook, Walter Chung, Alexa McCulloch, Randy Kendall, James Lee, John Brekke, Cindy Yen, Kevin Stattenfield, Luis Espinoza, Greg Loboda; especially fellow EIP graduate student Jon Strizzi and again Harvey Shew for always being there for me.

I would also like to express my heartfelt appreciation to my boyfriend Francis DeSouza, who kept me motivated throughout this process.

Above all, I am grateful to my family to whom I dedicate this thesis. Mom, Bob, Tim, and Nancy, thanks always for your love and encouragement.

Table of Contents

List of Figures

List of Tables

Chapter 1: Background

1.1 Introduction

Advanced systems ranging from large ground based astronomical telescopes to space based surveillance satellites require high performance, lightweight mirrors. Current focus on large aperture mirrors for increased resolution has placed great emphasis on minimizing mirror weight while maintaining structural and thermal stability. Using lightweight materials in conventional monolithic mirrors does not provide enough weight savings or deflection improvements, so lightweight structural designs such as tapered thickness mirrors are typically considered. Currently, the most popular approach is that of designing lightweight mirrors in a cellular configuration, using thin monolithic plates rigidly connected by a webbed framework (Figure 1-1). Ribbed cells, usually forming a network of hexagons, triangles or squares (Figure 1-2), make it possible to build a mirror that is three to four times lighter than a solid mirror of the same dimensions and exhibit comparable self-weight deflections. The structural complexity of these mirrors, however, makes analyzing and finding the best design for a given application a difficult process. A number of parameters such as cell size, cell shape, rib thickness and rib height must be chosen to simultaneously satisfy requirements such as maximum self-weight deflection, specified fundamental frequency, and manufacturing limitations. Current design processes are time consuming and inefficient for extensive trade studies. Consequently, designs are usually chosen based on past experience, and in some instances critical requirements are relaxed.

One way to improve such non-optimal designs is to provide the mirror with a means to adapt to its environment. The conventional method for deforming mirrors is by piston actuation on the back surface of the mirror. This is usually accomplished by using blocks or stacks of piezoelectric ceramics. The piezoelectric materials strain when an electrical field is applied across them, making them useful for shape control to correct mirror surface

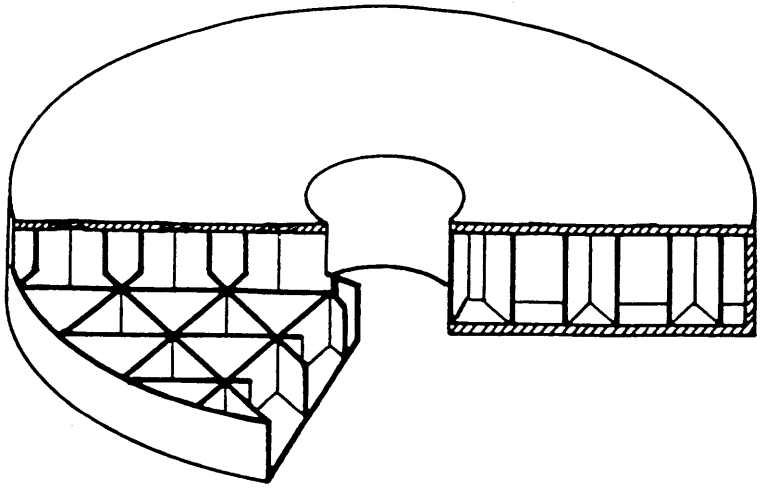

Figure 1-1 Lightweight Mirror Construction (Ref.[57])

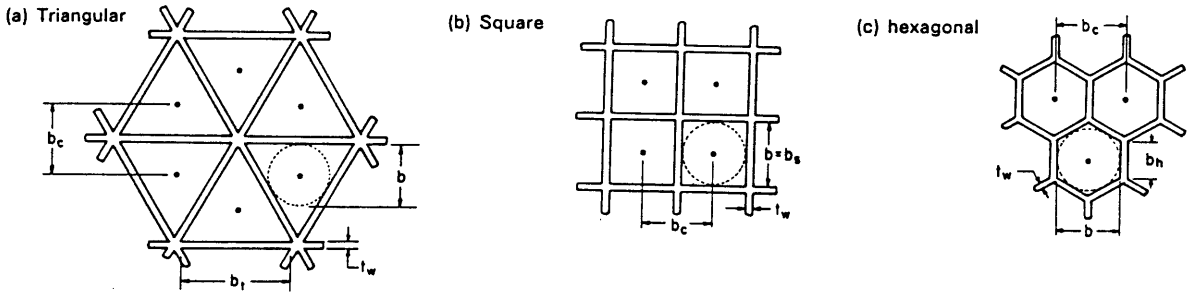

Figure 1-2 Several Types of Rib Patterns (Ref.[37])

distortions caused by gravity, temperature gradient, or fabrication errors. However, since piezoelectric ceramics are relatively dense compared to most mirror materials, considerable weight may be added to the mirror system. Recent studies have introduced an alternative concept, using actuators placed parallel to a mirror's surface to cause moment-induced deflections in the mirror. These so-called moment actuators seem to provide effective global transverse deflections whereas piston actuators tend to provide large deflections locally. However, to obtain large moment forces, the actuator must be supported by stand-off devices

(Figure 1-3), which increase the weight of the mirror system. Lightweight mirrors, on the other hand, are well suited for moment actuators because their cellular configuration provides a natural moment arm for pronounced actuator effects (Figure 1-4). A thin layer of piezoceramics may be attached directly onto the backsheet of a lightweight mirror without the stand-off devices needed for thin solid mirrors.

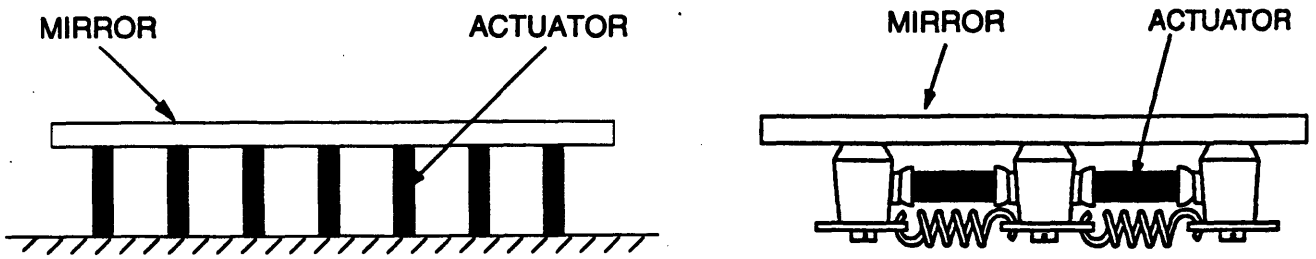

(a) With Piston Actuators **(b) With Moment Actuators**

Figure 1-3 Actuation Approaches for Adaptive Mirrors (Ref.[38])

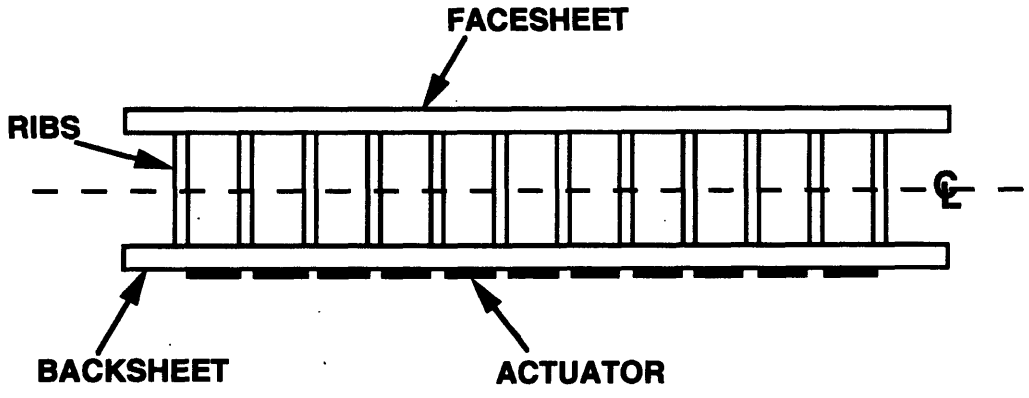

Figure 1-4 Lightweight Mirror with Moment Actuators

An adaptive mirror could potentially improve performance through every phase of its existence. This includes correcting gravity-induced deflections for more accurate ground tests and correcting wavefront aberrations for better focus and contrast enhancement during operation. Figure 1-5 summarizes some of the uses for such adaptive lightweight mirrors.

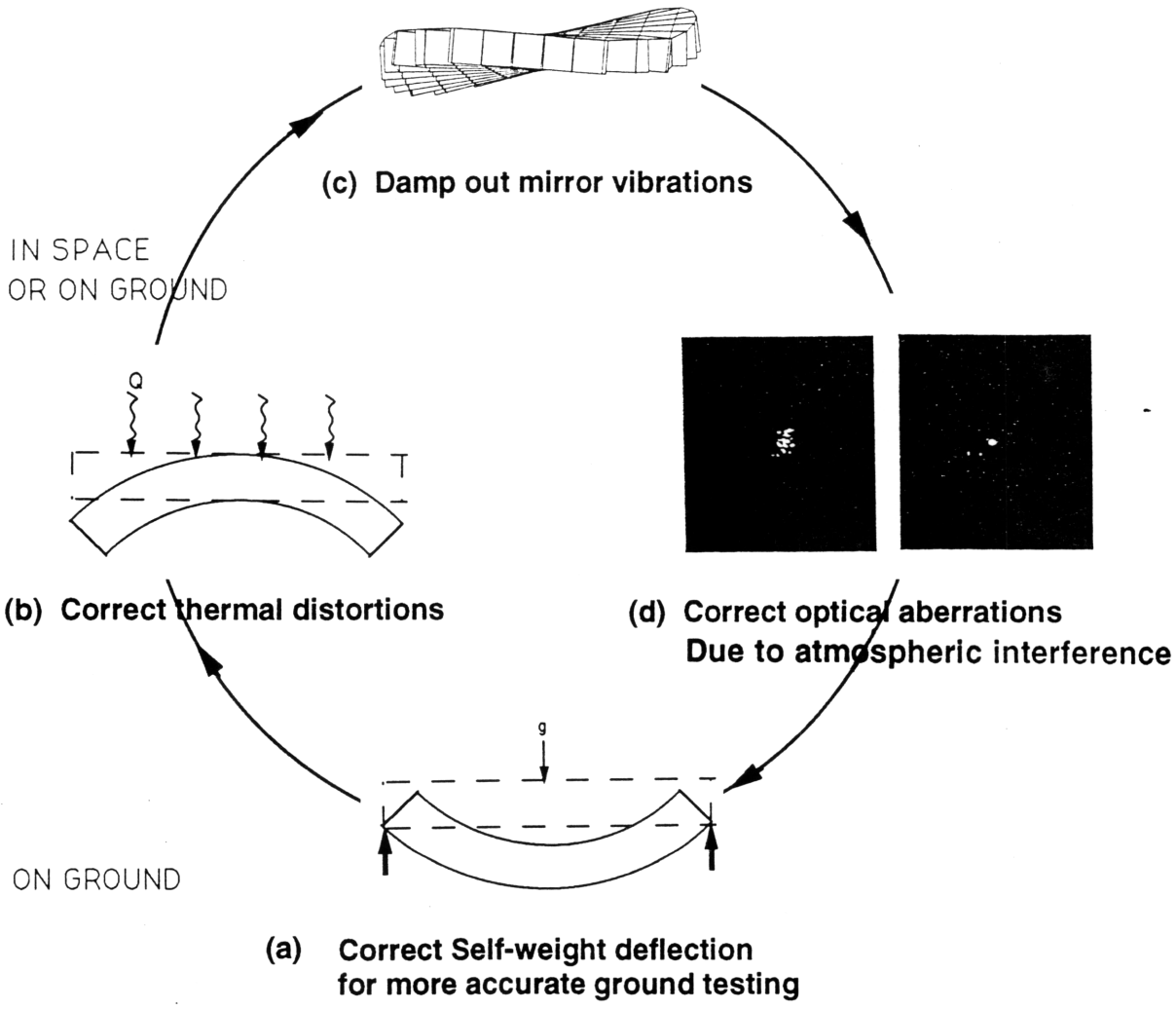

Figure 1-5 Summary of the Uses for Adaptive Lightweight Mirrors

This thesis intends to address two goals towards advancing lightweight mirror technology. The first goal is to improve lightweight mirror analysis capabilities so that structural deflections produced by gravity or temperature gradients may be more efficiently evaluated.

The second goal is to address the feasibility of using piezoceramics as moment actuators, specifically how they can be used to improve lightweight mirror deflection characteristics (as depicted by options (a) and (b) in Figure 1-5) to meet design requirements. To demonstrate the merits of the improved analysis capabilities and of piezoceramics for improving mirror performance, actuation profiles for the correction of self-weight deflection and thermal distortion of a circular mirror will be found. Emphasis is placed on developing a practical and efficient methodology using finite element analysis, which can be easily utilized by industry for conducting parametric studies of lightweight mirrors, leading to an efficient lightweight mirror design.

1.2 Motivation

Designing the best lightweight mirror for a given application involves many challenges. A number of parameters including mirror and rib dimensions, material, and mirror mounting locations play an important part in the static and dynamic performance of these mirrors. Consequently, parametric studies for design optimization are of considerable practical interest. Of the analytical methods for predicting mirror characteristics, the finite element method appears to be the most convenient and versatile method. Unfortunately, the process of building a finite element model to evaluate the structural and thermal performance of a lightweight mirror is time consuming because of the complexity of the ribbed designs. Automation of the repetitious mirror modeling process would improve mirror analysis capabilities by simplifying the process for parametric studies and by bypassing possible user modeling errors. In this way modifications in the mirror thickness, for example, could be accomplished to conduct mass and stiffness trade-offs in a matter of minutes, making the finite element analysis much more efficient and painless.

Building adaptivity into the mirror also has its merits. Trade-offs in mirror mass and stiffness might arrive at an optimal design for a minimal weight mirror that pushes the limit for one

requirement yet leaves margin in another requirement. For example, design criteria for self-weight deflection and natural frequency might be set such that they cannot be met simultaneously. In the case where a design leaves a large margin in fundamental frequency but approaches the self-weight deflection boundary, adaptive materials can provide significant corrections to the self-weight deflection. In this way a less stiff but lighter design could be arrived that still meets both requirements.

Even if minimizing weight is not the driving requirement or if a mirror adequately meets all requirements, adaptive materials can be used to improve the mirror performance. Since disturbances which degrade mirror performance are rarely fully correctable through proper design, incorporating adaptivity into the mirror can provide much more flexibility. Previous works have been documented where adaptive materials are used to damp out system disturbances as well as to correct thermal distortions. For optical devices, this flexibility can be very important since even minor distortions in the mirror surface caused by manufacturing or polishing tools can alter the mirror's expected performance. Finally, even the most ideally fabricated mirror may encounter less than ideal atmospheric conditions which can distort wavefront images. Here, adaptive optics can provide the flexibility to correct wavefront errors to restore the reflected image (Figure 1-6).

Designs of lightweight mirror constructions and adaptive optics date back to 1950's but the combination of the two concepts to form an adaptive lightweight mirror has been considered only recently. Understanding the advances in each of the two areas is essential to the final design and analysis of adaptive lightweight mirrors. The following two sections are devoted to discussion of each.

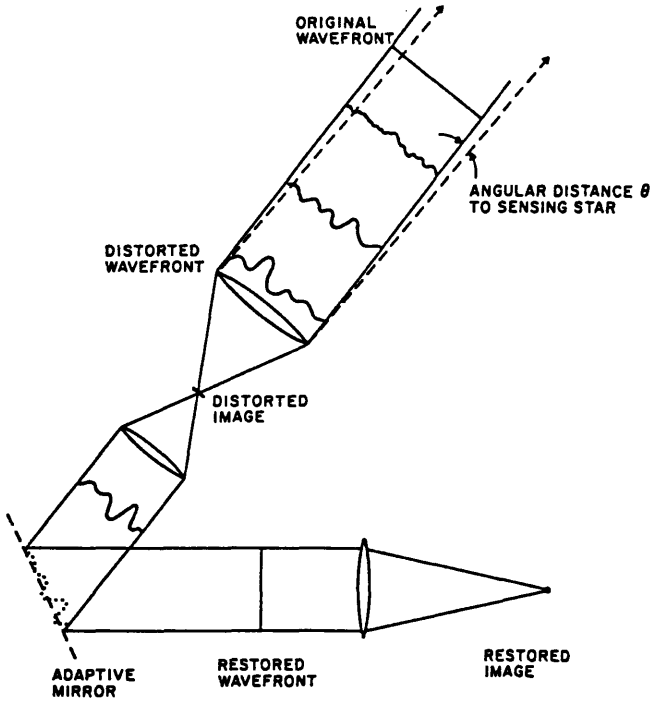

Figure 1-6 Principle of Adaptive Optics for Correcting Optical Aberrations (Ref.[12])

1.3 Lightweight Mirrors

This section will cover a brief history of the developments in lightweight mirrors, beginning with a description of the several weight-reducing possibilities. Then, a discussion of mirrors which were actually built, either for a specific application or for experimental work, will follow. Next, the many analytical methods which were developed to study lightweight mirrors will be discussed, followed by a brief synopsis of the efforts at The Aerospace Corporation, from which this thesis results.

Lightweighting a mirror can be accomplished by several different methods. Each technology attempts to reduce the material that is used to form the mirror while maintaining a "stiff" structure, where the self-weight induced deflection is small. There are three main categories

for lightweighting: contoured back mirror, ribbed back or cellular core mirror, and foam core mirror. Their differences are illustrated in Figure 1-7.

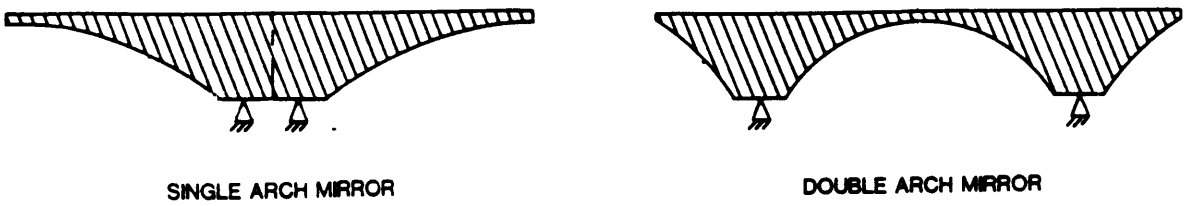

(a) Contoured Back Mirrors (Ref.[52])

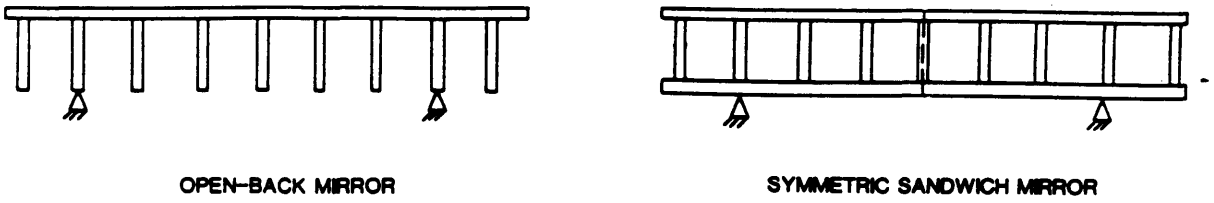

(b) Cellular Configuration Mirrors (Ref.[52])

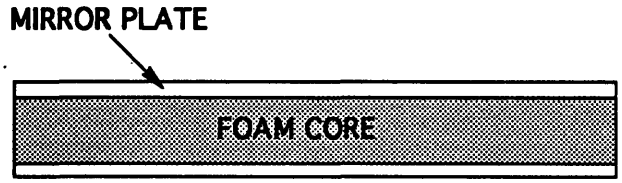

(c) Foam Core Mirror (Ref.[47])

Figure 1-7 Typical Lightweighting Techniques

Contoured back mirrors generally exhibit either a single-arch or double-arch on the back surface. This tapered design serves to reduce the self-weight induced optical surface figure

error when the mirror is in the horizontal position. This is a very straightforward idea whose merits can be illustrated with a simpler situation such as the beam. The deflection of a cantilevered beam is described by:

$$w = \frac{M}{EI}\frac{x^2}{2} \qquad (1\text{-}1)$$

where M = Bending moment

EI = Bending stiffness

Tapering the outer edge, which in effect decreases the self-weight induced bending moment M and inertia I at the edge, implies that a lighter beam can exhibit the same amount of deflection as a nominal flat beam. Therefore, the tapered edge mirror can provide the desired deflection characteristics and weigh less than a uniform flat mirror.

The ribbed back and sandwiched cellular core designs offer a similar deflection to weight advantage. By displacing material away from the centerline, thus increasing the moment of inertia I in the desired bending direction, a mirror of this design can exhibit a smaller deflection than a nominal flat mirror of the same weight. The foam core mirror also operates under this concept. The only difference is that a material of lower density is used instead of the cellular pockets.

A great deal of work has been devoted to studying each type of mirror and to determining their relative advantages and disadvantages. The 5.1m Hale telescope completed in 1950 had the first successful large mirror of lightweight ribbed construction, where a rib structure was cast directly into the back of a Pyrex disk (Ref.[57]). This design has two advantages over the conventional solid disk. First, the mirror's ability to reach thermal equilibrium quickly is enhanced since all ribs and faceplate are thin and exposed to the surrounding air. Second, it was found that the ribbed design permitted a weight saving of 50 percent for equal self-

weight deflection. Work was also conducted in evaluating optimal designs for these cored mirror structures. In 1969, Barnes (Ref.[11]) attempted to demonstrate some preferences for rib configurations and design dimensions through parametric variations.

Among the experimental comparison work, the Soviets seems to have led with a discussion of ribbed versus cellular core mirrors in 1977. Robachevskaya and Rodkevich (Ref.[48]) experimentally tested two lightweight fused quartz mirrors with and without a rear plate, and found that the open-back structure exhibited greater relative deformation than the symmetric sandwich structure under identical weight-relief conditions. Thermal and fabrication issues have also been studied for these lightweight mirror constructions. In response to technological needs for infrared telescopes operating at cryogenic temperatures, Eastman Kodak Company developed a 0.5 m fused silica mirror where face plates and core are frit bonded together. The mirror was evaluated at temperatures of 100 Kelvin down to 8 Kelvin, and Eastman and NASA concluded that such mirrors exhibited excellent thermal stability, comparable to that reported for conventional fusion and solid mirrors (Ref.[18]). Another thermal problem lies in distortions caused by thermal gradients. Wong (Ref.[56]) at the University of Texas tried to minimize thermal distortions by an internal ventilation system. Vukobratovich has also done considerable experimental work, concentrating however in contoured mirrors. In 1982, Vukobratovich *et al.* studied the single and double arch lightweight mirrors (Ref.[53]) and in 1989, expanded on this work by accounting for mirror supports as well (Ref.[15]). Also in 1989, Valente and Vukobratovich performed a comparison of the merits for contoured back mirrors against those of open-backed and symmetric sandwich mirrors (Ref.[52]). Merits were based not only on weight savings but also on cost and manufacturing difficulty. In 1990, these designs were considered for laser communications (Ref.[54]).

Because experimental studies of lightweight mirrors are very costly, several groups have tried to develop methods for producing accurate analytical solutions. The presence of the irregularities in the structure due to lightweighting greatly complicates this problem. This is especially true for predicting thermal stability of a lightweight mirror since deflection characteristics are determined not only by the material from which the mirror is fabricated but also by the geometrical parameters of the construction of each of the elements. In 1983, Paimushin *et al.* attacked this problem by formulating a boundary value problem with numerical finite-sums (Ref.[44]). They found thermal relationships for heat conductivity and thermal diffusivity coefficients, and claimed that these relationships give enough accuracy for engineering purposes to choose the type and construction of a lightweight mirror. In 1987, Pepi came up with general deflection approximations for lightweight mirrors under gravitational and thermal loading (Ref.[45]). Using well-documented results from Williams and Brinson (Ref.[55]) for various multipoint supports and conditions for a circular plate, Pepi extended these results for lightweight mirrors by replacing the solid thickness by equivalent thicknesses and weight density. This analysis seems to yield good first order results. Also in 1987, Mehta studied the characteristics of lightweight mirrors in an attempt to find theoretical relationships for optimal geometrical configurations based on flexural rigidity (Ref.[37]). He found a transitional point for which an openback configuration may be structurally superior to a sandwich configuration. In 1988, Khesin developed a complex computational-experimental approach (CCEA) for developing optimum designs of lightweight mirrors (Ref.[30]). This method combines three areas: the capabilities of a numerical analysis of the stress-strain state, a search for the optimum geometrical parameters on a computer, and an experimental check of the strength and stiffness limitations by a photoelasticity method.

The fact that so much work has been devoted to finding an accurate method to characterize lightweight mirror deflections indicates the complexity of this problem. The Aerospace

Corporation is also very interested in a method which can give accurate approximations to help evaluate practical mirror designs for space applications. In the concept design stage, simplicity was the main criterion for evaluation, and Luu (Ref.[33]) developed a first cut optics design program to quickly conduct a trade-off between the weight and dimensions for a lightweight mirror. As the detailed design phase begins, however, this program no longer meets the accuracy nor versatility required for complete evaluations. A more comprehensive method is needed. Several engineers have begun work in this area, which formed a practical basis for this thesis.

1.4 Adaptive Optics

Discussion of adaptive optics to compensate wavefront errors due to atmospheric disturbances by using an arbitrary deformable optical element with feedback from a wavefront sensor began with Babcock in 1953 (Ref.[32]). Since then, considerable progress has taken place, both in terms of finding new actuator materials and finding new methods to realize adaptive mirrors. There have even been publications which suggest the possibility of adaptive optics without the use of wavefront sensors (Ref.[35]).

A number of adaptive materials such as piezoelectric, electrostrictive, and magnetostrictive materials can potentially be used for accomplishing the actuation needed for an optical system. The most prevalent and mature material discussed in literature is piezoelectric ceramic. This material has been used in a variety of ways to deform mirrors, including the piston concept, piston plus tilt concept, and bending moment concept, in sizes ranging from thin films to an entire actuator block (Ref.[20]).

In 1980, Everson et al. (Ref.[21]) of the Itek Corporation published experimental findings for a discretely actuated deformable mirror which used the stacked piston concept. They found that this configuration, illustrated in Figure 1-8, presented a near-gaussian influence

function for each actuator, which involved very little "cross talk" with neighboring actuators. References [12], [14], and [19] give brief summaries of previous experimental studies in adaptive mirrors.

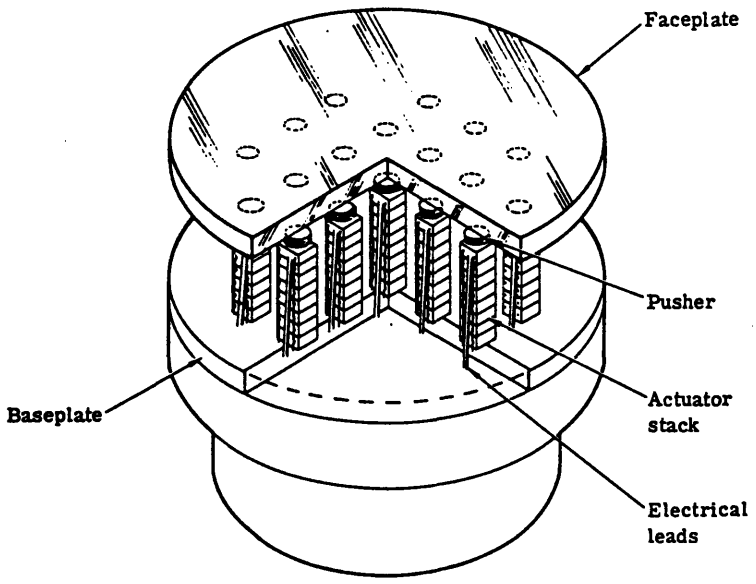

Figure 1-8 The stacked actuator mirror concept (Ref.[21])

In the area of deformable mirror analysis and design, studies related to both continuous facesheet and segmented facesheet mirrors have been performed. In 1989, Ealey and Wellman (Ref.[20]) examined a variety of these problems and developed basic design equations to account for an overall mirror system, including actuators, facesheet, support structure, and electronic drivers. In 1990, Mehta (Ref.[38]) produced analytical solutions for mirrors which are actuated through the moment actuation concept and obtained influence functions of the actuators at various locations and orientations. The results clearly show a more global deflection character in contrast to the piston type actuators.

More recently, requirements for large space mirrors have necessitated the development of segmented mirrors, and Niemiec (Ref.[40]) describes the process of structural analysis for an adaptive primary mirror through a finite element model. Loboda (Ref.[32]) also details the optical and structural analysis process for designing a large segmented mirror of lightweight construction.

There is a wealth of information on piezoelectric actuator dynamics and control of structures, including work by Crawley (Ref.[16] and [17]), Hagood (Ref.[22] and [23]), and How (Ref.[28]). There is also increased interest in the optimal locations of actuators for dynamic, quasistatic and static shape control (Ref.[6], [42], [49]).

All of these studies can very well be applied to lightweight mirrors, and within the last few years, efforts have been devoted in that direction. One such method (Ref.[10]) uses pressurized honeycomb cells to introduce small deformations in the optical surface of a sandwiched mirror. Using piezoelectric ceramics to deform a lightweight mirror remains an attractive option, and this thesis intends to address whether this technology is feasible.

1.5 Objectives and Approach

The principal objectives of this project are as follows:

(1) Develop an efficient and practical methodology for analyzing adaptive lightweight mirrors of any size and shape, and

(2) Utilize this method in a study to demonstrate the feasibility of using piezoelectric ceramics to correct self-weight deflections and thermal distortions

The process involves some parametric study of lightweight mirrors to identify critical parameters, as well as repetitive changes in piezo-actuation to find the appropriate piezoceramic actuation profile for deflection correction. These requirements set a secondary

objective that the chosen modeling method be fast and efficient. Finally, although circular mirrors will be used in all verification studies, the methodology must be adaptable to any shaped mirror.

An approach for analyzing lightweight mirrors should be consistent with the capabilities and convenience of current aerospace industry. Whereas finite element programs such as NASTRAN or ABAQUS could have been used for developing the analysis methodology, it was decided to utilize PC-based COSMOS/M Finite Element System. The primary motivation for such a selection was convenience and cost. The thermostructural capabilities of COSMOS/M also allow the evaluation of thermal deflections. This thesis addresses three important issues for analyzing and designing adaptive lightweight mirrors: (1) how to model lightweight mirrors, (2) how to model adaptive mirrors, and (3) how to choose piezoelectric actuation profiles to accomplish the necessary deflection corrections.

To insure that the methodology developed for adaptive lightweight mirror analyses is reasonably accurate as well as fast, the following tasks were performed. First, a routine which automatically generates lightweight mirror models is developed to facilitate the modeling process. This package must be general enough to accommodate lightweight mirrors of any shape. Second, an analytical self-weight deflection solution for a circular lightweight mirror is obtained to verify the accuracy of the mirror model. Third, the methodology for modeling piezoceramics is verified through a simple beam problem. Modeling piezoelectric effects as thermal "forces" to obtain a finite element solution is verified with analytical results for a piezoceramic actuated beam. Fourth, the process of designing an "optimal" mirror using the automatic mirror model generation routine is defined. Here, a nominal circular lightweight mirror with square cells is selected as a starting point design. Finite element models of this design with various mirror parameters are generated using COSMOS/M and trade-off studies are conducted to select a viable design. Once the most feasible mirror which

still meets self-weight deflection and frequency criteria is identified, piezoelectric ceramic elements are modeled on the back sheet of the mirror. The resulting mirror deflection and frequency characteristics are then found. Finally, detailed studies address the placement and actuation profile of piezoceramics in correcting self-weight deflection and thermal distortion of the designed mirror. The piezo-actuated strain capabilities are represented by thermal strains, where an equivalent thermal expansion coefficient is defined for the piezoceramic elements. Unit temperature "loads", representing the applied voltage which induces actuation strains, are applied to each of the piezoceramic elements. Thermostructural analyses are conducted and an actuation influence function is mapped out for the piezoceramic at each node. These influence functions are compiled into MATLAB and least squares solutions for the representative temperature values which pinpoints the appropriate actuation profiles for mirror deflection correction are found for both gravity and thermally induced distortions. Finally, a successive placement optimization routine is used to find piezo-placement locations for correcting these deformations with a restricted number of actuators.

Chapter 2: Lightweight Mirror Modeling

This chapter describes the lightweight mirror modeling method and the analytical solutions used to verify the finite element analyses. Section 2.1 defines the problems associated with the design of lightweight mirrors and provides the approach and assumptions which are used in the finite element modeling. Section 2.2 presents a description of the methodology for automating lightweight mirror modeling. Section 2.3 presents the analytical solution for the mirror's self-weight deflection. An analytical approach based on small deflection theory is adapted for a lightweight mirror and the results are compared with finite elements. These analyses confirm that the lightweight mirror modeled using COSMOS/M finite element program give good first-cut results.

2.1 Problem Statements and Assumptions

Several considerations must be addressed in the design of lightweight mirrors, including gravity-induced deflections, fundamental frequency, and quilting deflections. Mirror parameters which affect these deflections include the overall mirror height, rib thickness, and facesheet to cell width ratio. For the following analyses, it is assumed that optimization of mirror geometry and support locations to reduce mechanical deflection of a mirror in meeting its specified structural requirements will also meet the desired optical performance. In general, this will not necessarily be true since tilt of the mirror surface is equally important in determining the mirror's performance.

Lightweight mirrors are modeled by a series of plate elements (Figure 2-1) where facesheet and rib interfaces are assumed to be fritted or fused together such that there are no local weaknesses in the mirror structure. The finite element model is generated by using quadrilateral and triangular thick shell elements (Ref.[1]). Although the usual convention for structural modeling and analyses recommends: modeling plates as thin elements if the

smallest plate dimension to thickness ratio is greater than ten; as thick shell elements when this ratio is between seven and ten; and not be modeled as a two-dimensional element at all should this ratio be any less; the construction of the lightweight mirror is such that it makes this decision quite difficult. Although such a mirror is made up of "thin" rib and face sheets where the dimensions in two directions are much larger than the third dimension, shear deformations or in-plane deformations may play an important role in rib plate deflections. The four-node quadrilateral thick shell and the three-node triangular thick shell elements will allow for such shear deformation effects should they play an important part. Otherwise, deflection results should not differ from thin shell analyses. The structural shell elements are assumed to be isotropic with constant thickness for self-weight deflection and thermal deflection problems. The piezoelectric elements, discussed in later chapters, are assumed to be orthotropic since normal strains are neglected.

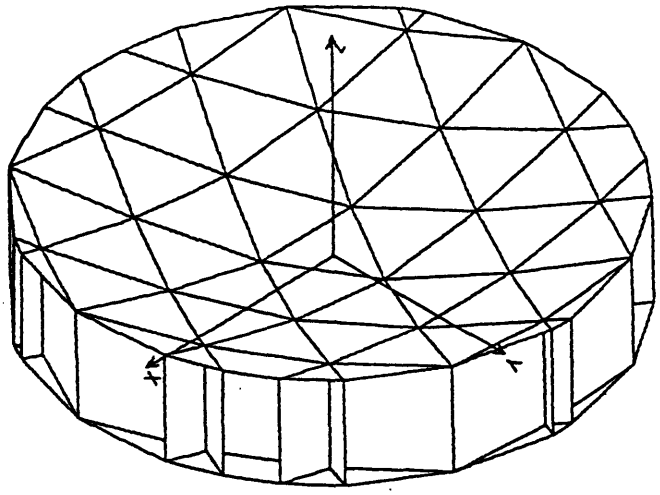

Figure 2-1 Finite Element Model of a Lightweight Mirror

Finite element for surfaces is generated in such a way as to keep the aspect ratio as close to unity as possible to assure the accuracy of the numerical results (Ref.[41],[43]). For the first

cut analyses desired for the correction of self-weight and thermal deflections, each cell will be modeled by one element on each surface.

Boundary conditions for the lightweight mirrors are assumed to be simply supported multipoints. This assumption is reasonable for characterizing mirror mounts that have a ball-in-socket type construction. Various support mounts can be designed and, again for meeting weight requirements, a minimum number is best. For the purpose of this thesis, the number of constraints is chosen to be three because it is the minimum number of supports necessary for keeping the mirror aligned in a specified plane. Each support point constrains displacement in the x, y and z directions, for a total of nine constraints. In reality, mirror supports may be kinematic, containing only six constraints, which allow free thermal expansion and contraction capabilities.

Finite element analysis provides good results for mirror deflections and natural frequencies in a fairly efficient manner, but the finite element modeling process is repetitive, time-consuming, and prone to user error. The model featured in Figure 2-1 might take an experienced user half a day to complete. This process involves specifying the geometrical shape, making the connective surfaces for the face sheets and ribs, and meshing these surfaces with appropriate element types and material properties. Automation of such a process can greatly ease the study of lightweight mirrors by allowing changes to be made quickly and accurately. The Automatic Mirror Modeling and Analysis Package (AMMAP) is developed to interface with the COSMOS/M finite element analysis program to build mirror models in an efficient manner. In order for the package to be useful, it must provide wide-ranging capabilities for generating mirror models of any size and shape. The following is a description of AMMAP's approach and capabilities. An abridged version of this software program is featured in Appendix A.

2.2 Modeling Automation Description

Similar to popular modeling and analysis software, the COSMOS/M Finite Element System contains a defined library of commands for generating, meshing, and analyzing structural models. The automatic mirror modeling and analysis program (AMMAP) is designed to utilize these commands to model a lightweight mirror by translating important mirror and rib dimensions into COSMOS/M commands. To accomplish this goal, a versatile graphics routine called NODE_GEN was developed to provide the capability to generate and display important mirror dimensions and cell coordinates needed for mirror modeling. These parameters are then read into AMMAP and manipulated into a manageable sequence to generate the appropriate COSMOS/M commands for creating and meshing mirror facesheets and rib support surfaces. Because the objective is to provide a method which can accommodate various sizes, shapes, and intersection of mirror and rib surfaces, an algorithm which accounts for all possible combinations of rib cell shapes was developed. In consultation with Eric K. Hall of the Structural Technology Department and Kiet T. Luu of the Electro-Optical Systems Department at The Aerospace Corporation, the author wrote AMMAP and developed a methodology for interfacing each of the different software packages (NODE_GEN Graphics Routine, AMMAP, and COSMOS/M) to achieve a versatile and efficient lightweight mirror analysis package.

Data points are provided by the graphics routine NODE_GEN developed by Armando Cardona of the Software Development Department at The Aerospace Corporation. NODE_GEN reads input parameters from the user (Table 2-1), creates graphics showing important mirror dimensions and cell coordinates (Figure 2-2), and outputs into a file the rib intersection coordinates as well as data for rib and mirror edge intersections (Table 2-2). It is designed to plot a variety of geometries as shown in Figure 2-2.

Table 2-1 Graphics Routine Input Parameters

INPUT PARAMETER	OPTIONS AND DESCRIPTION
cell shape	0: Square 1: Triangle 2: Hexagon
cell dimension	Edge length for square and triangular cells Radius for hexagonal cell
mirror shape	0: Circle 1: Rectangle 2: Pseudoellipse
mirror dimensions	Diameter for circular mirror Width and length for rectangular mirror Width, length, and radius for pseudoellipse
x offset	Offset of mirror center from cell center
y offset	Offset of mirror center from cell center
tolerance	Tolerance for differentiating data points
file name	Output file name
option 1	Y or N to show nodes on screen
option 2	Y or N to show node numbers on screen
option 3	Y or N to obtain a printout

Table 2-2 Sample of Graphics Routine Output File

Node Number	M-coordinate	N-coordinate	Status	X-coordinate	Y-coordinate
52	10	3	0	-350.000000	349.999000
53	10	2	1	-357.072402	349.999000
54	11	3	1	-350.000000	357.071421
55	11	4	2	-250.000000	433.012702
56	11	6	0	-50.000000	449.999000
57	11	5	0	-150.000000	449.999000
58	11	6	2	-217.947012	449.999000
59	12	5	1	-150.000000	476.969601
60	12	6	1	-50.000000	497.493717

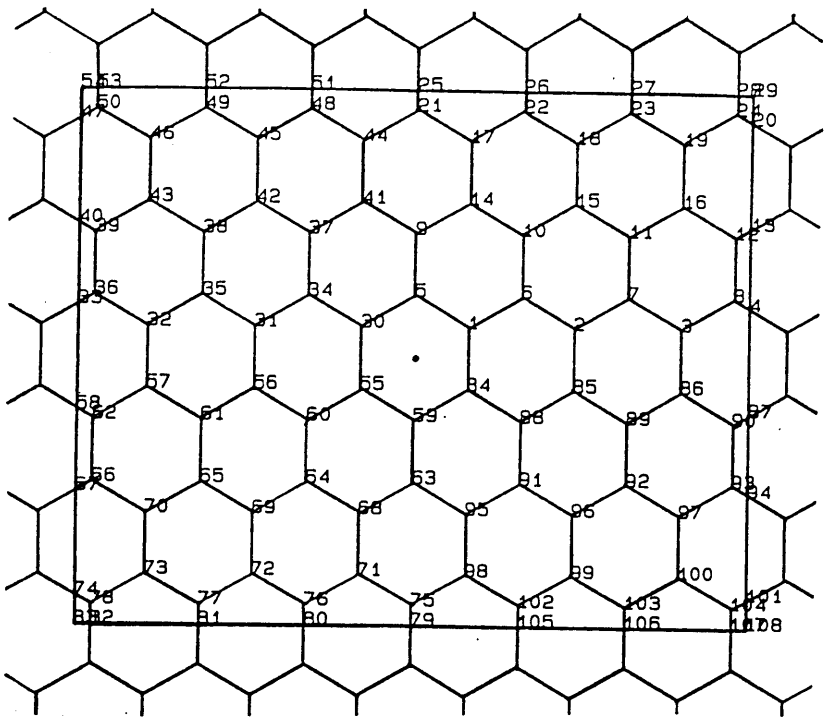

(a)

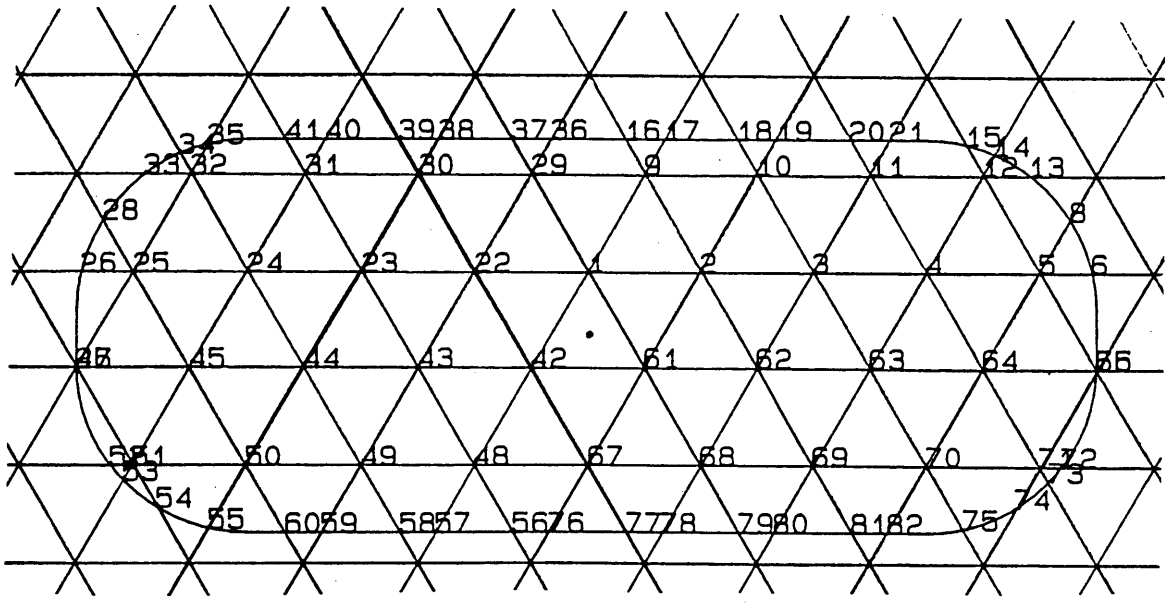

(b)

Figure 2-2 Examples of Graphics Routine Capabilities

The conversion of these data points into a finite element model poses several problems. First, how can the relative location of each node be systematically distinguished from one another and, second, how can an algorithm "know" which nodes to connect to produce a surface? This is where a systematic way of defining "matrix" coordinates for each node (designed to be provided by the graphics routine as shown in Table 2-2) becomes essential for specifying the location of each point. This information eases AMMAP's modeling process tremendously. Unlike the x and y-coordinates which give the absolute two-dimensional position of a point, the "matrix" coordinates (m,n) represent an integer grid overlay to which a point is assigned. In this way, the relative positions of a point with respect to other points are defined and the integer assignment can be used in a programming loop for easy repetitions. More appropriately, this is easy for points connecting rib cells completely, but problems are encountered when the rib wall intersects with the edge of the mirror. Here, cells may be "cut off" and multiple points will share the same m and n-coordinates (Figure 2-3).

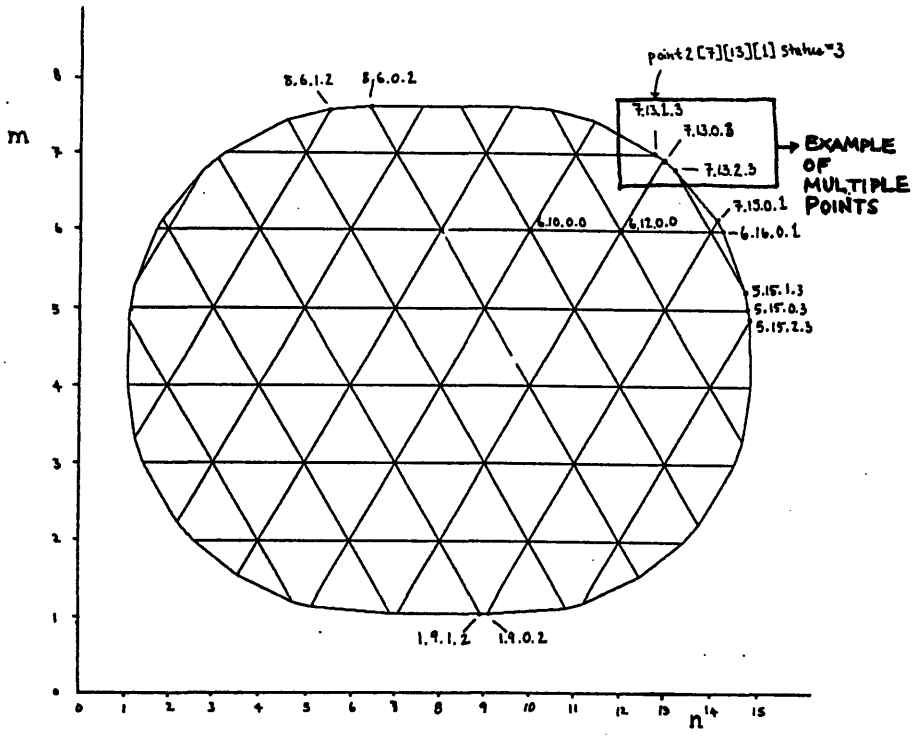

Figure 2-3 Array Assignment of Points for Triangular Cells

In order to distinguish these "problem" points at the edge from one another and from the "no problem" interior points, a third parameter "status" is devised. These numbers range from zero to three and are assigned to the points depending on where the point is relative to the mirror and to other points. All interior points intersecting two rib surfaces are assigned a status of zero. The edge points gravitate outwards from the mirror center along a rib to the nearest m and n-coordinate, where they are assigned a status number depending on the total number of points sharing those same (m,n) coordinates. All the data needed for distinguishing nodes from one another is designed to be provided by NODE_GEN so that AMMAP can simply apply the information given to generate 3-D models.

AMMAP interfaces between the graphics routine and COSMOS/M and runs interactively by prompting the user for mirror and cell shapes, mirror dimensions, and mirror material (Table 2-3). Figure 2-4 shows the general flow of this program, and Figure 2-5 shows some finite element mirror models generated by this program.

AMMAP creates a three-dimensional array of structures where the first two dimensions contain the "matrix" (m,n) coordinates and the third dimension allows storage of multiple points. Each structure contains information about each point: node number, status, and the values in x, y, and z coordinates. Then, to generate the surfaces which make up the mirror facesheets and ribs, the program loops through the array of points and performs a series of checks on the neighboring points' status. This distinguishes the cell type, whether three, four, or five pointed surfaces, and evokes commands which create the appropriate surface. Notice, however, that since COSMOS/M does not have the capability to generate five pointed surfaces easily, a five pointed surface is divided into a combination of three and four pointed surfaces. Thus, future graphics depicting mirrors may appear to have surfaces separating cells, but these are simply the lines which make up the three and four pointed surfaces.

Because of the "brute force" logic of using conditional statements to distinguish cell shapes and the large variety of surface combinations, the program turned out to be quite lengthy. However, this methodology allows much more versatility, including the ability to easily incorporate mirror curvature parameters using standard optical conventions. This advantage may not be obvious at first glance, but the capability is essential to practical mirror designs. More complete description of the modeling and meshing process can be obtained from the actual program in Appendix A.

Table 2-3 AMMAP Input Parameters

INPUT PARAMETER	OPTIONS AND DESCRIPTION
mirror type	1: Open back mirror 2: Close back mirror
material type	1: Silicon Carbide (SiC) 2: Beryllium (Be) 3: Fused Silica (SiO2) 4: Aluminum (Al) 5: Zerodur
mirror dimensions	Mirror, facesheet, backsheet thickness
rib support shape	1: Square 2: Triangular 3: Hexagonal
rib dimension	Rib support thickness
edge band option	1: No edge band 2: Edge band
edge band dimension	Edge band thickness
mirror curvature parameters	curv, K, A, B, C, and D from Code 5
offsets	Mirror center offset from parent mirror Mirror center offset from cell center
tolerance option	Y or N
tolerance	COSMOS/M tolerance for merging nodes

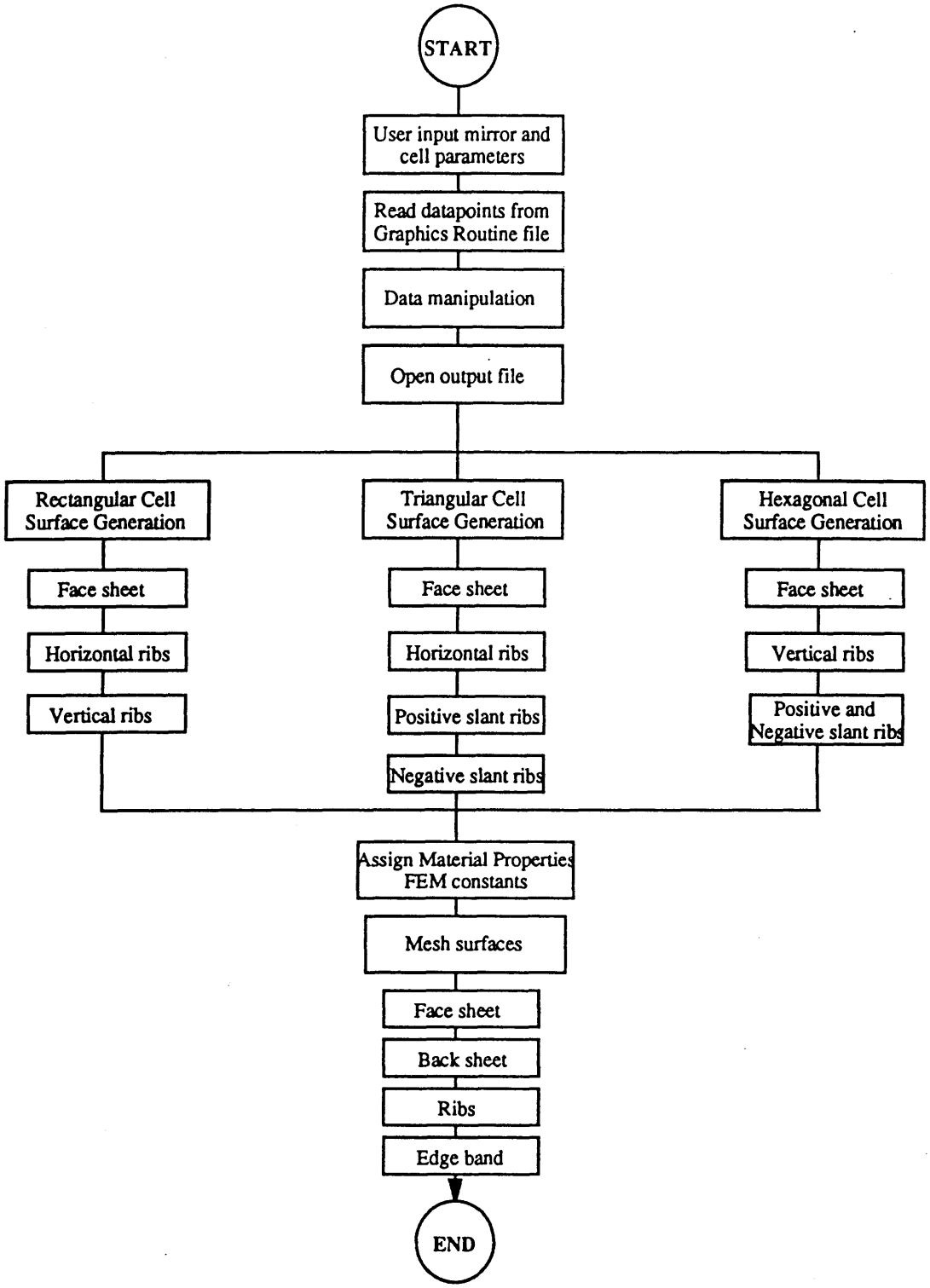

Figure 2-4 AMMAP Flow Chart

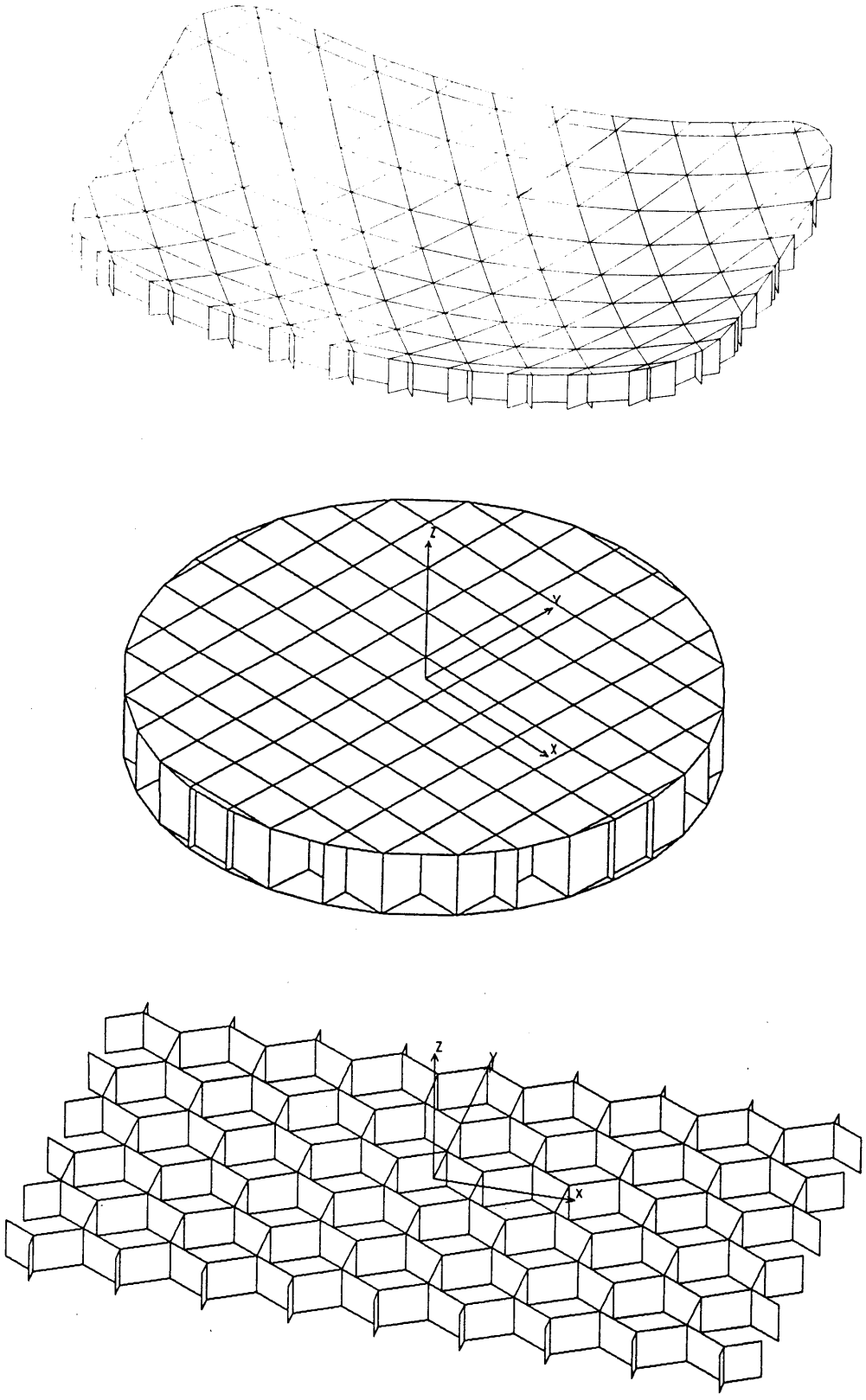

Figure 2-5 Models Generated by AMMAP

2.3 Modeling Verification

Models which are automatically generated by AMMAP can be readily adapted by a finer mesh should this provide more accuracy, but it is desirable first to show that a simple model is adequate for trade studies. Analytical solutions are used to verify the accuracy of a "coarsely" meshed finite element model. Some theoretical equations pertinent to solving the mechanical deflections of a lightweight plate and later to designing a lightweight mirror are presented, followed by a comparison between analytical and finite element gravity-induced deflections.

First, finite element deflection solutions for a flat plate supported on three points is checked with the deflection solution for a general circular plate on equally spaced points developed by Williams and Brinson (Ref.[55]). Since their results also correlated with experimental data, the comparison will ascertain that COSMOS/M finite element program gives good results. Section 2.3.1 contains a discussion of this analytical problem. Next, to extend this application to a circular lightweight mirror, equivalent lightweight plate properties are found to replace solid plate properties. The analytical solutions are again compared with finite element solutions. This is detailed in Section 2.3.3 and 2.3.4.

2.3.1 Plate Deflection Solution

The deflection for a circular plate with constant thickness supported on point supports and subjected to uniformly distributed load W can be found on the basis of classical small-deflection theory. Figure 2-6 illustrates the problem at hand. Williams and Brinson arrived at a solution, in terms of real variables that can be used directly for engineering applications. The transverse deflection w_T of this system is found by combining solutions published by Timoshenko and Woinowsky-Krieger (Ref.[51]) and solving for an unknown solution through superposition. Figure 2-7 illustrates the components used to define the total system.

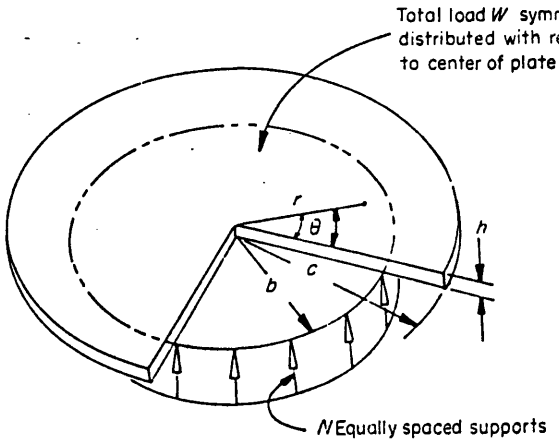

where

c	plate radius
h	uniform plate thickness
b	support radius
N	number of supports
q	uniform load intensity
r	radius of interest
θ	angle of interest
α	angle between supports

Figure 2-6 Uniformly Loaded Circular Plate on Multipoint Supports (Ref.[55])

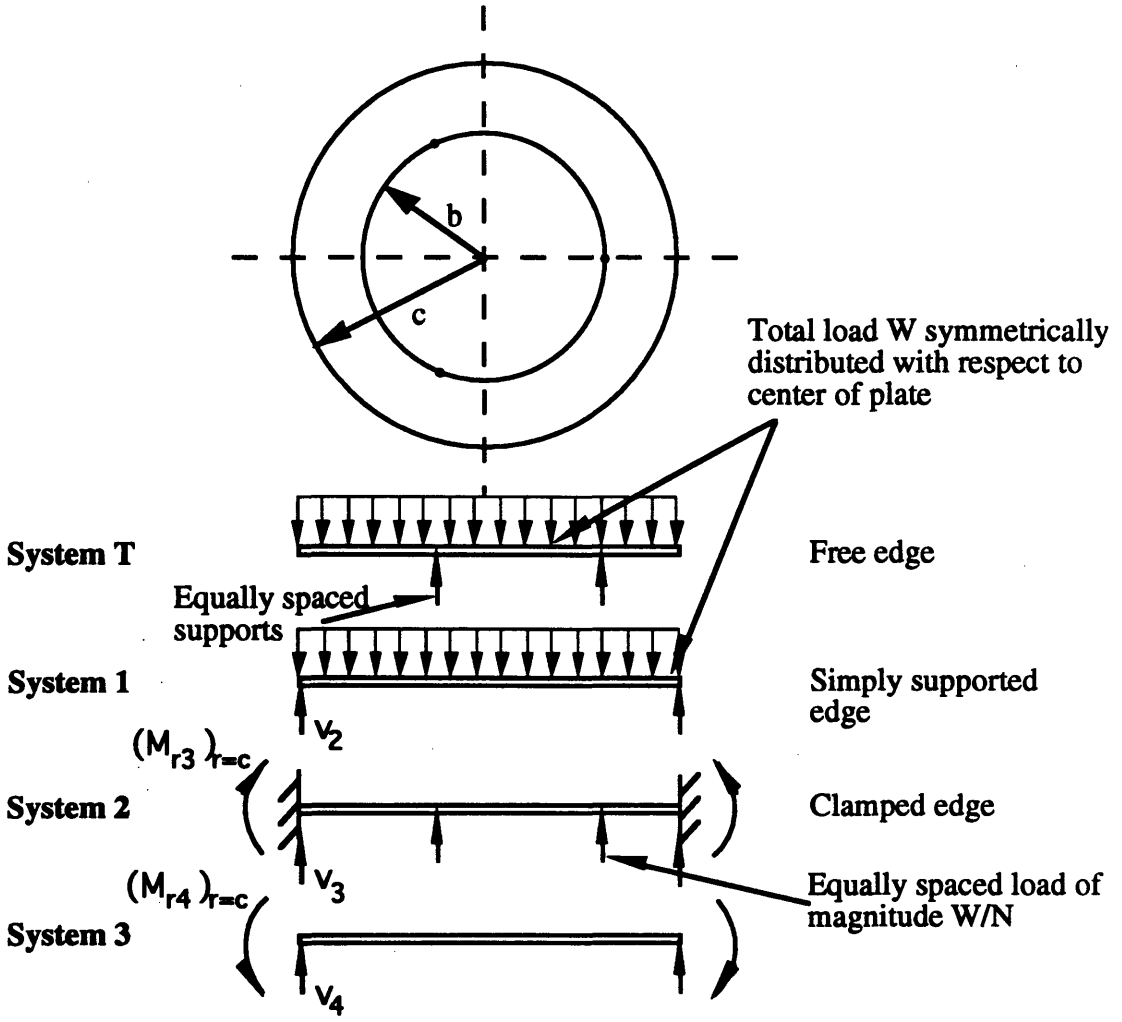

Figure 2-7 Total System T broken down to System 1, 2, and 3 (Ref.[55])

Solutions to the first two systems can be found in Ref.[51] and manipulated for the following cases, with

$$x = \frac{r}{c} \qquad \text{and} \qquad \nabla^2 = \frac{1}{c^2}\left(\frac{\delta^2}{\delta x^2} + \frac{1}{x}\frac{\delta}{\delta x} + \frac{1}{x^2}\frac{\delta^2}{\delta\theta^2}\right)$$

Case (1) is a simply supported circular plate of radius c subjected to symmetrically distributed load W,

$$\nabla^4 w_1 = \frac{1}{r}\frac{d}{dr}\left\{ r\frac{d}{dr}\left[\frac{1}{r}\frac{d}{dr}\left(r\frac{dw_1}{dr}\right)\right]\right\} = \frac{q(r)}{D} \tag{2-1}$$

$$(M_{r1})_{r=c} = -D\left(\nu\nabla^2 w_1 + \frac{1-\nu}{c^2}\frac{\delta^2 w_1}{\delta x^2}\right)_{x=1} = 0 \tag{2-2}$$

$$(V_1)_{r=c} = -D\left[\frac{1}{c}\frac{\delta\nabla^2 w_1}{\delta x} + \frac{1-\nu}{c^3 x}\frac{\delta^2}{\delta x\delta\theta}\left(\frac{1}{x}\frac{\delta w_1}{\delta\theta}\right)\right]_{x=1} = -\frac{W}{2\pi c} \tag{2-3}$$

where D is flexural rigidity and q(r) is related to W by

$$W = 2\pi\int_0^c q(r)\, r\, dr \tag{2-4}$$

Case (2) is a clamped circular plate of radius c subjected to N concentrated supports equally situated on radius b, each of magnitude $-\frac{W}{N}$, where $\alpha = \frac{2\pi}{N}$,

$$w_2 = \frac{Wc^2}{16\pi ND}\left\{(x^2-1)(1-s^2) + \frac{1}{N}\sum_{n=1}^{N}\left[x^2+s^2-2xs\cos(\theta-n\alpha)\right]\log\left[\frac{1+x^2s^2-2xs\cos(\theta-n\alpha)}{x^2+s^2-2xs\cos(\theta-n\alpha)}\right]\right\} \tag{2-5}$$

$$\begin{aligned}(M_{r2})_{r=c} &= -D\left(\nu\nabla^2 w_2 + \frac{1-\nu}{c^2}\frac{\delta^2 w_2}{\delta x^2}\right)_{x=1} \\ &= \frac{W(1-s^2)}{4\pi} + \frac{W(1-s^2)}{2\pi N}\sum_{n=1}^{N}\sum_{m=2}^{\infty} s^m\cos m(\theta-n\alpha)\end{aligned} \tag{2-6}$$

$$\begin{aligned}(V_2)_{r=c} &= -D\left[\frac{1}{c}\frac{\delta\nabla^2 w_2}{\delta x} + \frac{1-\nu}{c^3 x}\frac{\delta^2}{\delta x\delta\theta}\left(\frac{1}{x}\frac{\delta w_2}{\delta\theta}\right)\right]_{x=1} \\ &= \frac{W}{2\pi c}\left[1 + \frac{1}{N}\sum_{n=1}^{N}\sum_{m=2}^{\infty}\left[2 + m(1-s^2)\right] s^m\cos m(\theta-n\alpha)\right]\end{aligned} \tag{2-7}$$

The third system can be solved by following the assumption that the resulting total system have the boundary conditions of a free edge,

$$(M_{rT})_{r=c} = -D\left(\nu \nabla^2 w_T + \frac{1-\nu}{c^2}\frac{\delta^2 w_T}{\delta x^2}\right)_{x=1} = 0 \tag{2-8}$$

$$(V_T)_{r=c} = -D\left[\frac{1}{c}\frac{\delta \nabla^2 w_T}{\delta x} + \frac{1-\nu}{c^3 x}\frac{\delta^2}{\delta x \delta\theta}\left(\frac{1}{x}\frac{\delta w_T}{\delta\theta}\right)\right]_{x=1} = 0 \tag{2-9}$$

so that,

$$-(M_{r3})_{r=c} = (M_{r1})_{r=c} + (M_{r2})_{r=c} \tag{2-10}$$

$$(M_{r3})_{r=c} = -D\left(\nu \nabla^2 w_3 + \frac{1-\nu}{c^2}\frac{\delta^2 w_3}{\delta x^2}\right)_{x=1}$$
$$= -\frac{W(1-s^2)}{2\pi}\left[\frac{1}{2} + \frac{1}{N}\sum_{n=1}^{N}\sum_{m=2}^{\infty} s^m \cos m(\theta - n\alpha)\right] \tag{2-11}$$

$$-(V_3)_{r=c} = (V_1)_{r=c} + (V_2)_{r=c} \tag{2-12}$$

$$(V_3)_{r=c} = -D\left[\frac{1}{c}\frac{\delta \nabla^2 w_3}{\delta x} + \frac{1-\nu}{c^3 x}\frac{\delta^2}{\delta x \delta\theta}\left(\frac{1}{x}\frac{\delta w_3}{\delta\theta}\right)\right]_{x=1}$$
$$= -\frac{W}{2\pi N c}\sum_{n=1}^{N}\sum_{m=2}^{\infty}\left[2 + m(1-s^2)\right] s^m \cos m(\theta - n\alpha)\Big] \tag{2-13}$$

Equations (2-11) and (2-13) suggest a deflection equation for Case (3) of this form,

$$w_3 = A + Bx^2 + \sum_{n=1}^{N}\sum_{m=2}^{\infty}\left(A_m + B_m x^2\right) x^m s^m \cos m(\theta - n\alpha) \tag{2-14}$$

where the coefficients A, B, A_m, and B_m can be solved when substituted into the equations above. Now that all the deflection characteristics are known, manipulations will give a solution which only depends on the deflection of the first system, the simply supported plate with the desired loading conditions (Consult Ref.[55] for all the details).

$$w_T = w_1 - [w_1]_{x=s} + \Phi(x, \theta) \tag{2-15}$$

$$\Phi(x,\theta) = \frac{K(\lambda^2-s^2)(x^2-s^2)}{\lambda(\lambda+1)} + \frac{Ks^2}{N\lambda}\sum_{n=1}^{N-1}(1-\cos n\alpha)\log\left\{\frac{[2s^2(1-\cos n\alpha)]^\lambda}{1+s^4-2s^2\cos n\alpha}\right\} \tag{2-16}$$

$$+\frac{K}{2N\lambda}\sum_{n=1}^{N}[x^2+s^2-2xs\cos(\theta-n\alpha)]\log\left\{\frac{1+x^2s^2-2xs\cos(\theta-n\alpha)}{[x^2+s^2-2xs\cos(\theta-n\alpha)]^\lambda}\right\}$$

$$+\left(K\frac{\lambda^2-1}{\lambda}\sum_{(m=N,2N,\ldots)}^{\infty}\frac{x^m s^m}{m^2(m-1)}\cos m\theta\right) - \left(K\frac{\lambda^2-1}{\lambda}\sum_{(m=N,2N,\ldots)}^{\infty}\frac{s^{2m}}{m^2(m-1)}\right)$$

where $$K = \frac{qc^4}{8D} = \frac{Wc^2}{8\pi D} \qquad D = \frac{Eh^3}{12(1-\nu^2)} \tag{2-17}$$

$$\lambda = \frac{3+\nu}{\nu-1} \qquad x = \frac{r}{c} \qquad s = \frac{b}{c}$$

and W total load on plate

ν Poisson's ratio

For the uniformly loaded plate under discussion here, Ref.[51] p. 57 gives:

$$w_1 = \frac{q(c^2-r^2)}{64D}\left(\frac{5+\nu}{1+\nu}c^2 - r^2\right) \tag{2-18}$$

substituting in consistent parameters from Eq.(2-17), modified equations are found which can be easily substituted into Eq.(2-15)

$$w_1 = \frac{K(1-x^2)}{8}\left(\frac{5+\nu}{1+\nu} - x^2\right) \tag{2-19}$$

$$[w_1]_{x=s} = \frac{K(1-s^2)}{8}\left(\frac{5+\nu}{1+\nu} - s^2\right) \tag{2-20}$$

to give a surface deflection

$$w_T = \frac{K}{2N\lambda}\sum_{n=1}^{N}[x^2+s^2-2xs\cos(\theta-n\alpha)]\log\left\{\frac{1+x^2s^2-2xs\cos(\theta-n\alpha)}{[x^2+s^2-2xs\cos(\theta-n\alpha)]^\lambda}\right\}$$

$$+\frac{Ks^2}{N\lambda}\sum_{n=1}^{N-1}(1-\cos n\alpha)\log\left\{\frac{[2s^2(1-\cos n\alpha)]^\lambda}{1+s^4-2s^2\cos n\alpha}\right\} \tag{2-21}$$

$$+\frac{K(\lambda^2-1)}{\lambda}\{\sum_{m=N,2N,\ldots}^{\infty}[\frac{x^m s^m \cos m\theta}{m^2(m-1)}] - \sum_{m=N,2N,\ldots}^{\infty}[\frac{s^{2m}}{m^2(m-1)}]\}$$
$$+\frac{K(x^4-s^4)}{8} - \frac{K(\lambda^2-2s^2)}{2\lambda(\lambda+1)}(x^2-s^2)$$

A numerical deflection coefficient β to ease the manipulation of this equation can be found:

$$w_T = \beta\frac{qc^4}{Eh^3} = \beta\frac{Wc^2}{\pi Eh^3} \qquad (2\text{-}22)$$

where β is a dimensionless deflection coefficient that is a function of these variables:

x	radius of interest	s	radius of support
θ	angle of interest	N	number of supports
ν	Poisson's ratio		

Table 2-4 presents the deflection coefficients at three different locations (Figure 2-8) for the three point support problem (N=3) with a typical material used in mirrors, fused silica (ν=0.17).

Table 2-4 Deflection Coefficients β for Fused Silica Plate on Three Equally Distributed Support Points (Ref.[55])

S	Point A (x=1, T= 60°)	Point B (x=1, T=0°)	Point C (x=0)
0.1	-1.088692	-1.087507	0.027370
0.2	-0.932069	-0.922659	0.068665
0.3	-0.749346	-0.718001	0.099569
0.4	-0.570584	-0.497664	0.105003
0.5	-0.419801	-0.280705	0.071502
0.6	-0.318866	-0.085446	-0.015179
0.7	-0.289646	0.068472	-0.171589
0.8	-0.356112	0.157924	-0.418307
0.9	-0.548326	0.152540	-0.783557
1.0	-0.916689	0	-1.317198

β provided here are relative to the plane of the supports and upward deflections are assumed to be positive. Point A, Point B, and Point C are used as descriptive terms for the deflections as illustrated in Figure 2-8. Since the plate is uniformly loaded and the supports are arranged in a symmetrical manner, the maximum and minimum deflection values of the plate under any support radius could be obtained from these three points.

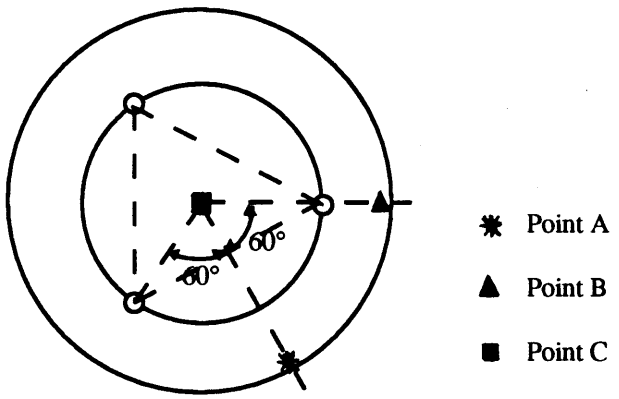

Figure 2-8 Points of Deflection Measurement

2.3.2 Analytical and Finite Element Plate Solution Comparison

For the comparison test, a finite element model of a fused silica plate was generated on COSMOS/M with the following dimensions and properties:

Diameter:	270.75 mm
Thickness:	36.27 mm
Young's Modulus:	7.308E7 N/mm^2
Poisson's Ratio:	0.17
Mass:	4.59 kg

The point support radius was varied between one-tenth of the radius (s=0.1) to the edge of the plate (s=1) and deflections were taken at the points A, B, and C as depicted in Figure 2-8. These were compared with the analytical results as given by equation (2-22). Since the analytical solution is based on small deflections, analysis using thin shell elements correlated

very well with these results (Figures 2-9 through 2-11). Realistically, however, this particular plate should be modeled by thick shell elements since the plate diameter to thickness ratio is quite small. Here one sees quite a difference between results with (thick shell) and without (thin shell) shear effects (Figure 2-9). This demonstrates that the lightweight mirror models need to be modeled by thick shells should transverse shear play an important part in mirror deformations, and that mirror deflection results could very well differ from analytical results due to shear.

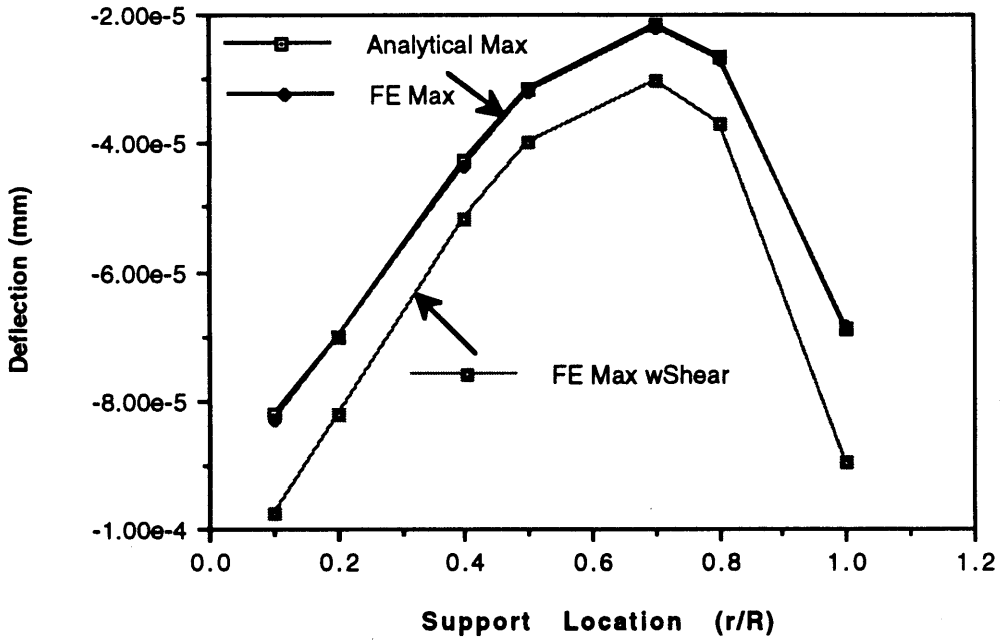

Figure 2-9 Plate Solutions at Maximum Point A

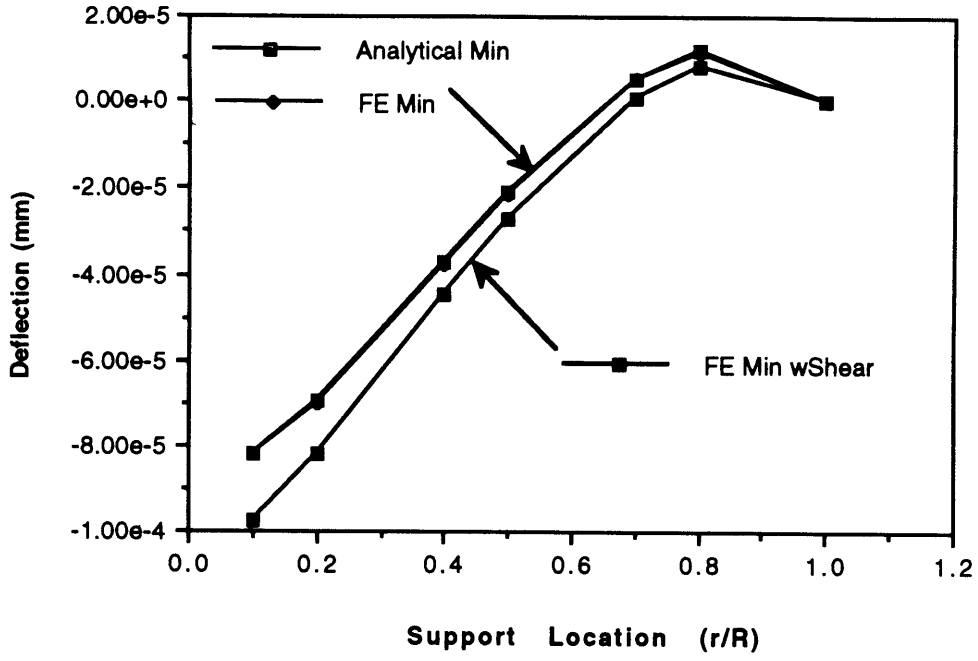

Figure 2-10 Plate Solutions at Minimum Point B

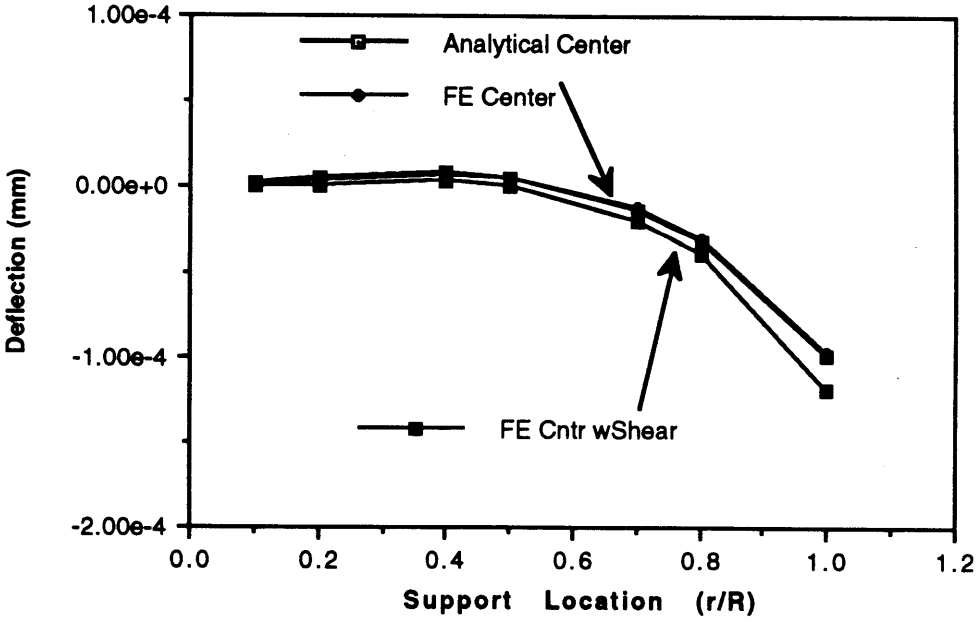

Figure 2-11 Plate Solutions at Center Point C

2.3.3 Equivalent Plate Properties for Lightweight Plate Deflection

It has been shown that finite element solutions for a thin plate correlate quite well with analytical solutions for a thin plate. Now a comparison between solutions and analyses of a lightweight mirror can be conducted by extending this analytical solution for a thin plate to include lightweight mirror properties. Since the analytical deflection solution is conveniently in real variables, one can easily replace the solid plate properties with equivalent lightweight plate properties to arrive at a solution for a lightweight mirror. Instead of a solid mirror, relationships which distribute the materials to represent a lightweighted plate can be used. Specifically, lightweight properties can be defined either by a different modulus of elasticity E or by an effective plate thickness h. Two previous works document how this is done. Mehta (Ref.[37]) defined an equivalent thickness h_e of a solid plate with the same flexural rigidity of the lightweight plate. By using a rib solidity ratio, where mirror variables are illustrated in Figure 2-13,

$$\eta = \frac{(2B+t_w)t_w}{(B+t_w)^2} \tag{2-23}$$

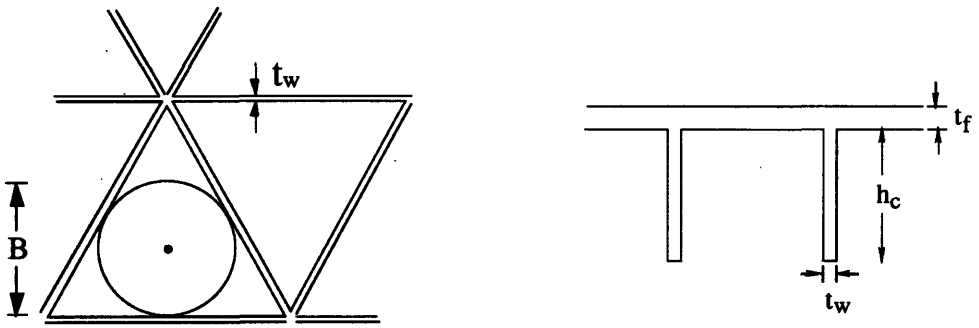

Figure 2-12 Nomenclature for Rib Solidity and Equivalent Thickness Calculations

the flexural rigidity and the weight of the lightweight mirror can be defined in these terms,

$$D = \frac{Eh_e^3}{12(1-\nu^2)} \qquad W = \rho A\,(mt_f + \eta h_c) \tag{2-24}$$

where for an open-back mirror

$$h_e^3 = \frac{\{(1-\frac{\eta}{2})\,(t_f^4 - \eta\frac{h_c^4}{2}) + (t_f + h_c)^4\,\frac{\eta}{2}\}}{(t_f + \eta\frac{h_c}{2})} \tag{2-25}$$

and for a closed-back mirror

$$h_e^3 = (2t_f + h_c)^3 - (1-\frac{h}{2})\,h_c^3 \tag{2-26}$$

Then, to obtain the lightweight mirror deflection, h_e is simply substituted in for h,

$$w_T = \beta\frac{Wc^2}{\pi Eh_e^3} \tag{2-27}$$

This method equates the flexural rigidity of the lightweight mirror to that of a solid plate by varying one parameter h_e, but in order to equate both the flexural and extensional rigidities of the lightweight structure to a solid plate, two parameters must be varied. Such is done in Meyers' work (Ref.[39] and [3]) on isogrids, which is developed to provide efficient, stiffened structures and can be extended to lightweight mirrors. The structural properties are identical since the isogrid structure resembles the triangular celled mirror with its pattern of equilateral triangles. By applying plane stress theory which states that the stiffness property can be assumed isotropic should it contain three or more discrete lines of symmetry, of which this structure exhibits, this gridwork can be "smeared out" and its elastic properties are related to isotropic materials in generalized plane stress.

An isotropic material requires two elastic constants. Here E and ν are chosen to be,

$$E = E_o\frac{b}{h} \qquad \text{and} \qquad \nu = \frac{1}{3} \tag{2-28}$$

where E_o is the base grid material property. Then the extensional rigidity K and flexural rigidity D of the isogrid can be defined in terms of the skin thickness t and two nondimensional shape factors, a and d. Figure 2-14 illustrates the variable definitions.

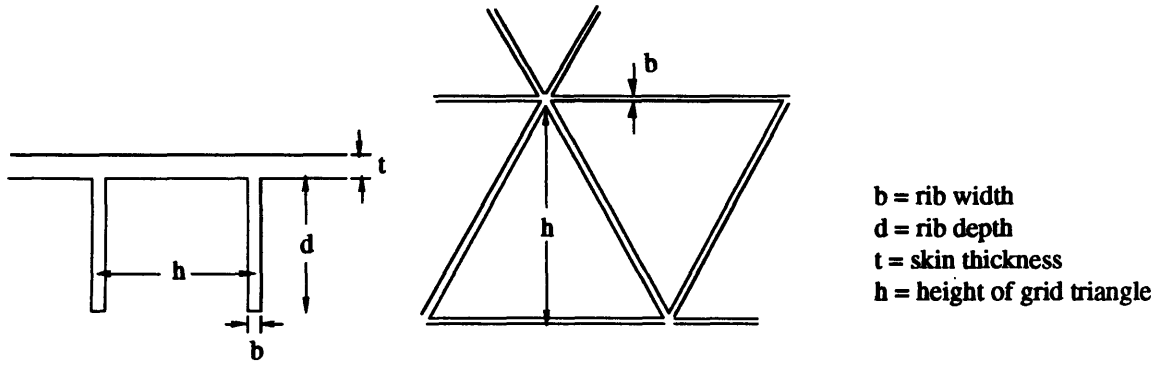

Figure 2-13 Nomenclature for Isogrid Structure

By definition, $\alpha = \frac{bd}{th}$ and $\delta = \frac{d}{t}$ (2-29)

then,

$$K = \frac{1}{1-\nu^2} \int E(z)dz = \frac{E_o t}{1-\nu^2}(1+\alpha) \quad (2\text{-}30)$$

$$D = \frac{1}{1-\nu^2} \int E(z)\, z^2\, dz = \frac{E_o t^3}{12(1-\nu^2)} \frac{\beta^2}{1+\alpha} \quad (2\text{-}31)$$

where $\beta = [\, 3\alpha\,(1+\delta)^2 + (1+\alpha)(1+\alpha\delta^2)]^{1/2}$ (2-32)

The first factors E_o, t, and ν give the rigidity of the base skin material, and this is multiplied by the second factors to account for the lightweighting. For monocoque solutions which are not given in terms of K and D, equivalent variables t* and E* must be determined to give the correct isogrid rigidities.

Defining $$K = \frac{E^*t^*}{1-\nu^2} \quad \text{and} \quad D = \frac{E^*t^{*3}}{12(1-\nu^2)} \tag{2-33}$$

t* and E* can be solved

$$t^* = \sqrt{\frac{12D}{K}} = t\,\frac{\beta}{1+\alpha} \tag{2-34}$$

$$E^* = (1-\nu^2)\sqrt{\frac{K^3}{12D}} = E_o\,\frac{(1+\alpha)^2}{\beta} \tag{2-35}$$

These variables can be substituted in for E_e and h_e, respectively, to give,

$$w_T = \beta\frac{Wc^2}{\pi E_e h_e{}^3} = \beta\frac{Wc^2}{\pi E^* h^{*3}} \tag{2-36}$$

In theory, the isogrid method should give more accurate results since it accounts for both the extensional and flexural rigidities in equating lightweight mirror properties to a solid plate. However, it has not been developed to account for a backsheet surface, which is an advantage which the Mehta method contains. The deflections defined by each of the two lightweighting methods can now be used to see how accurate the finite element model of a lightweight mirror is.

2.3.4 Analytical and Finite Element Lightweight Plate Solution Comparison

For the comparison test, a finite element model of a fused silica lightweight mirror was generated on COSMOS/M with the dimensions and properties illustrated in Figure 2-14. This design was chosen such that support locations can be varied between a normalized radius of s between 0.1 and 1.0. Using Table 2-4 and Eq.(2-25) and Eq.(2-34), analytical mirror deflections can be found. Deflection solutions from the analytical models and the finite element model at the three locations of interest are plotted (Figures 2-15 through 2-17).

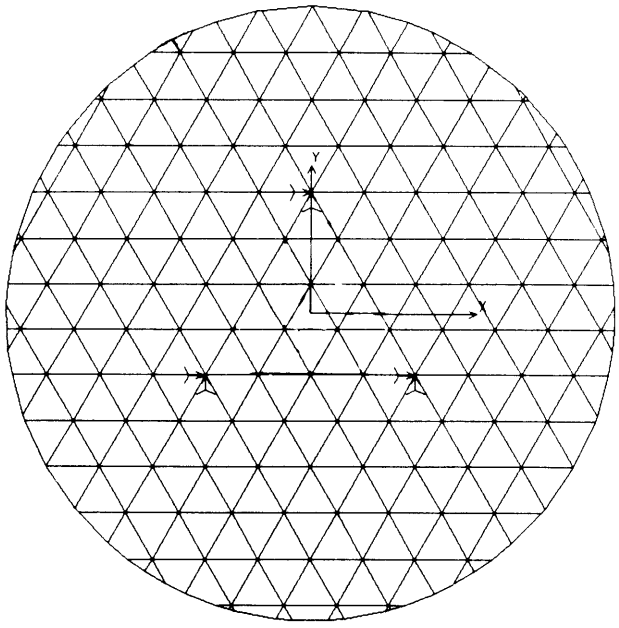

Mirror Material: Fused Silica

Mirror Radius: 135.38mm

Facesheet Thickness: 36.27mm

Cell Side Width: 23.45mm

Cell Height: 20.31mm

Rib Height: 55mm

Rib Thickness: 1.5mm

(Shown:Support Radius s=0.4)

Figure 2-14 Lightweight Mirror Dimensions

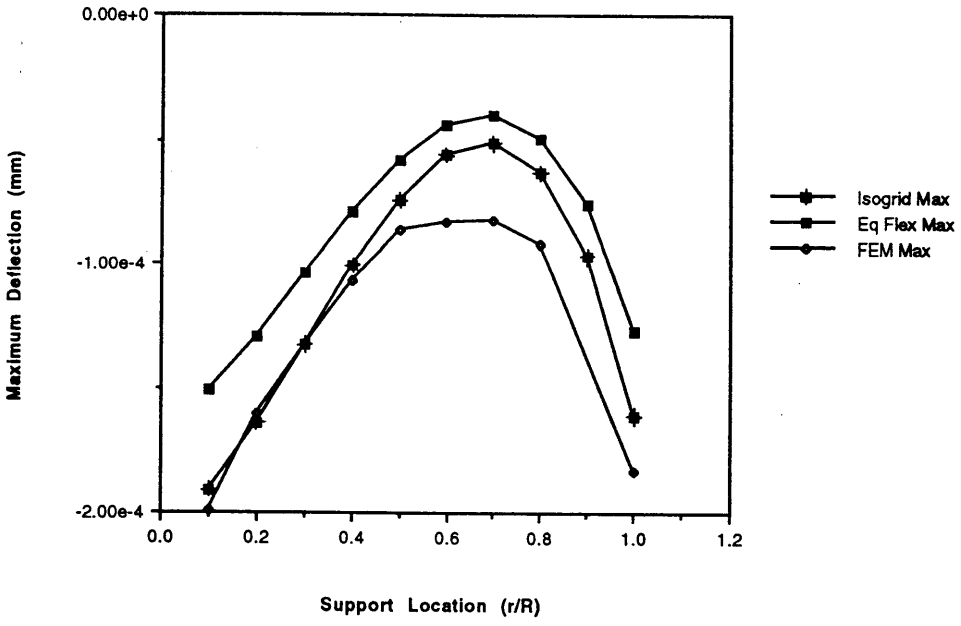

Figure 2-15 Lightweight Mirror Deflection at Maximum Point A

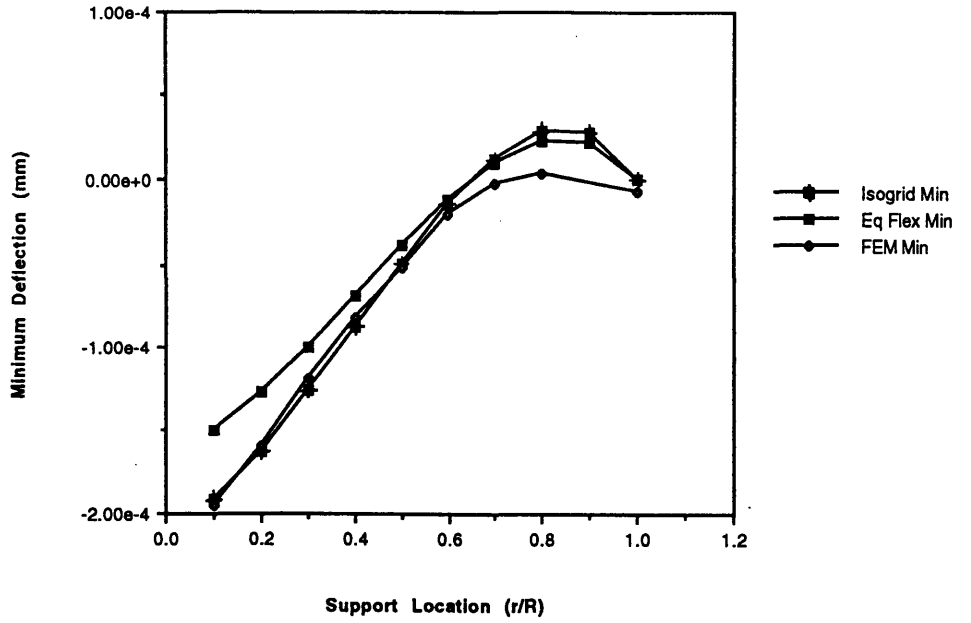

Figure 2-16 Lightweight Mirror Deflection at Minimum Point B

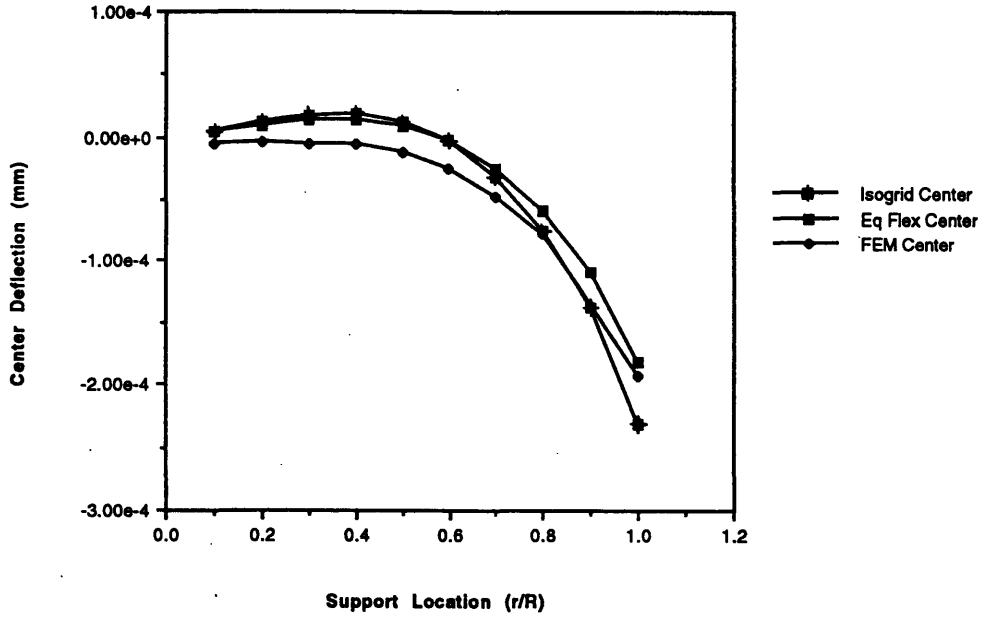

Figure 2-17 Lightweight Mirror Deflection at Center Point C

As mentioned before, flexural rigidity is a measure of stiffness and not a measure of deflection, and other factors need to be examined for more accurate deflection results. Indeed, calculations show a noticeable discrepancy between the results given by the equivalent flexural rigidity model and the isogrid model. Finite element solutions also show a wide discrepancy with either of these solutions but tend to have a closer correlation to the analytical solutions given by the isogrid method, when deflections are observed far away from the support locations. This difference is due to either inaccuracies in the analytical models or inaccuracies in the finite element model. The first case is more likely the problem. Analytical models assume a continuum structure, but this is definitely not the case for lightweight mirrors since they exhibit discrete ribs. Not only does this assumption exclude accounting for localized effects such as rib compression due to the weight of the facesheet, but it also does not account for shearing of the ribs. The shearing does not occur in the facesheet or backsheet or the rib plates, but across the thickness of the entire mirror structure. The simplifying assumption of a continuum structure would not be a problem for studying lightweight mirror characteristics under no loading or under uniformly distributed loads as was studied in the original papers (Ref.[37] and [39]). However, the boundary conditions of a lightweight mirror supported by discrete point forces poses a problem because local effects are very important. Especially around support points, the structure of the mirror itself shears and the thin facesheet must carry not only its own weight but also the weight of the ribs.

For the purpose of this thesis, the analytical models helped to verify the shape of the deflection characteristics, but not the exact deflection. No apparent problems can be found in the finite element analysis, and the discrepancy between analytical models and finite element model emphasizes the importance of performing finite element analysis for this type of problems. The inaccuracy of the analytical model due to the effects described above may be

checked by modeling several finite element lightweight mirrors with increasingly small cells, thus making the localized area effects and compression effects less prominent.

In summary, the lightweight mirror modeling method for this study appears to be an accurate representation of a real lightweight mirror. Deflection characteristics show good correlation with analytical results, and the discrepancies between their exact deflection solutions can be explained by several factors, each pointing in favor of the finite element results.

Chapter 3: Adaptive Material Modeling

This chapter describes the adaptive material modeling method. Section 3.1 details the problems which need to be addressed in adaptive material modeling and how actuator element properties can be modeled to simulate piezoelectric behavior. Section 3.2 presents a methodology for modeling an adaptive structure using finite elements. Two approaches are then demonstrated for an adaptive beam and compared to analytical solutions. The better approach is selected for modeling adaptive mirrors.

3.1 Problem Statements and Assumptions

COSMOS/M finite element program cannot directly model electromechanical behavior, therefore, a different method is necessary. A popular way is to relate the in-plane piezo-actuation strain as an equivalent thermal strain, leaving the normal strain unmodeled. Before this method is discussed further, a thorough understanding of the actuator behavior would be helpful.

Piezoelectric ceramics are electromechanical in nature, straining in the presence of an electric field, and conversely producing a charge when they are stressed. This effect is fundamentally nonlinear (Ref.[31]). However, when the piezoelectric ceramic is operated at low voltage levels, its behavior can be modeled as essentially linear. In addition, since the nonlinearity is strain dependent, a piezoceramic which is bonded to or embedded in a structure would strain less and, therefore, exhibit less nonlinearity. Therefore, the linear model will be the standing assumption throughout this analysis. Thus, fundamental constitutive relations for a piezoelectric can be described as,

$$\begin{bmatrix} D \\ S \end{bmatrix} = \begin{bmatrix} e^T & d \\ d_t & s^E \end{bmatrix} \begin{bmatrix} E \\ T \end{bmatrix} \tag{3-1}$$

where (Ref.[5] and [23])

$$D=\begin{bmatrix} D_1 \\ D_2 \\ D_3 \end{bmatrix} \quad E=\begin{bmatrix} E_1 \\ E_2 \\ E_3 \end{bmatrix} \quad S=\begin{bmatrix} S_{11} \\ S_{22} \\ S_{33} \\ 2S_{23} \\ 2S_{13} \\ 2S_{12} \end{bmatrix}=\begin{bmatrix} S_1 \\ S_2 \\ S_3 \\ S_4 \\ S_5 \\ S_6 \end{bmatrix} \quad T=\begin{bmatrix} T_{11} \\ T_{22} \\ T_{33} \\ T_{23} \\ T_{13} \\ T_{12} \end{bmatrix}=\begin{bmatrix} T_1 \\ T_2 \\ T_3 \\ T_4 \\ T_5 \\ T_6 \end{bmatrix} \tag{3-2}$$

D vector of electrical displacements (charge/area)

S vector of material strains

E vector of electrical field in the material (V/m)

T vector of material stress (force/area)

Direction "3" is associated with the direction of piezoelectric poling as depicted in the following figure, and the engineering notation is assumed for the variable indices.

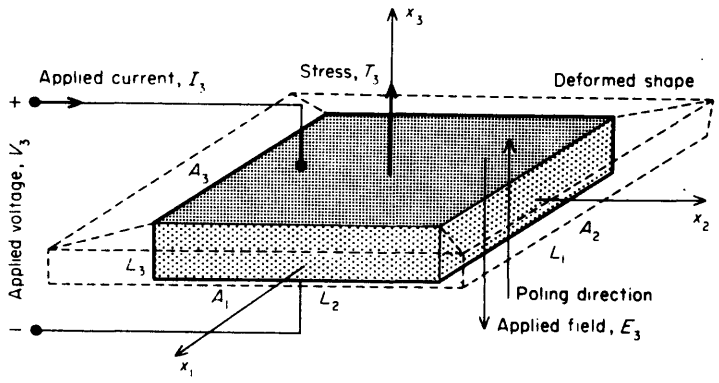

Figure 3-1 Piezoelectric Action from Applied Voltage (Ref.[23])

The material is approximately isotropic in the planar direction. Therefore, material properties are identical in the "1" and "2" directions, and other material constants may be described as follows for poled ferroelectric ceramics (Ref.[36]).

$$e^T = \begin{bmatrix} e_1^T & 0 & 0 \\ 0 & e_1^T & 0 \\ 0 & 0 & e_3^T \end{bmatrix} \qquad s^E = \begin{bmatrix} s_{11}^E & s_{12}^E & s_{13}^E & 0 & 0 & 0 \\ s_{12}^E & s_{11}^E & s_{13}^E & 0 & 0 & 0 \\ s_{13}^E & s_{13}^E & s_{33}^E & 0 & 0 & 0 \\ 0 & 0 & 0 & s_{55}^E & 0 & 0 \\ 0 & 0 & 0 & 0 & s_{55}^E & 0 \\ 0 & 0 & 0 & 0 & 0 & s_{66}^E \end{bmatrix} \qquad (3\text{-}3)$$

$$d = \begin{bmatrix} 0 & 0 & 0 & 0 & d_{15} & 0 \\ 0 & 0 & 0 & d_{15} & 0 & 0 \\ d_{31} & d_{31} & d_{33} & 0 & 0 & 0 \end{bmatrix}$$

e^T is the dielectric constant measured under constant stress, and it relates the electrical displacement with the electrical field. s^E is the elastic compliance constant measured at constant electrical field (shorted electrodes E=0) and it relates the stress and strain of the material. d is the matrix of piezoelectric constants and d_t is its matrix transpose, and they relate the interchangeable mechanical and electrical properties of the piezoelectric. From Eq.(3-1), it can be seen that the piezoelectric constants d relate the strain S to applied field E where d_{31} refers to the strain developed in the "1" direction in response to an applied field in the poling direction "3". In this way, when a piezoelectric ceramic is mounted onto the backsheet of a mirror, its in-plane strain in the "1" direction can cause deformations in the mirror. Specifically, by straining, it can induce stress in the mirror structure, causing an effective moment about the midline of the mirror. As mentioned in Chapter 1, the lightweight mirror provides quite a large moment arm for pronounced actuation effect.

By convention, the piezoelectric charge constant in the poling direction d_{33} is positive and in the planar direction d_{31} negative, since the piezoceramic expands in the poling direction and contracts in the planar direction when an electric field is applied in the poling direction.

Since piezoelectric strain can be described linearly, it can be related to thermal strain, which COSMOS/M does have the capability to model and analyze.

$$S_{piezo} = S_{thermal} \tag{3-4}$$

Taking the strain in the planar direction and ignoring any strain in the normal or poling direction, a relationship between the piezoelectric constant and a thermal expansion coefficient can be found.

$$S_{piezo} = d_{31}E_3 \tag{3-5}$$

$$d_{31}E_3 = \alpha_1 \Delta T \tag{3-6}$$

Then, describing the electric field by

$$E_3 = \frac{V}{t_a} \tag{3-7}$$

where V is the voltage applied across the actuator and t_a is the thickness of the actuator, an equivalent coefficient of thermal expansion (CTE) in the planar direction can be found,

$$\alpha_1 = \frac{d_{31}\, V}{t_a \Delta T} \tag{3-8}$$

where the relationship between V and ΔT can be chosen arbitrarily.

Many non-idealities in the piezoelectric behavior cannot be easily modeled and are either ignored or avoided in this analysis. As illustrated in Figure 3-2, d_{31} is temperature dependent, where an applied voltage is not as effective at a lower operation temperature. This

would not be a problem if an unlimited amount of voltage could be applied to the actuator. In reality, however, a strong electric field can depolarize the piezoelectric element, destroying any predictable actuation effects. This depoling field, also known as the material coercive field, is published material property, and the typical operating limit is between 500V/mm and 1000V/mm (or 12.7V/mil and 25.4 V/mil) for AC applications. To avoid any problems associated with depolarization, maximum applied voltage will be limited to 85% of the material's coercive field.

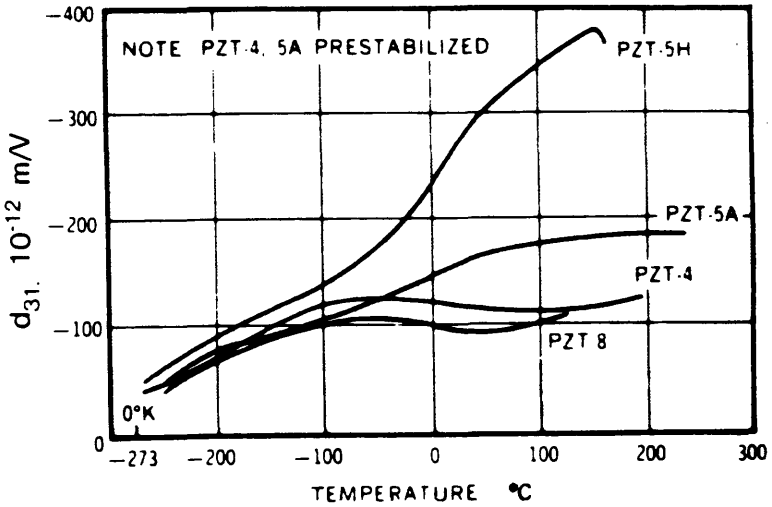

Figure 3-2 d_{31} vs. Temperature

Limiting the applied voltage serves to limit other inaccuracies as well. As mentioned before, piezoelectric behavior becomes more non-linear with increased actuation. Another factor which enters into inaccuracies of modeling piezoceramics as linear elements is that these actuators actually exhibit considerable hysteresis when strained cyclically at low frequencies (Ref.[32]). All these reasons give support to limiting the operating voltage.

3.2 Approach and Modeling Verification

Given an equivalent CTE, the piezoelectric element can be modeled on COSMOS/M. In general, this can be done by either creating a composite plate with layers to represent mirror

and piezo-materials, or creating separate plates for each material and attaching them with rigid bars. Either way, verification of its accuracy is needed. The beam is chosen for modeling verification because of its simplicity. The goal of this analysis is to verify that piezoelectric properties are adequately modeled by the equivalent thermal coefficient. Comparing the accuracy of finite element solutions to analytical solutions for piezoelectric effects on a plate is left for future studies.

3.2.1 Analytical Solution

Several analytical models are available for solving the deflection of a beam due to actuator deformations (Ref.[16], [17], and [24]). The Uniform Strain model (Figure 3-3) is only applicable to surface bonded actuators since it assumes a uniform extensional strain throughout the thickness of the actuator. Bernoulli-Euler bending model, on the other hand, can be applied to both bonded and embedded actuators as both extension and bending are accounted for in the actuator. Shear lag may be incorporated in either model to account for adhesive properties. Based on comparison with detailed finite element models and experiments, Crawley and Anderson (Ref.[17]) found that the Bernoulli-Euler bending model was more accurate for predicting extensional and bending deformations. The Uniform Strain with Perfect Bond Model developed by Crawley and de Luis (Ref.[16]) was found to be accurate in describing the actuator-induced stretch, but not as accurate in describing induced bending for thin structures.

For the purpose of verifying that piezoceramics can be modeled with an equivalent coefficient of thermal expansion as described above, a structure with a small piezo to beam thickness is used. Using an actuator which is thin enough relative to the beam so that its actuation strain can be essentially described uniformly justifies the use of the Uniform Strain model for providing adequate accuracy for this study. The comparison analysis assumes that the bond between the actuator and beam is perfect.

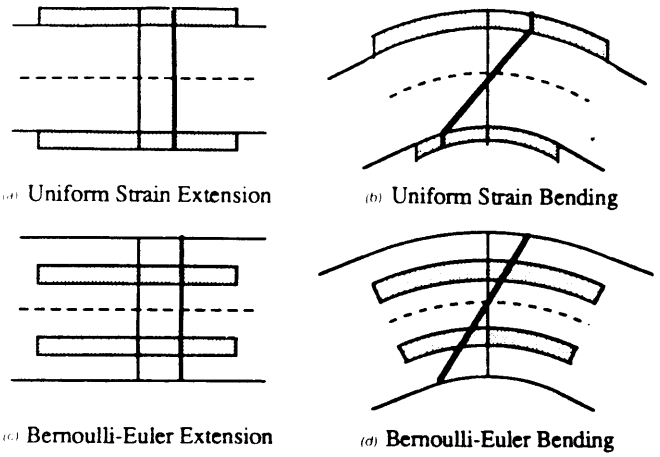

Figure 3-3 Induced Strain Distributions in Analytical Beam Models(Ref.[17])

Consider a beam which is clamped at one end and free at the other, with piezoelectric ceramics attached on both the top and bottom surfaces near the root of the clamped end. See Figure 3-4 for the nomenclature used in this derivation and Figure 3-5 for definitions of the forces developed in this problem. Since only the in-plane piezo-actuation strain is considered, appropriate substitution of the equivalent thermal strain from Eq.(3-8) arrives at a piezoelectric constitutive relationship of,

$$\sigma_a = E_a\left(\varepsilon_a - \frac{d_{31}V}{t_a}\right) \tag{3-9}$$

The uniform strain model assumes that when actuation strain is commanded in the actuators, a shear force is applied to the beam along the actuator-substructure interface; and for perfectly bonded actuator, the shear is concentrated in an infinitesimal zone near the edge of the actuator. Thus, compatibility of the actuator and substructure can be assumed (Ref.[17]), and the strain in the actuator can be equated to the strain at the surface of the beam structure,

$$\varepsilon_a = \varepsilon_b{}^s \tag{3-10}$$

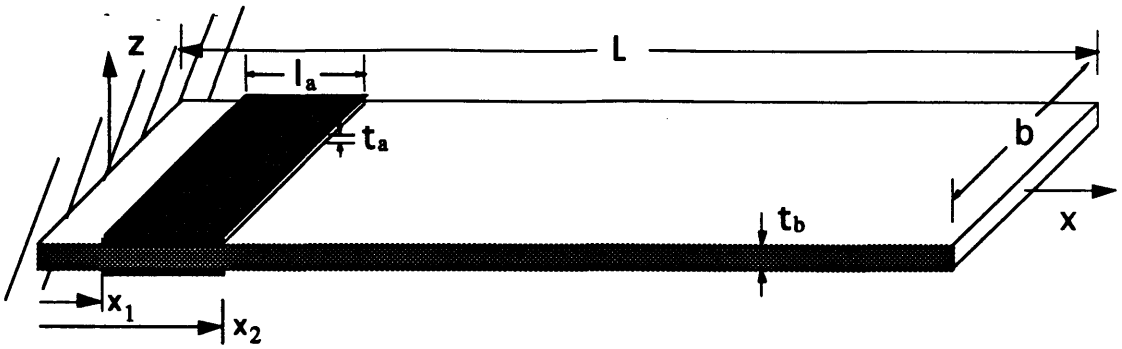

Figure 3-4 Nomenclature for Beam Model

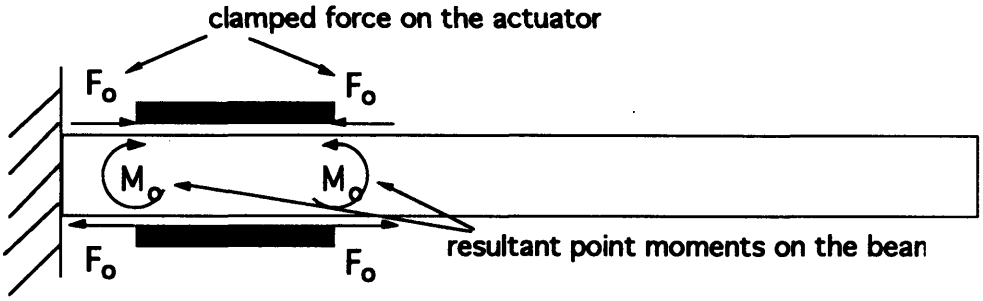

Figure 3-5 Development of Point Moments in the Beam (Ref.[24])

The strain in the actuator can be derived from Eq.(3-9), giving

$$\varepsilon_a = \frac{d_{31}V}{t_a} + \frac{\sigma_a}{E_a} \tag{3-11}$$

where σ_a can be expressed in terms of the forces described in Figure 3-5,

$$\sigma_a = \frac{F_o}{t_a b} = \frac{M_o}{t_a t_b b} \tag{3-12}$$

Similarly, the strain on the surface of the beam can be described by,

$$\varepsilon_b{}^s = -\frac{M_o t_b}{2E_b I_b} \tag{3-13}$$

Substituting Eqs.(3-11) through (3-12) to solve Eq.(3-10), an expression for M_o can be found,

$$M_o = \frac{-2E_bI_bE_abt_at_b}{2E_bI_b + E_abt_at_b^2}\frac{d_{31}V}{t_a} \tag{3-14}$$

The point moment induced in the beam at one end of the actuator creates a tip deflection of,

$$w_{t1} = \frac{M_o}{2E_bI_b}(L - x_1)^2 \tag{3-15}$$

while the other end creates an opposing moment of,

$$w_{t2} = -\frac{M_o}{2E_bI_b}(L - x_2)^2 \tag{3-16}$$

These point moments combine to produce a tip deflection,

$$w_t = \frac{M_o}{2E_bI_b}[(L - x_1)^2 - (L - x_2)^2] \tag{3-17}$$

which can be compared with finite element results.

3.2.2 Analytical and Finite Element Beam Solution Comparison

Equation (3-17) is used to obtain the tip deflection of a rectangular beam with the following characteristics. PZT-5A is chosen arbitrarily for this study and the relevant properties are given below.

ALUMINUM BEAM	PZT-5A ACTUATOR
E_b = 6.89e10 N/m^2	E_a = 6.9e10 N/m^2
t_b = 0.002083 m	t_a = 0.000254 m
I_b = 3.108e-11 m^4	d_{31} = -1.66e-10 m/V

STRUCTURAL DIMENSIONS

$b = 0.0413$ m

$L = 0.35$ m

$l_a = 0.0635$ m

$x_1 = 0.0087$ m

The same beam is modeled on COSMOS/M by both the composite layer method and the rigid bar method. The equivalent CTE is simply modeled into the representative piezoceramics elements with a one-to-one relationship between V and ΔT. Then, five units of temperature "force" was applied to the finite element nodes to represent five units of applied voltage. Static deflection analysis is shown in Figures 3-6 and 3-7.

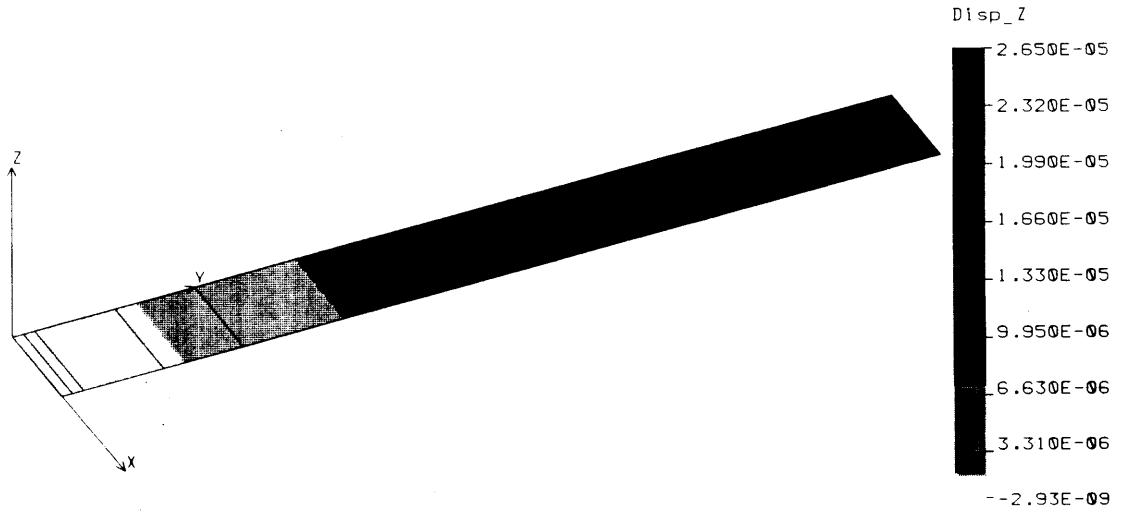

Figure 3-6 Beam Deflection Solution for Model with Composite Elements

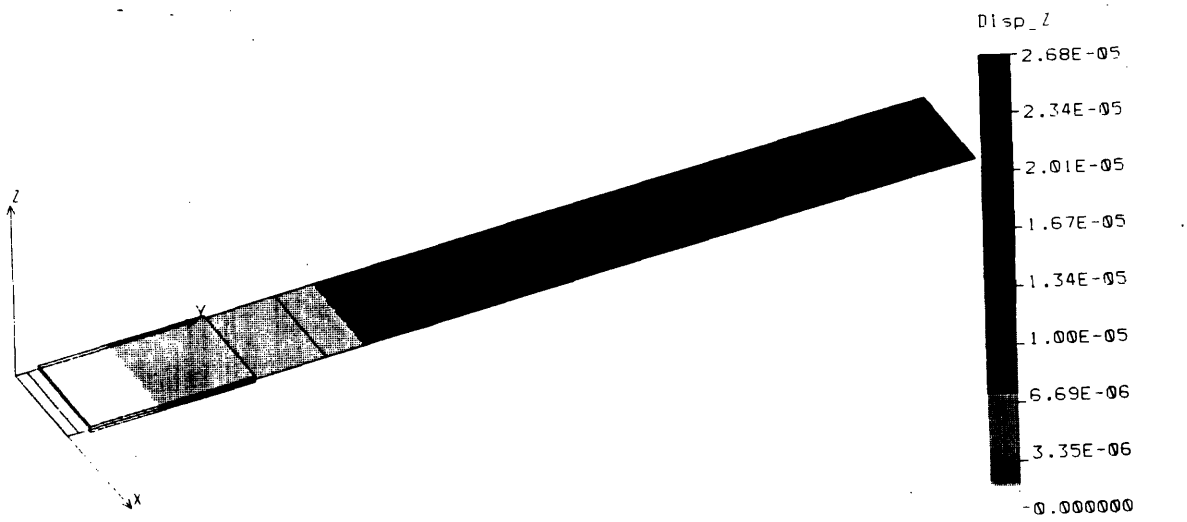

Figure 3-7 Beam Deflection Solution for Model with Rigid Bar Elements

Tip deflection varies linearly with applied voltage. Plotting this relationship, comparison between the analytical solutions and finite element solutions can be seen below in Figure 3-8.

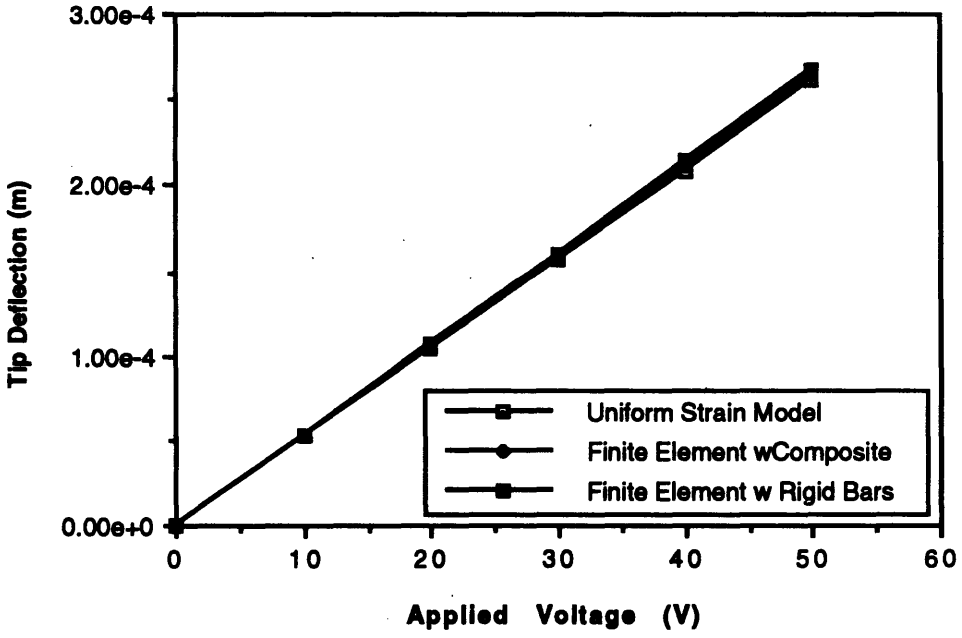

Figure 3-8 Tip Deflection of Actuated Beam

Notice that either finite element modeling method gives results within 3% of analytical results. The composite layer method is easier to model and is therefore chosen as the method for modeling adaptive lightweight mirrors in the next chapters.

On the lightweight mirrors, piezoceramic elements can be modeled in a composite layer with mirror elements (Figure 3-9). Therefore, each backsheet element may have its own discrete piezoceramic, which makes discrete placement studies possible. Piezo elements are modeled with orthotropic properties, where the equivalent coefficient of thermal expansion is identical in both the "1" and "2" directions.

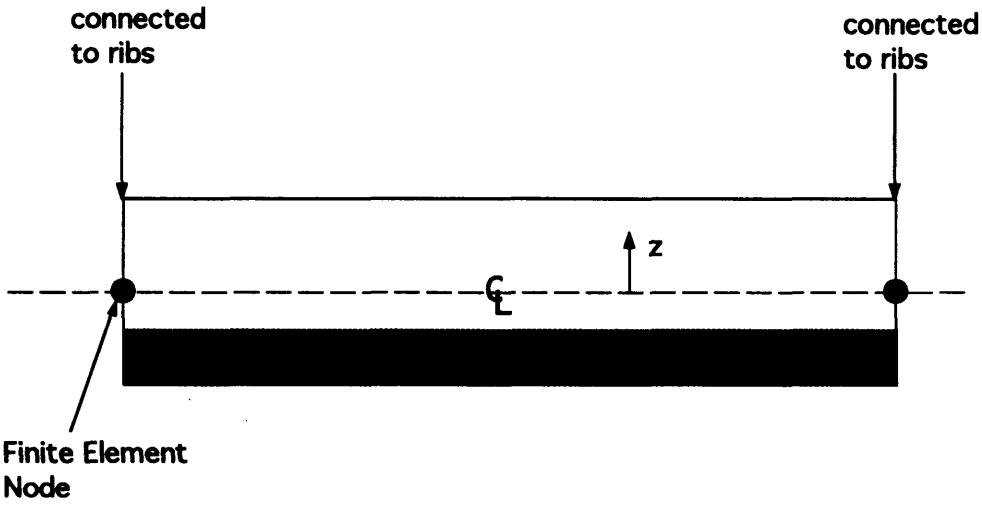

Figure 3-9 Typical Backsheet Element

Chapter 4: Lightweight Mirror Case Study

This chapter presents the self-weight deflection and thermal deflection of a lightweight mirror designed to meet infrared applications. Section 4.1 details the process by which an "optimal" lightweight mirror design was developed to meet specific requirements. Section 4.2 presents mirror deflection characteristics. Section 4.3 discusses the process of choosing the appropriate actuator and its dimensions. Then, in Section 4.4, piezoelectric ceramic materials are added onto the backsheet of the lightweight mirror, and deflection characteristics due to the addition of the actuators are determined.

4.1 Designing a Lightweight Mirror

Several issues must be addressed when designing a lightweight mirror. Cell wall thickness, core cell structure, and quilting or print-through during mirror polishing are all important parameters and issues. For a given application, a mirror design is determined by several requirements including the following:

(1) Maximum Self-Weight Deflection: This requirement is usually set by testing engineers who determine how accurately ground tests reflect actual performance of mirrors in operations. This is especially crucial for space mirrors since mirrors will not be operating under earth's gravity.

(2) Minimum Resonant Frequency: This requirement is usually set by the structures and controls engineers who determine the kind of disturbances which the mirror is likely to encounter and the mirror's response to such disturbances. This natural frequency requirement is usually set at some arbitrarily high value so that the mirror would not resonate due to any expected disturbances.

(3) Mass:. The maximum allocated mass is determined by the payload engineers and is dependent upon the telescope or satellite requirements and structure.

(4) Surface Figure Error: This requirement sets the maximum allowable errors due to fabrication or polishing. Since facesheets are thin, the pressure applied for polishing the mirror may indent areas which are not directly supported by ribs. This is called quilting deflection because "dimples" appear on the mirror surface. Performance criteria for quilting deflection generally requires it to be less than one-tenth of a wavelength at the frequency of interest (Ref.[45]), and for very sensitive systems this is set at one-twentieth of a wavelength (Ref.[34]).

Typically, lightweight mirror designing begins with varying parameters to satisfy the quilting deflection requirement. This sets the cell width and facesheet thickness of the mirror. Then, the mirror thickness, or rib height, and the support locations are varied to meet the self-weight deflection and frequency requirements. Throughout the process, the mass of the mirror must be kept within requirements. This design process is detailed below.

For the purpose of this thesis, requirements for a one-meter diameter fused silica mirror are defined. The mirror is assumed to satisfy a mid-wave infrared wavelength, usually from 4.4μm to 5μm, and therefore, requires cryogenic temperatures for operation (Ref.[27]). Design criteria are assumed to be:

Maximum Self-Weight Deflection = 1μm

Natural Frequency = 400 Hz

Maximum Mass = 30 kg

Maximum Quilting Deflection = $\frac{\lambda}{20}$ = 0.22μm

Operating Temperature = 200K

Assuming a typical polishing pressure of 0.3 psi or 2069.254 N/m^2 (Ref.[52]) and using the physical properties for fused silica (Table 4-1), mirror parameters to meet quilting deflection can be found.

Table 4-1 Fused Silica Material Properties

Modulus E	10.6e6 psi or 7.308e10 Pa
Poisson's Ratio ν	0.17
Density ρ	0.0796 lb/ in3 or 2203.32 kg/ m3
Thermal Expansion Coefficient α	5.6e-7 /K

By focusing on each cell surface, the quilting deflection can be derived from the solution for the maximum deflection at the center of a uniformly loaded plate with clamped edges. This is a reasonable method because each cell is supported on all sides by ribs which keep the deflection and slope zero at these boundary edges. Ref.[51] p. 202 gives the deflection solution for a square plate:

$$w_{max} = 0.00126 \frac{qa^4}{D} \tag{4-1}$$

Adapting this to lightweight mirror variables gives:

$$\delta_q = \Psi \frac{PB^4}{D} \tag{4-2}$$

where δ_q quilting deflection

Ψ deflection coefficient determined by cell configuration

P polishing pressure

B cell width or inscribed circle diameter

$D = \frac{Et_f^3}{12(1-\nu^2)}$ flexural rigidity of facesheet

and t_f facesheet thickness

ν Poisson's ratio

Ref.[8] gives the deflection coefficient for square, triangular, and hexagonal cell shapes:

$$\Psi_{sq} = 0.00126 \qquad \Psi_{tri} = 0.00151 \qquad \Psi_{hex} = 0.00111$$

In this thesis, a nominal circular mirror with square cells was designed. Following the requirement that quilting deflection must be less than or equal to 2.2E-7 m,

$$\delta_q = \frac{12(1-\nu^2)\,\Psi_{sq}\,P\,B^4}{E\,t_f^3} < 2.2E\text{-}7 \text{ m} \qquad (4\text{-}3)$$

two variables are left at the designer's disposal, the cell dimension B and the facesheet thickness t_f. To meet the same deflection characteristics, thicker facesheets would allow larger cells, while thinner facesheets must be supported by smaller cells. Figure 4-1 presents facesheet dimensions with the corresponding cell dimension as calculated from Eq.(4-3).

From this set, an "optimal" design may be chosen. The basis for choosing an "optimal" design for a given application depends on fabrication technology, cost and manageability. For instance, current manufacturing limitations require that facesheets be greater than 3mm and ribs be no thinner than 1.5mm. The designer must also keep in mind that as the number of cells increases, fabrication costs increase; and that smaller cell size increases fabrication complexity and the risk of manufacturing errors.

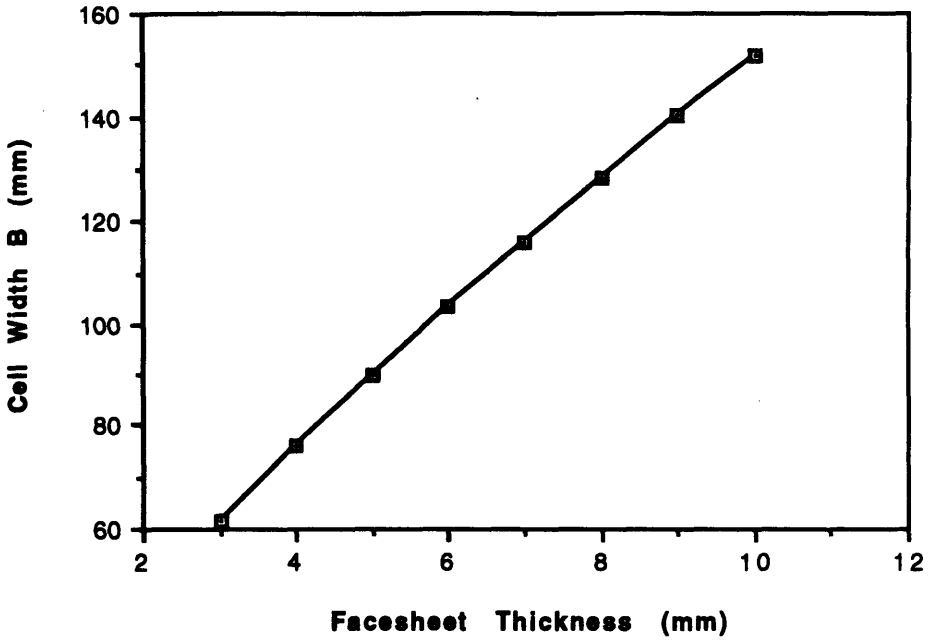

Figure 4-1 Facesheet Thickness vs. Cell Width to Meet Quilting Deflection

A finite element model was generated for each possibility with facesheet thickness between 3 mm and 8 mm on COSMOS/M. The 9 mm and 10 mm were not examined because they did not contain good choices for support locations. For comparison purposes, all mirrors were generated with the same rib height of 100 mm. Backsheet thickness is 3 mm for all designs. Then, within each design, mirror support points were varied to obtain the minimum deflection characteristic which still met the fundamental frequency requirement of 400 Hz. The following figures (Figures 4-1 through 4-6) summarize these results.

As one can see, different support locations give different maximum self-weight deflections and fundamental frequencies. From the plate study in Section 2.3.1, it was found that minimum deflection of a circular plate occurs for a support location around s = 0.7. For this reason, support locations were chosen around this area for the following studies, and their associated characteristics are illustrated. Two different designs of the 7 mm mirror are shown

because one gave clearer choices for support locations. The 8 mm facesheet mirror contained limited support location choices, and they could not be varied to meet design requirements. For this reason, the 9 mm and 10 mm facesheet mirrors were not even examined.

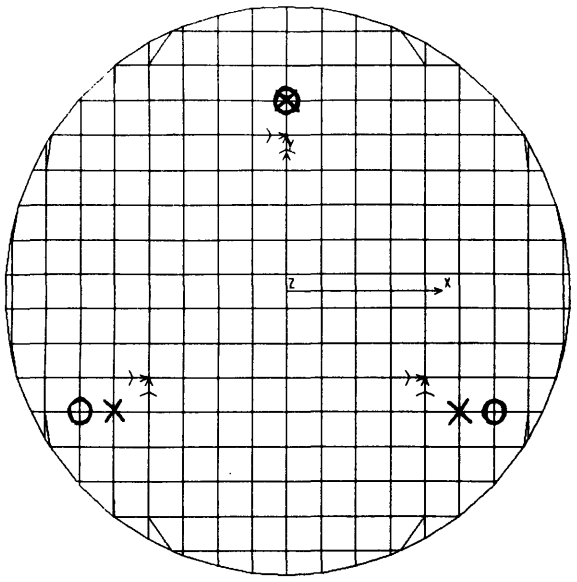

Diameter = 1 m for all mirrors

MASS = 18.89 kg

O
s = 0.72
SWD = -0.00106 mm
Freq = 454 Hz

X
s = 0.67
SWD = -0.00103 mm
Freq = 426 Hz

s = 0.56
SWD = -0.000927 mm
Freq = 420 Hz

Figure 4-1 Lightweight Mirror Characteristics for 3 mm Facesheet as a Function of Support Locations

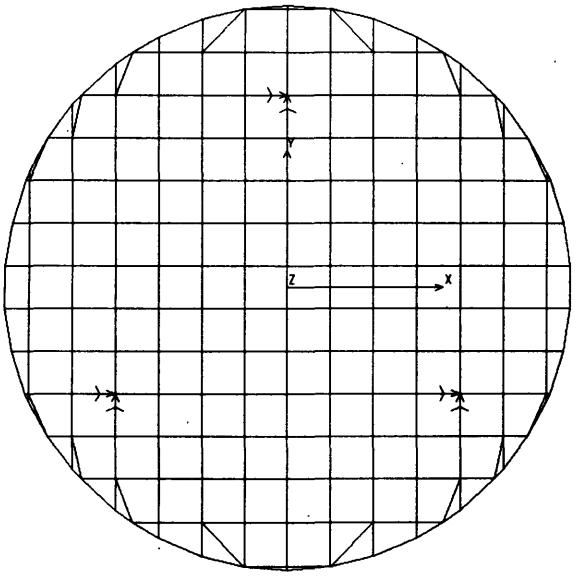

MASS = 18.92 kg

s = 0.70
SWD = -0.000946 mm
Freq = 452 Hz

Figure 4-2 Lightweight Mirror Characteristics for 4 mm Facesheet as a Function of Support Locations

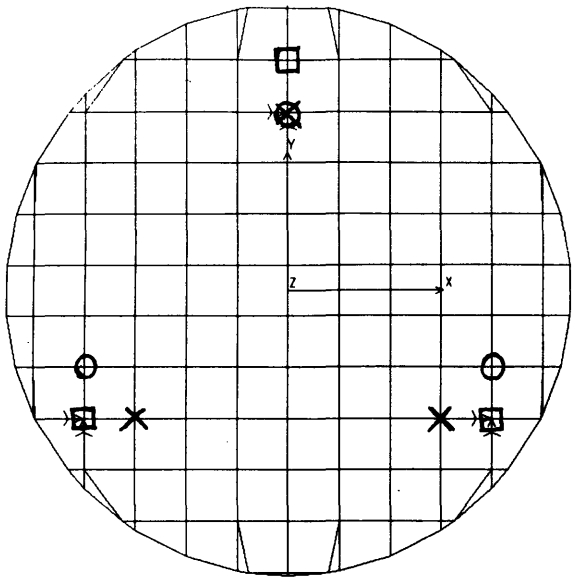

MASS = 19.54 kg

○
s = 0.68
SWD = -0.00189 mm
Freq = 370 Hz

×
s = 0.68
SWD = -0.00123 mm
Freq = 389 Hz

□
s = 0.80
SWD = -0.00123 mm
Freq = 441 Hz

s = 0.72
SWD = -0.00108 mm
Freq = 441 Hz

Figure 4-3 Lightweight Mirror Characteristics for 5 mm Facesheet as a Function of Support Locations

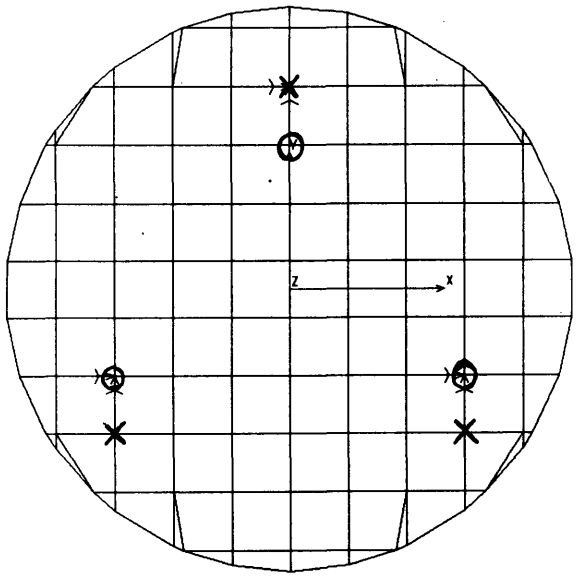

MASS = 20.50 kg

○
s = 0.60
SWD = -0.00114 mm
Freq = 376 Hz

×
s = 0.76
SWD = -0.00120 mm
Freq = 345 Hz

s = 0.70
SWD = -0.00131 mm
Freq = 419 Hz

Figure 4-4 Lightweight Mirror Characteristics for 6 mm Facesheet as a Function of Support Locations

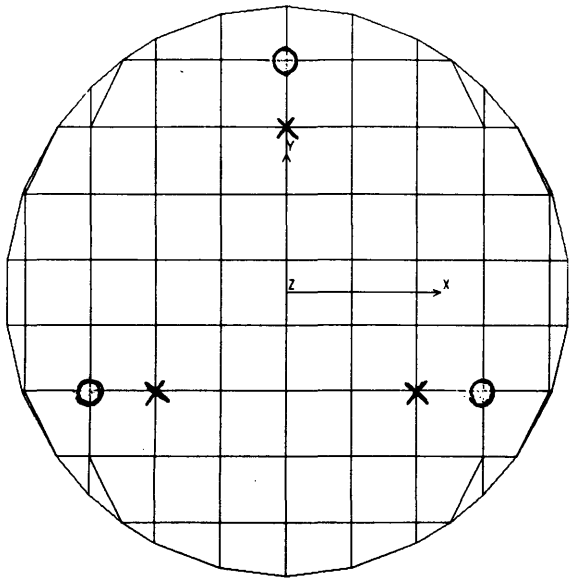

MASS = 21.65 kg

○
s = 0.81
SWD = -0.00154 mm
Freq = 407 Hz

×
s = 0.58
SWD = -0.00125 mm
Freq = 354 Hz

(a)

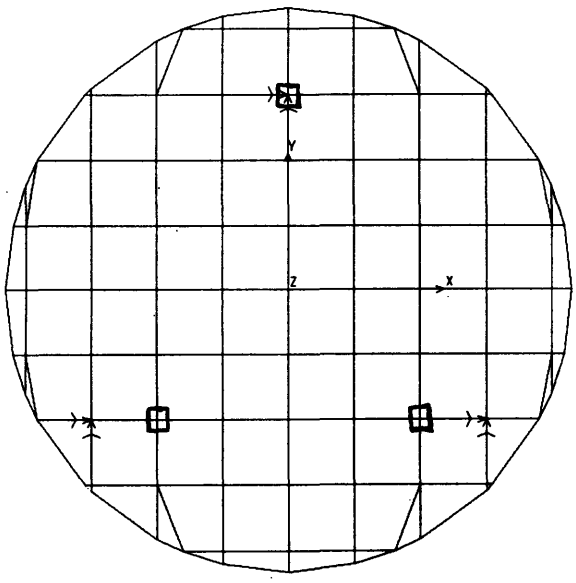

MASS = 21.71 kg

□
s = 0.67
SWD = -0.00156 mm
Freq = 326 Hz

s = 0.75
SWD = -0.00138 mm
Freq = 403 Hz

(b)

Figure 4-5 Lightweight Mirror Characteristics for 7 mm Facesheet as a Function of Support Locations

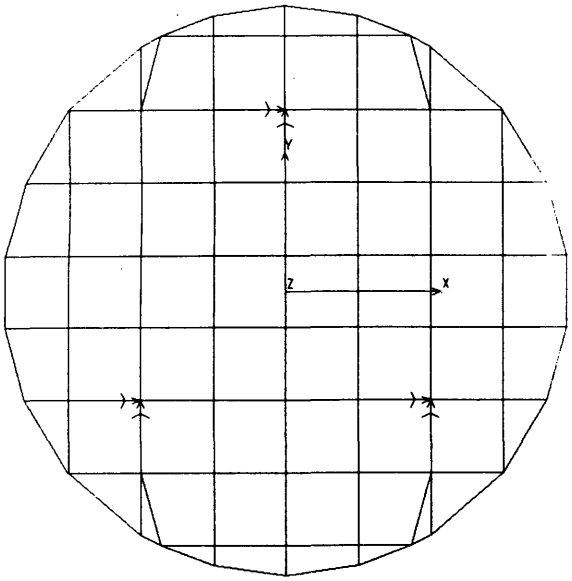

MASS = 22.82 kg

s = 0.64
SWD = -0.00140 mm
Freq = 356 Hz

Figure 4-6 Lightweight Mirror Characteristics for 8 mm Facesheet as a Function of Support Locations

Once the best deflection characteristic for each mirror which meet all requirements is obtained, trade-offs may be made to arrive at a design. Table 4-2 summarizes the choices of mirrors with the lowest maximum deflection which still meet the 400 Hz frequency requirement.

Table 4-2 Dimensions Trade-Off

Facesheet Thickness (mm)	Mirror Mass (kg)	Number of Cells	Self-Weight Deflection (mm)	Minimum Frequency (Hz)
3	18.89	238	-0.000927	420
4	18.92	162	-0.000946	452
5	19.54	116	-0.001080	441
6	20.50	94	-0.001310	419
7	21.71	76	-0.001380	403

Plotting these variables with respect to the facesheet thickness gives a better picture of their characteristics.

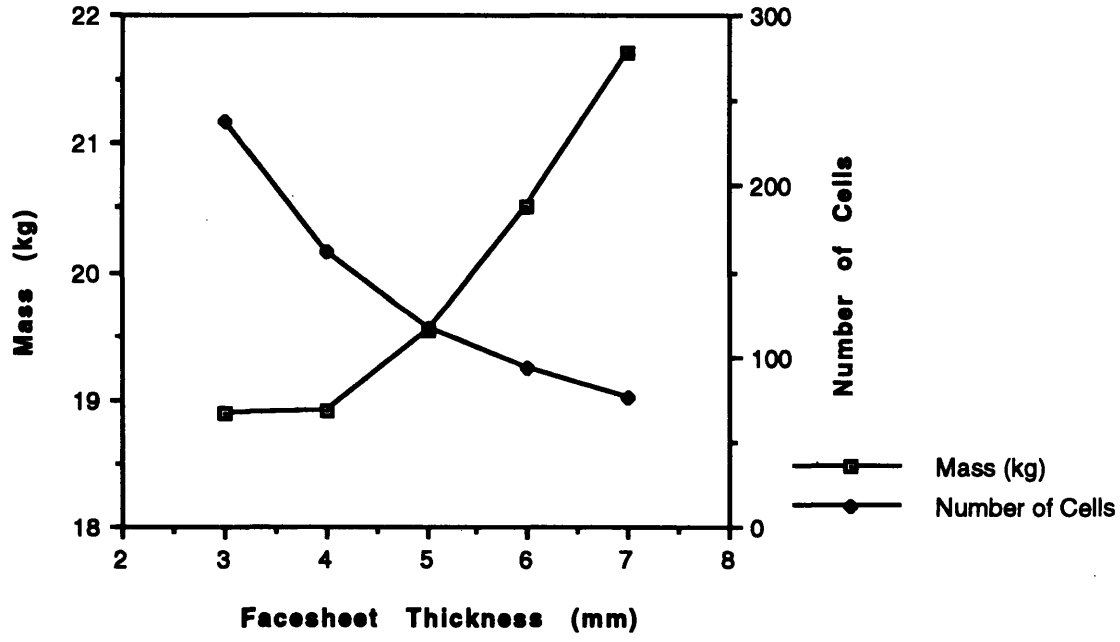

Figure 4-7 Mass and Number of Cells Trade-Off

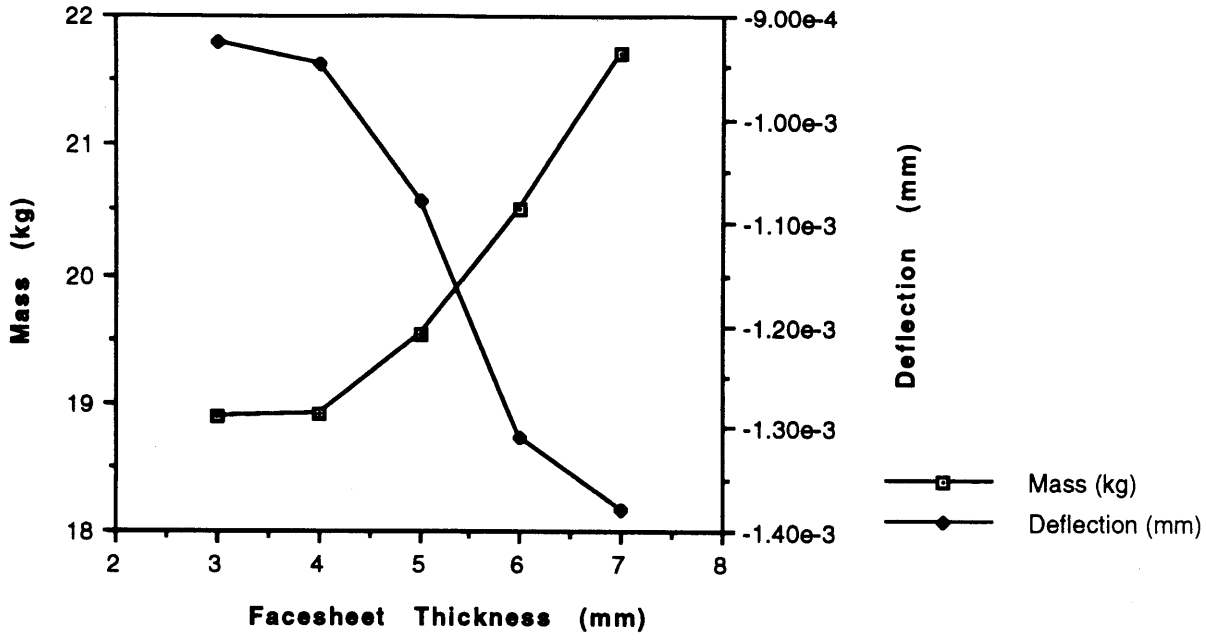

Figure 4-8 Mass and Self-Weight Deflection Trade-Off

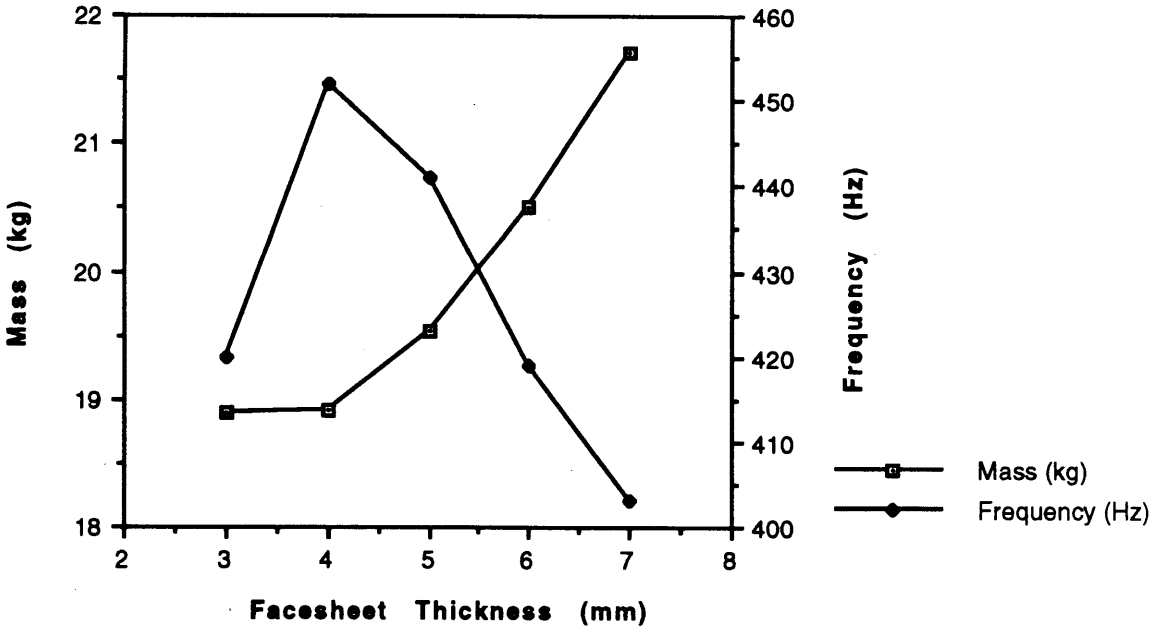

Figure 4-9 Mass and Frequency Trade-Off

From the figures, a facesheet thickness of 5 mm appears to be a good design that gives good deflection characteristics with a relatively small number of cells. Its mass is not much greater than those exhibited by the 3mm and 4mm facesheets. However, its rib height must be increased such that the maximum deflection will not exceed one micron. Finite element analysis shows that this can be done by increasing the rib height from 100 mm to 110 mm, which increases the mirror mass from 19.54 kg to 20.12 kg.

4.2 Lightweight Mirror Deflection Characteristics

The 5 mm facesheet mirror with 1.5 mm ribs and 3 mm backsheet is chosen. After increasing its rib height to 110 mm, the mirror exhibits the following characteristics, which meet all design requirements.

Maximum Self-Weight Deflection = -0.000982 mm

Fundamental Frequency = 467 Hz

Mass = 20.12 kg

Figures 4-10 through 4-15 shows the self-weight deflection and thermal deflection profiles. Since mirrors are generally made to reach equilibrium quickly, thermal deflections are obtained for a one Kelvin change throughout the entire mirror. All contour values are in millimeters.

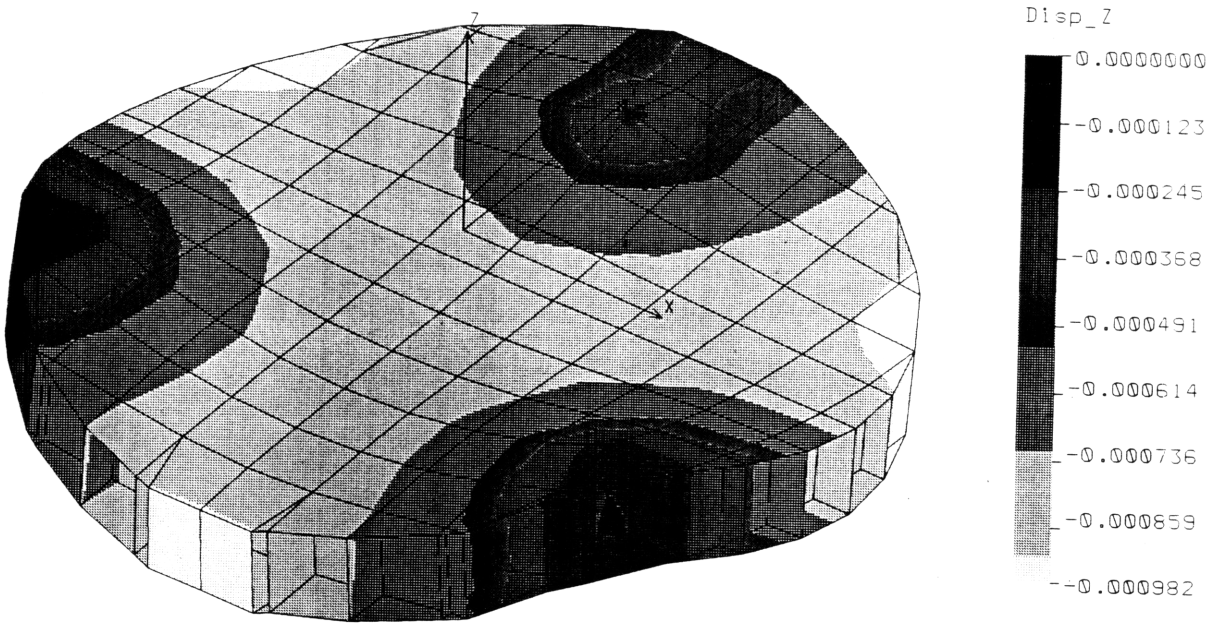

Figure 4-10 Self-Weight Deflection Profile (z displacement in mm)

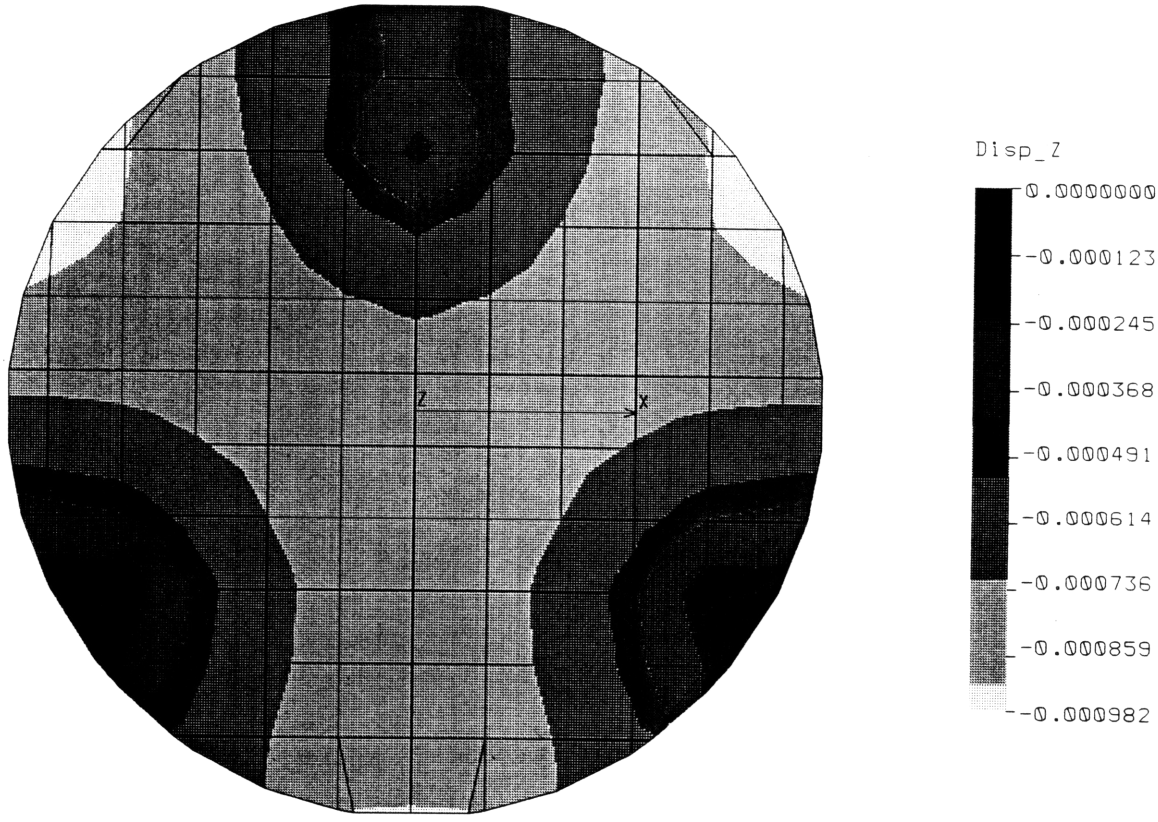

Figure 4-11 SWD Profile of the Facesheet (z displacement in mm)

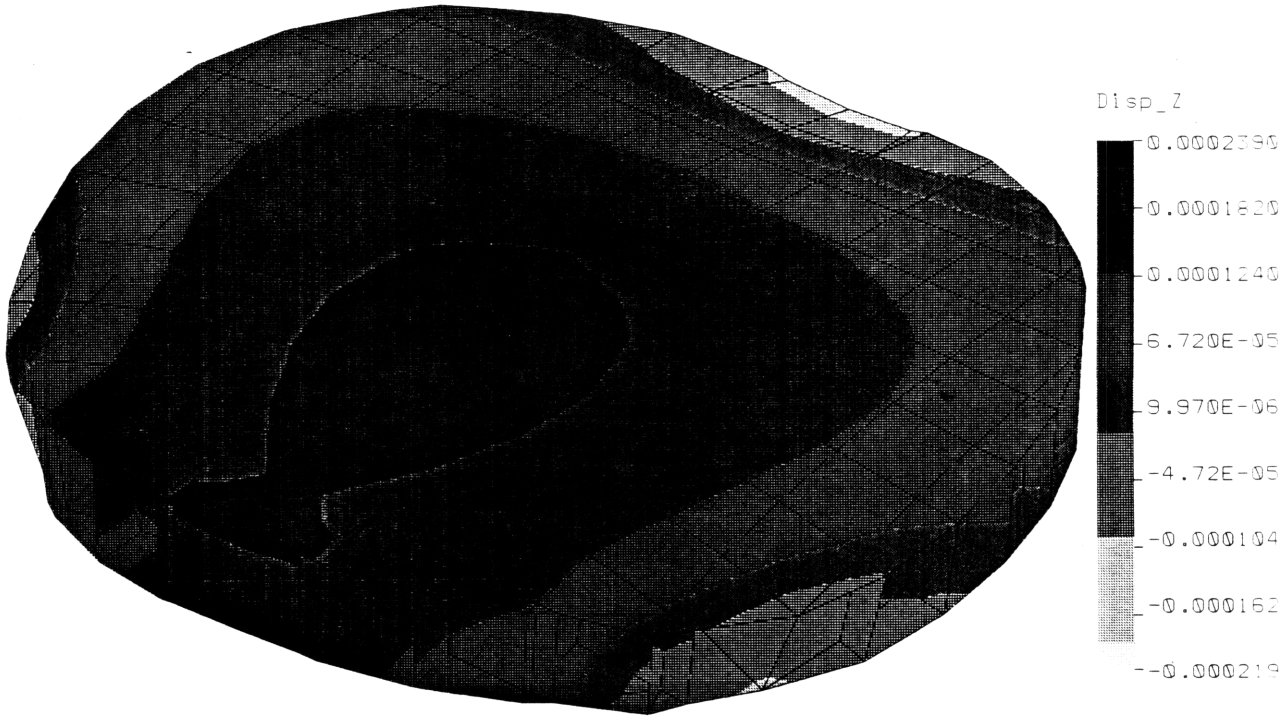

Figure 4-12 Thermal Deflection Profile (z displacement in mm)

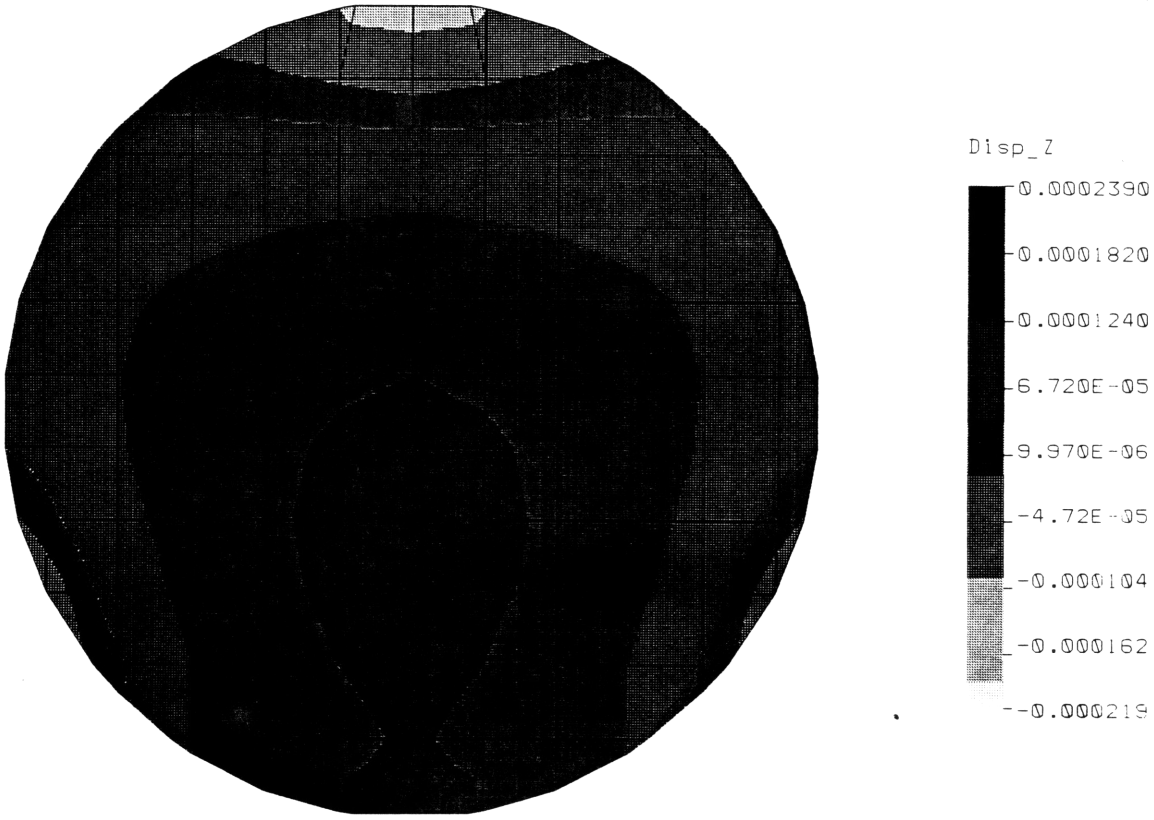

Figure 4-13 Thermal Deflection Profile of the Facesheet (z displacement in mm)

4.3 Choosing the Actuator Material and Dimensions

Piezoelectric ceramics may now be added onto the backsheet of the mirror, and a design trade-off is needed to determine the right thickness for the piezoceramic. For comparison purposes, piezoelectric ceramic elements are assumed to be attached to the entire back surface of the mirror. From this, the added mass and deflection may be found, as well as the resulting frequency of the mirror.

Several different piezoelectric materials are available for use. Table 4-3 presents material properties for some of the promising piezoceramics for this study. Vernitron PZT-5H was used in previous studies of mirrors under cryogenic temperatures (Ref.[32]) and is used for this study. Its low Curie temperature, which is the absolute maximum exposure temperature for the piezoceramic before all piezoelectric properties are lost, is normally a limiting factor for many applications, but is not a concern for this design since the lightweight mirror is expected to operate in cryogenic temperatures. However, other parameters must also be considered.

As can be seen in Table 4-3, PZT-5H possesses the highest piezoelectric charge constant d_{31}, even at cryogenic temperatures, but its modulus E is relatively low compared to PZT-4. Its limiting voltage, or coercive field, is also lower than either PZT-4 or PZT-5A. Since a piezoelectric's strength depends on all three parameters, a figure of merit may be based on the product of all three, called the maximum induced stress. Using this parameter, PZT-5H does not appear to be the best material for actuation corrections requiring large forces. However, because this material exhibits excellent sensitivity (strain per applied voltage) at low temperatures, and in space applications voltage limitations can be important, high sensitivity may be the design driver. For the feasibility study, demonstrating that lightweight mirrors can be adequately corrected with PZT-5H would demonstrate that most other piezoelectric

materials could be used for this purpose. Under this assumption, the appropriate PZT-5H material thickness can now be chosen.

Table 4-3 Piezoceramic Material Properties (Ref.[2], [4], and [36])

Properties @ 200K	Vernitron PZT-4	Vernitron PZT-5A	Vernitron PZT-5H
Modulus E (N/m^2)	9.9e10	6.9e10	7.1e10
Piezoelectric Charge Constant d_{31} (m/V) (from Figure 3-2)	-120e -12	-110e -12	-150e -12
Density ρ (kg/m^3)	7600	7700	7500
Poisson's Ratio ν	0.31	0.31	0.31
Curie Temp (K)	598	638	468
Coercive Field (V/mm)	> 1000	~700	~400
Maximum Induced Stress (Product of Max Field, Modulus, and d_{31})	-11,880	-4,830	-4,260

Trade-offs are needed for choosing the appropriate piezoceramic thickness due to mirror requirements on weight, deflection, and frequency. As discussed in Chapter 3, strain is proportional to the applied field, and the thicker the piezoceramic, the more force it can impart into the mirror. However, thicker actuators also add considerable weight to the mirror system since piezoelectric materials are very dense compared to mirror materials. This added weight would in turn affect mirror deflection and frequency characteristics. To determine the appropriate material thickness that would still meet requirements for this design, two types of

tests must be performed. One is a passive test to determine the self-weight deflection and frequency characteristics of an adaptive mirror with various piezo thicknesses. The other is an active test which analyzes the amount of actuation effect which a piezo of certain thickness has on the adaptive mirror. A trade-off could then be made to determine the most effective thickness for the piezoceramic based on actuation strength verses added weight-induced deflection.

Finite element analyses were conducted for various material thicknesses, and Table 4-4 shows results from the passive test and summarizes how piezoceramic dimensions affect mirror characteristics. The applied field limit is calculated based on 85% of the maximum coercive field of 400V/mm for PZT-5H.

Table 4-4 PZT Thickness Trade-Off

Piezoceramic Thickness (mm)	Total Mass of Mirror (kg)	Self-Weight Deflection (mm)	Fundamental Frequency (Hz)	Applied Field Limit (V)
0.1	20.71	-0.000992	458	34
0.5	23.05	-0.001080	442	170
1.0	25.98	-0.001180	423	340
1.5	28.90	-0.001290	407	510
2.0	31.83	-0.001400	391	680

This test shows that the 2mm piezoceramic can be eliminated because it pushes over the weight limit of 30kg and does not meet frequency requirement. The 0.1 mm piezoceramic is also eliminated because preliminary studies show that it would be unable to provide the actuation needed to correct mirror deflections. Therefore, only the 0.5mm, 1mm, and 1.5mm

piezoceramics are examined further to see whether the advantages afforded by more actuation capabilities of a thicker piezoceramic outweigh the added deflection due to its presence. Keeping a one-to-one ratio between T and ΔV, their effective thermal expansion coefficients are, respectively: -3e-7mm/mmV, -1.5e-7mm/mmV, and -1e-7mm/mmV as calculated from Eq.(3-8). These properties were modeled into the COSMOS/M finite element system, and actuation profiles were obtained for a one volt actuation of a piezoceramic located in the middle of the mirror. The process was accomplished by only modeling the equivalent thermal expansion property into the specified piezo element. All other piezo elements contain only stiffness characteristics, and are not allowed to induce expansions or contractions to the mirror. Figures 4-16 through 4-18 show the actuation profiles of displacements in the z direction. All dimensions are in millimeters.

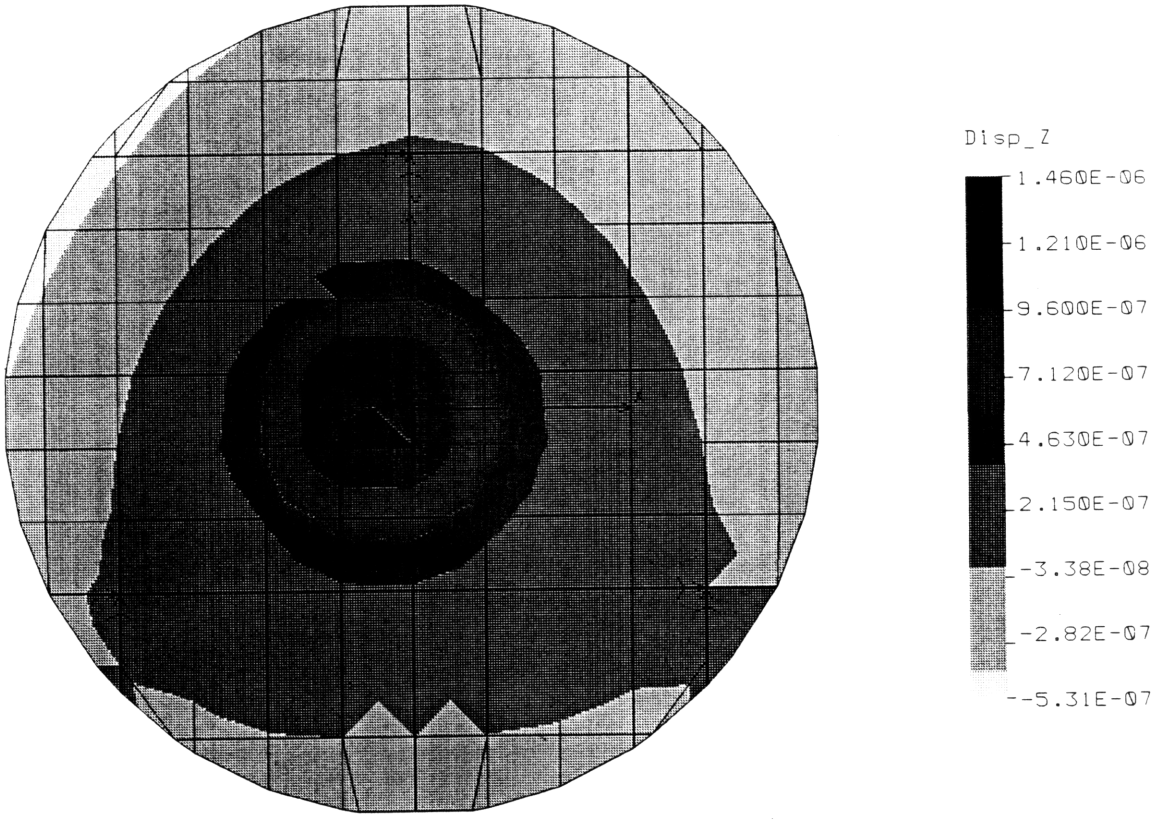

Figure 4-14 Actuation Profile for 0.5 mm Piezoceramic Layer

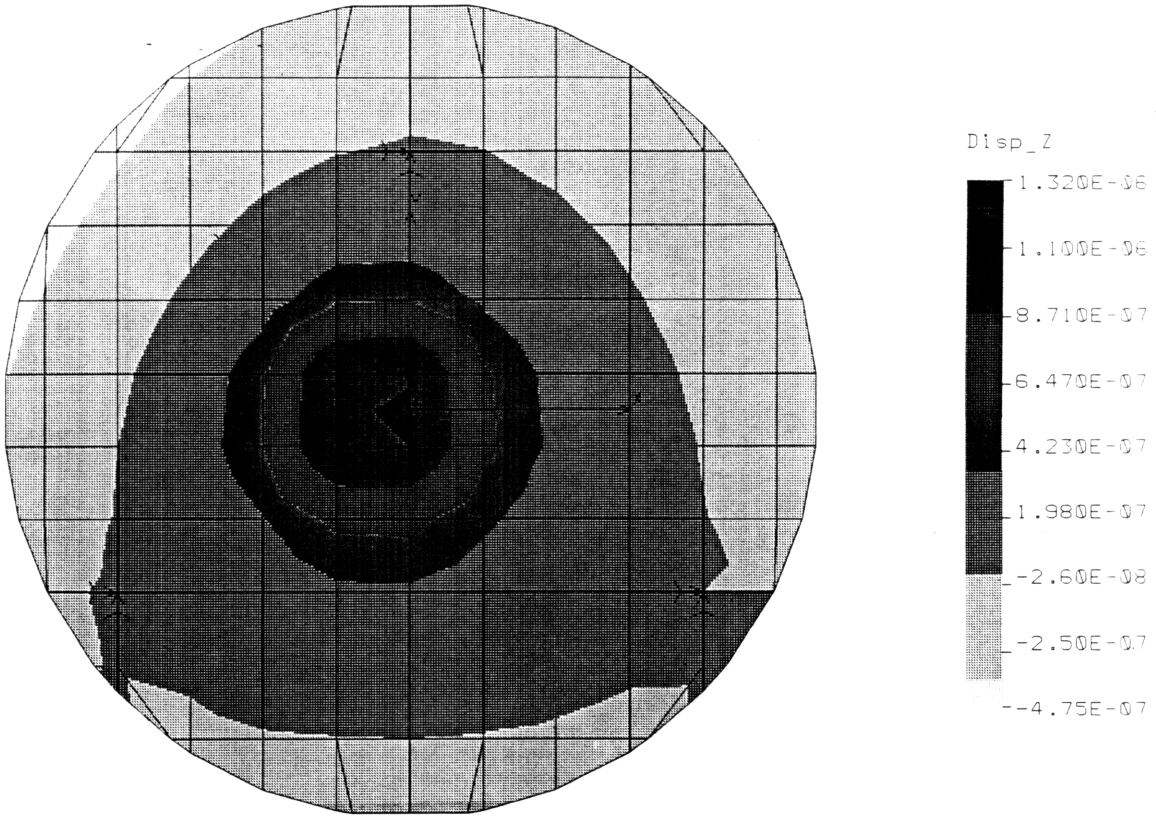

Figure 4-15 Actuation Profile for 1.0 mm Piezoceramic Layer

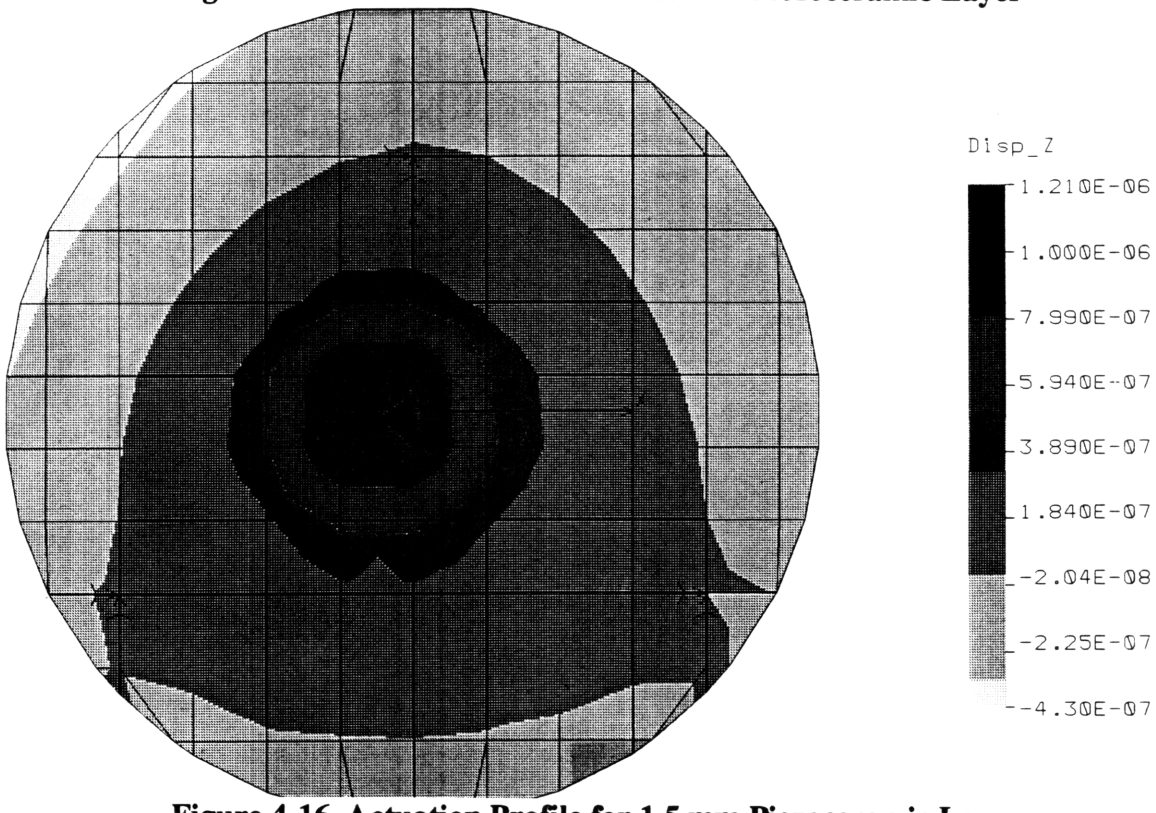

Figure 4-16 Actuation Profile for 1.5 mm Piezoceramic Layer

From these two analyses, it can be seen that the thicker 1.5mm piezoceramic layer provides actuation profile characteristics on the same order as the 0.5mm and 1.0mm layers. The added deflection to the mirror due to the increased weight is also on the same order of magnitude. Assuming a linear actuation increase of deflection due to an applied field, the higher voltage limit of the 1.5mm piezo implies that it would be able to provide more deflection correction. Based on this observation, the 1.5 mm layer is chosen.

4.4 Adaptive Lightweight Mirror Deflection Characteristics

With the 1.5 mm PZT-5H piezoelectric layer built onto the lightweight mirror model, the effects of the additional weight and stiffness must be examined. Once again, the thermal deflection profile is for a one Kelvin change throughout the mirror. Due to lack of published data for piezoceramic thermal properties at cryogenic temperatures, the coefficient of thermal expansion at zero degree Celsius was used, α = 1e-6 /K.

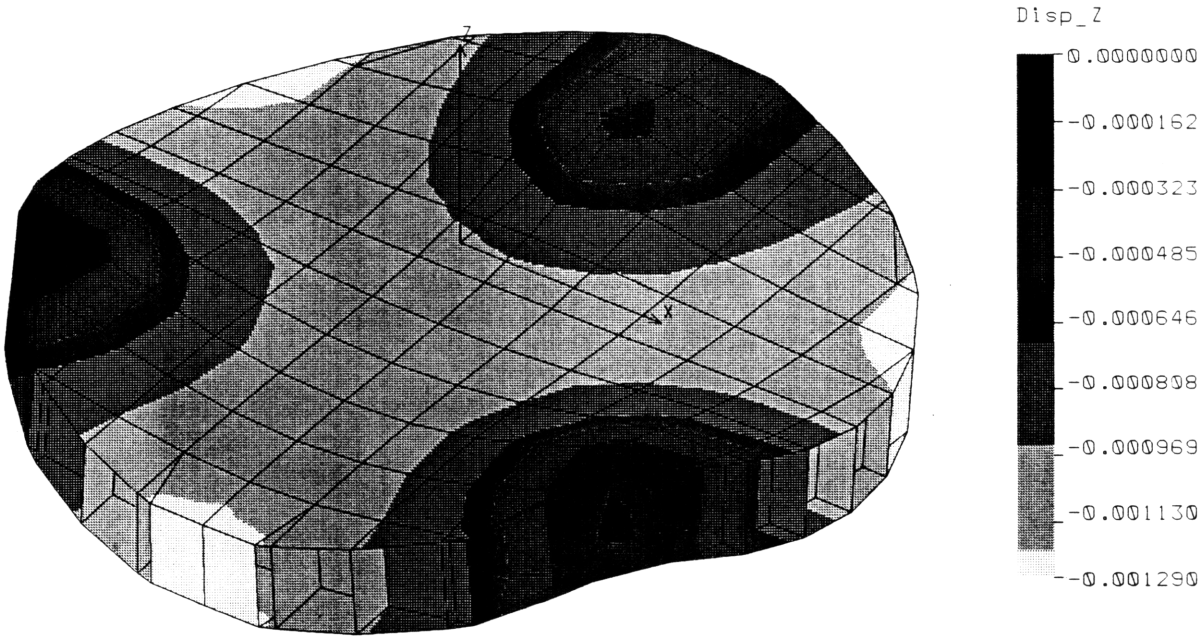

Figure 4-17 Self-Weight Deflection Profile with 1.5 mm Piezoceramic Layer (z displacement in mm)

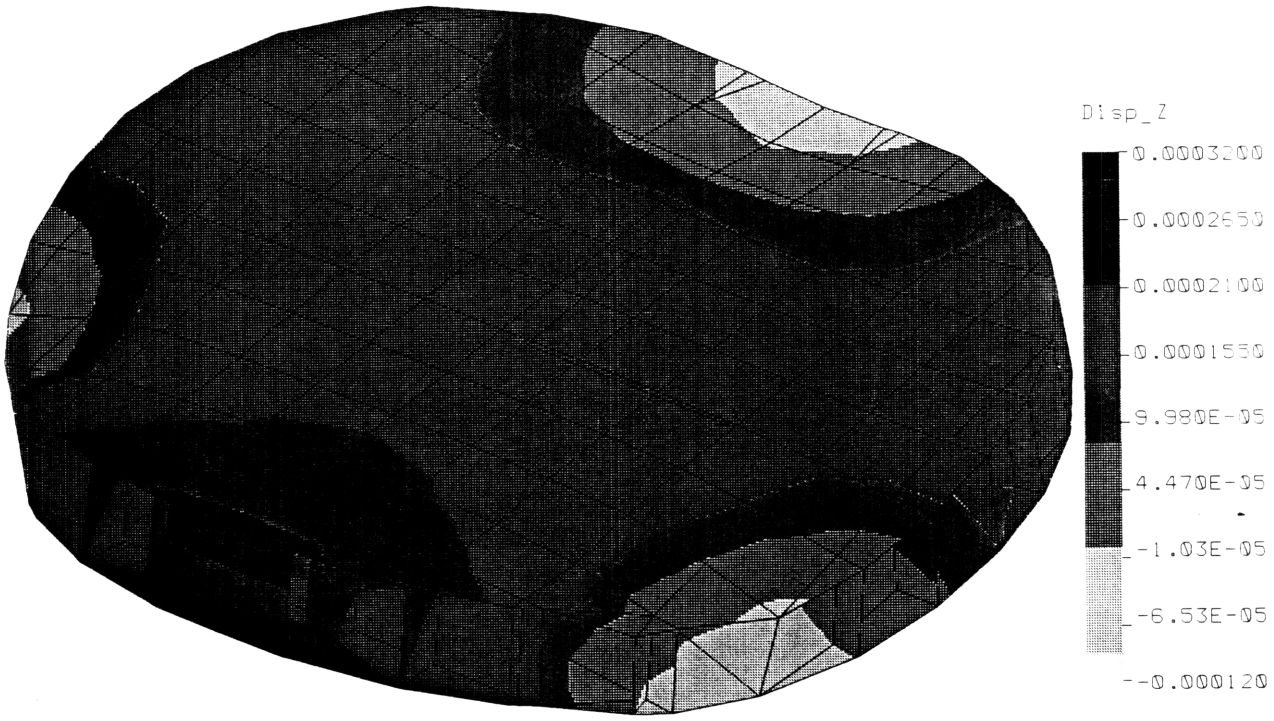

Figure 4-18 Thermal Deflection Profile for 1 Kelvin Change with 1.5 mm Piezoceramic Layer (z displacement in mm)

The piezoceramics add 8.78 kg to the entire mirror system, which induces greater self-weight deflection in the mirror. The effect of its thermal expansion also changes the original thermal deflection somewhat. Therefore, the piezoceramics must also be able to correct any deflection effects caused by its own presence. This is explored in the next chapter.

Chapter 5: Deflection Correction Results

Using the adaptive lightweight mirror designed in Chapter 4, deflection correction profiles can now be found. Section 5.1 begins with the least squares correction for self-weight deflection and thermal deflection. These results give the minimum root-mean-squares (RMS) error which can be expected in correcting mirror deformations when all actuators are present. Then, the focus shifts from using all available actuators to picking the best locations for actuators given a limited number of them. Section 5.2 contains a brief discussion of the difficulties of such a problem and the optimization scheme which is used in this study. Section 5.3 details the optimization profiles for self-weight deflection correction, and Section 5.4 addresses the optimization for thermal distortion correction.

5.1 Least Squares Correction

In this section, piezoceramic actuation profiles which minimize the mirror's surface error through least squares are found. Various cost factors are used to limit piezo-actuation voltages and their results are presented.

Since the designed mirror is flat, deflection in the planar direction is relatively unimportant compared with deflection in the z-direction. For this reason, actuation profiles are only composed of z-displacements of the static mirror analysis as described in section 4.3. Each actuator in the backsheet was individually actuated by one unit of voltage, and the corresponding z-displacement profile, called the actuation profile, was obtained. Figure 5-1 shows the numbering scheme which was assigned to the actuator location, and Figure 5-2 shows the numbering scheme assigned to displacement locations. There are 116 possible locations for piezoceramics and 136 nodes for deflection correction.

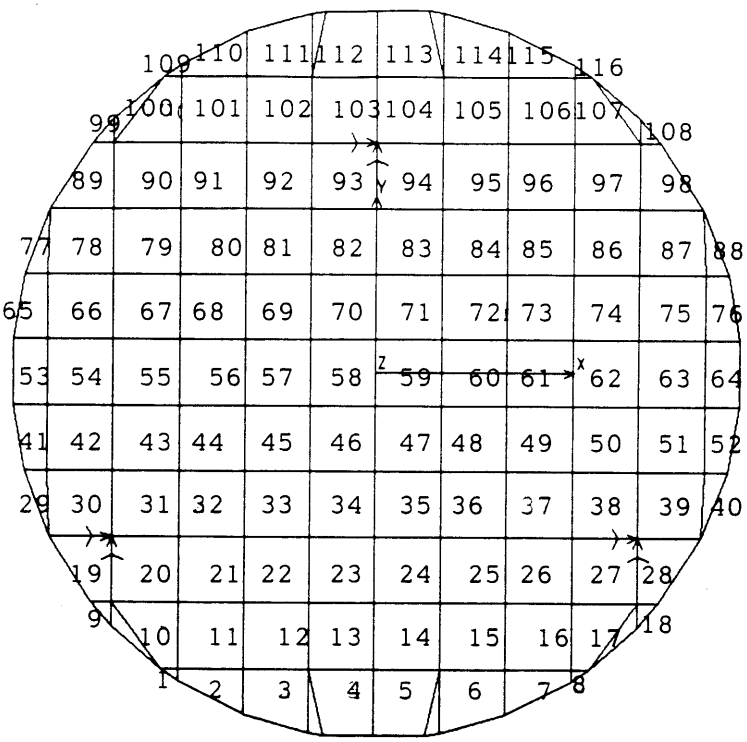

Figure 5-1 Location Scheme for Piezoceramics

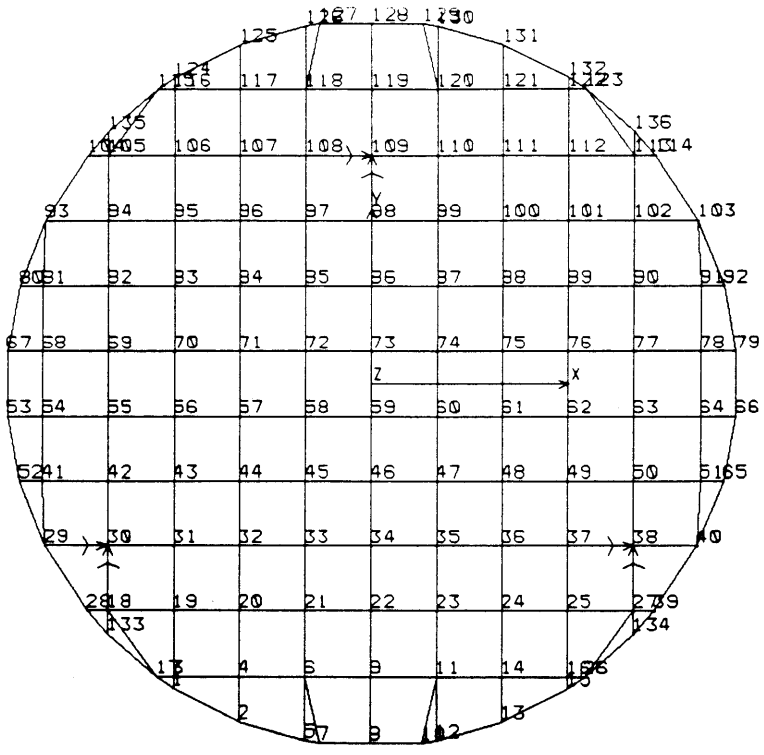

Figure 5-2 Location Scheme of Nodes for Deflection Measurement

Each piezoceramic was actuated with one unit of temperature "load" to represent one unit of voltage using the finite element method as described in Chapters 3 and 4, and these were compiled into a matrix, P, where the deflection induced by all the piezoceramics can be described by a combination of their actuation profiles with their corresponding applied voltages,

$$W_p = P\,V_p \tag{5-1}$$

P has 136x116 elements which denote the deflection influence of each piezoceramic on each nodal location. The elements are composed in the following fashion, where $a_{1,3}$ denotes the effect which the piezoceramic at location #3 has on the node at location #1.

$$P_{136x116} = \begin{bmatrix} a_{1,1} & a_{1,2} & a_{1,3} & \cdots & a_{1,116} \\ a_{2,1} & a_{2,2} & a_{2,3} & \cdots & a_{2,116} \\ a_{3,1} & \cdot & & & \\ \cdot & & \cdot & & \\ \cdot & & & \cdot & \\ \cdot & & & & \cdot \\ \cdot & & & & \\ \cdot & & & & \cdot \\ \cdot & & & & \\ \cdot & & & & \cdot \\ a_{136,1} & \cdots & \cdots & \cdots & a_{136,116} \end{bmatrix}$$

PZ#1 PZ#2 PZ#3 ... PZ#116

Location #1
Location #2
Location #136

(5-2)

As is indicated, each piezo actuation profile contributes a vector of displacements at every nodal point.

Similarly, deflection and voltage characteristics can be put into vector form, where w_3 is the deflection at nodal location #3, and V_3 is the voltage of piezo #3,

$$W = \begin{bmatrix} w_1 \\ w_2 \\ \cdot \\ \cdot \\ \cdot \\ \cdot \\ \cdot \\ \cdot \\ \cdot \\ \cdot \\ w_{136} \end{bmatrix} \qquad V_p = \begin{bmatrix} V_1 \\ V_2 \\ \cdot \\ \cdot \\ \cdot \\ \cdot \\ \cdot \\ \cdot \\ \cdot \\ \cdot \\ V_{116} \end{bmatrix} \tag{5-3}$$

The problem of finding appropriate actuation voltages for each piezoceramic is overdetermined since the number of locations describing each piezoceramic's influence profile exceeds the total number of voltage solutions which need to be solved. The system is not likely to have a solution, and only a least squares solution which arrives at piezo voltages giving the minimum squares error can be found (Ref.[50]). For deflection correction, the resulting piezoelectric deflection characteristics W_p must offset the original deflection W,

$$W_p + W = 0 \tag{5-4}$$

Substituting the influence matrix P into W_p,

$$P V_p + W = 0 \tag{5-5}$$

the actuation voltage which minimizes the error $\|PV_p+W\|^2$ with respect to voltage may be found. The squares error can be expanded using linear algebra,

$$E = \|PV_p+W\|^2 = (PV_p + W)^T(PV_p + W) \tag{5-6}$$

$$E = (PV_p)^T(PV_p) + 2P^TWV_p + W^TW \tag{5-7}$$

Taking the derivative of the error with respect to voltage and setting it to zero (Ref.[50]),

$$\frac{\delta E}{\delta V_p} = 2P^T P V_p + 2P^T W = 0 \tag{5-8}$$

a least squares solution for voltage V_p can be found.

$$P^T P V_p = -P^T W \tag{5-9}$$

$$V_p = -(P^T P)^{-1} P^T W \tag{5-10}$$

The parameters P and W as obtained from finite element analyses were compiled into MATLAB and solutions for the appropriate voltage profile were obtained. These were then used to correct the surface figure error of the mirror. Beginning with the deflected surfaces due to self-weight deflection (Figures 5-3) and thermal deflection (Figure 5-5), the least squares method arrived at corrected RMS surface deflections which are more than an order of magnitude below the uncorrected deflections. Self-weight deflection (SWD) of the nominal lightweight mirror with piezoceramics distributed throughout the back surface began with an RMS surface error of 9.2905e-4 mm and was corrected to 1.6782e-5 mm, or 1.8% of the original error. Thermal change of the same mirror under one Kelvin change as discussed in Section 4.4 began with an RMS surface figure error of 1.5799e-4 mm and was corrected to 7.6744e-6 mm, corresponding to 4.9% of the original error. The corrected contours are shown in Figures 5-4 and 5-6, respectively. Each contour plot contains the maximum and minimum deflection values, and contour lines are defined at an incremental step of 0.1μm for self-weight deflection plots and 0.01μm for thermal deflection plots.

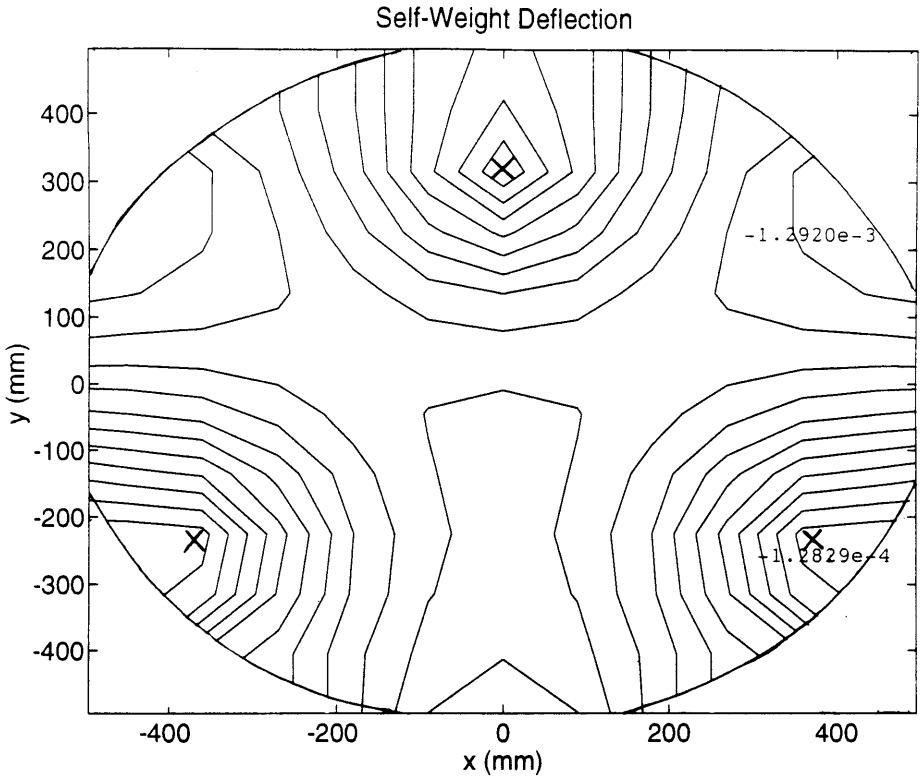

Figure 5-3 Self-Weight Deflection Surface Contour with All PZTs (0.1μm contour spacing)

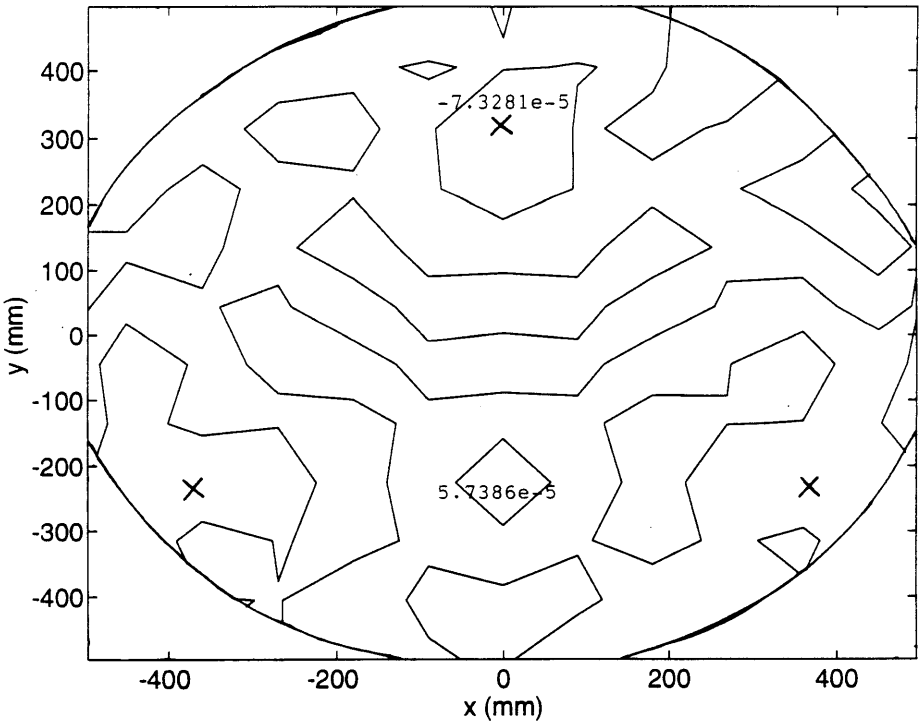

Figure 5-4 Corrected Surface Contour for Self-Weight Deflection (0.1μm contour spacing)

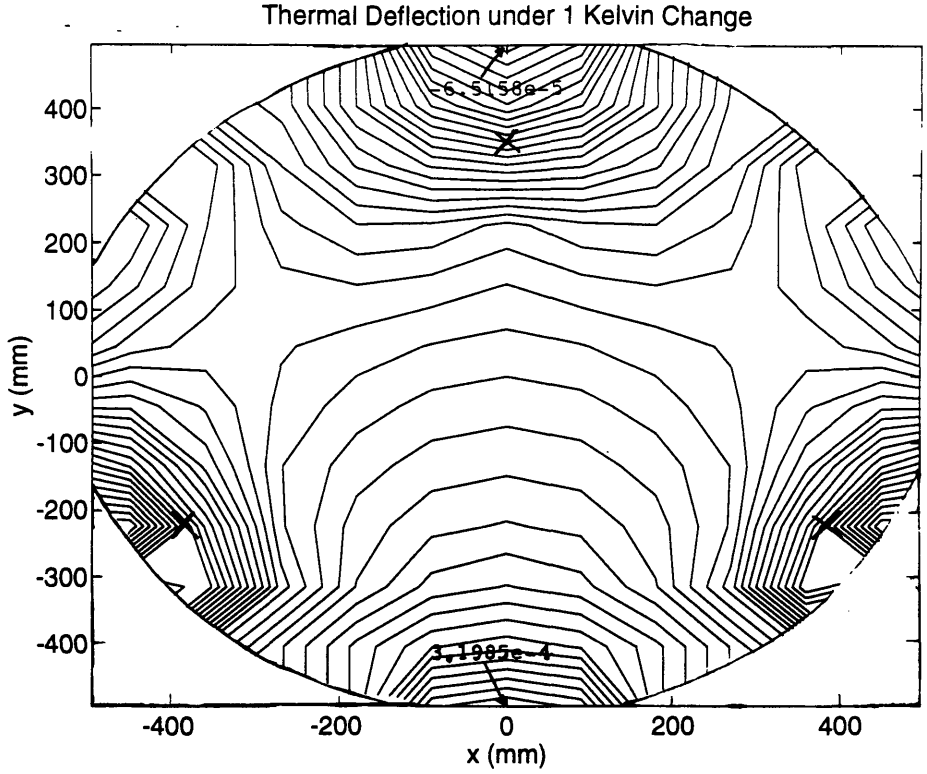

Figure 5-5 Thermal Deflection Surface Contour with All PZTs (0.01μm contour spacing)

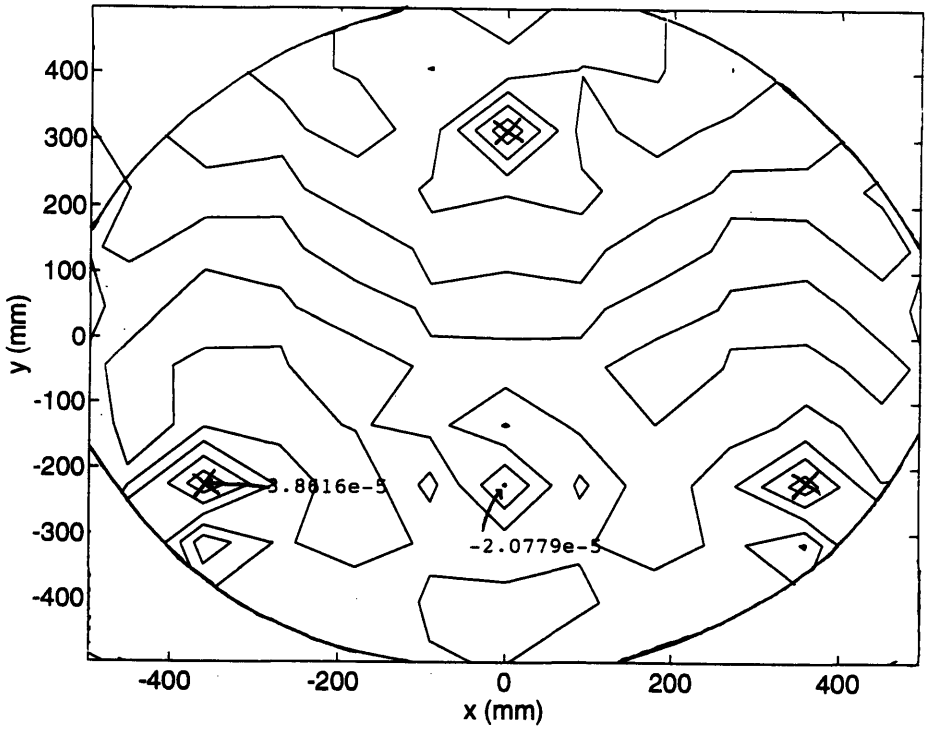

Figure 5-6 Corrected Surface Contour for Thermal Deflection (0.01μm contour spacing)

Unfortunately, because there was no constraint or cost associated with the magnitude of the voltages applied, actuation voltages exceed the 510V limit (or 85% of the coercive field of PZT-5H) at several locations. Appendix B contains the actuation voltages found for all cases. In fact, the highest actuation voltage for this least squares case was 5532V for self-weight deflection correction and -2200V for thermal deflection correction. This is due partially to very small piezoceramic elements at the corners of the mirror, which require greater electric field to obtain the necessary actuation characteristics, and partially to the fact that each piezoceramic is fighting with its neighboring piezos, as can be seen from the erratic expansion and contraction voltage profile (Appendix B). In any case, this implies that the actual performance which can be expected would be less than that predicted above, whether through truncating the applied voltages at 510V, or through adding a cost function for voltages. How much less performance needs to be determined. Afterall, it is not feasible to actuate piezoceramics to the current level of voltage field.

To constrain voltage values, a cost factor R can be added to penalize the magnitude of the voltage by a proportional factor into the RMS error. Thus, mathematically, high voltage values would actually induce more error into the system. The least squares method can still be used to solve for the optimal actuation profile with this constraint on voltage, where the larger the cost factor R associated with voltage values, the lower the least squares values for voltages would be. The squares error now has an additional cost factor term,

$$E = (PV_p + W)^T (PV_p + W) + R\, IV_p^T V_p \qquad (5\text{-}11)$$

$$E = (PV_p)^T(PV_p) + 2P^TWV_p + W^TW + R\, IV_p^T V_p \qquad (5\text{-}12)$$

where I is a 116x116 identity matrix which expands the scalar R factor for matrix manipulations. Once again, taking the derivative with respect to voltage,

$$\frac{\delta E}{\delta V_p} = 2P^T P\, V_p + 2P^T W + 2RI\, Vp = 0 \qquad (5\text{-}13)$$

the least squares solution for V_p can be derived. It now incorporates the cost factor R.

$$P^T P V_p + R I V_p = - P^T W \tag{5-14}$$

$$V_p = - (P^T P + RI)^{-1} P^T W \tag{5-15}$$

Various cost factors can be applied to obtain an appropriate actuation profile that gives reasonable deflection correction and does not exceed the voltage limit. These are performed in the following two sections.

5.1.1 Self-Weight Deflection Correction

Table 5-1 shows a summary of the results for SWD correction with various cost factors. The RMS surface error ratio is calculated based on the corrected error over the uncorrected error.

Table 5-1 Least Squares Self-Weight Deflection Correction Summary

Cost Factor R	RMS Error (mm)	RMS Error Ratio	Highest Voltage |V|
0 (Full Control)	1.6782e -5	0.01806	5532
1e -16	1.7707e -5	0.01906	1707
1e -15	1.8834e -5	0.02027	756
1e -14	2.2675e -5	0.02441	565
1e -13	2.9993e -5	0.03228	478
1e -12	4.7826e -5	0.05148	387
1e -11	9.0622e -5	0.09754	269
1e -10	2.9439e -4	0.31687	165
1e -9	7.4450e -4	0.80136	48
1e -8	9.0573e -4	0.97490	6.2
1e -7	9.2665e -4	0.99742	0.64
1e -6	9.2881e -4	0.99974	0.064
1e -5	9.2903e -4	0.99998	0.0064
1e -4	9.2905e -4	1	0.00064
∞ (No Control)	9.2905e -4	1	6.4e -8

Notice that R=0 represents the full control of the nominal least squares correction case as presented earlier, and that as R approaches infinity, actuation voltages are restricted to such a low level that the RMS surface error is not corrected at all. Thus, at R= ∞, the RMS surface error is the same as uncorrected surface error.

Plotting the RMS surface error with respect to maximum voltage, one sees an exponential increase in error when the maximum voltage is constrained to within 500V (Figure 5-7). Using the quilting deflection requirement as a guide for determining the level of acceptable deformations, it can be seen that maximum voltages as low as 250V can help to constrain mirror RMS surface error within a range of 1e-4 mm, still about an order of magnitude less than uncorrected deflection error.

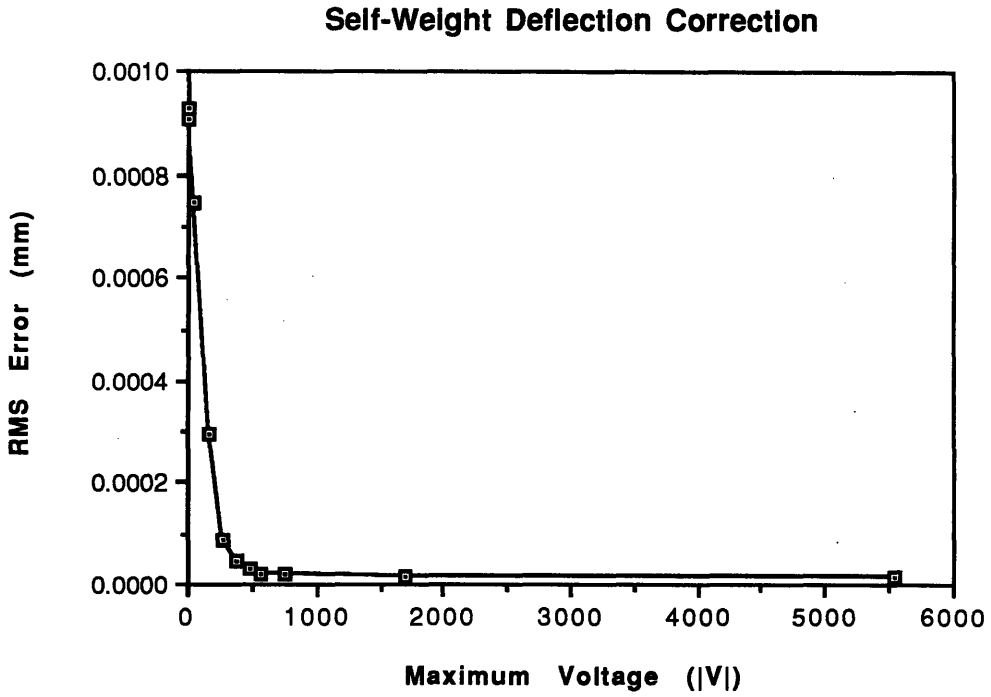

Figure 5-7 Maximum Voltage vs. RMS Error Given by Various Cost Factors for Self-Weight Deflection Correction

More detailed deflection characteristics can be seen in the contour plots in Figures 5-8 through 5-12, which feature deflection correction profiles with a few select cost factors, namely for R=1e-5, 1e-9, 1e-10, 1e-12, and 1e-16. Notice that cost factors less than 1e-12 give deflections less than quilting deflections at all points. The corresponding maximum applied voltage for R of 1e-12 is much less than 510V, which indicates that piezoceramic actuators are capable of providing excellent deflection corrections.

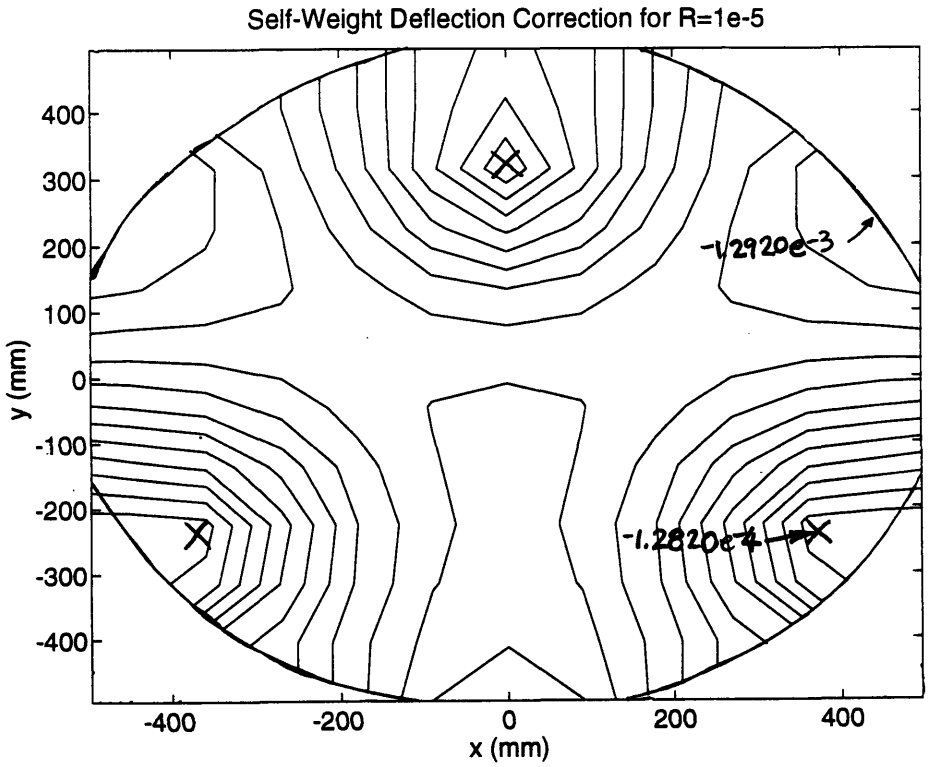

Figure 5-8 Least Squares SWD Correction for R=1e-5 (0.1μm contour spacing)

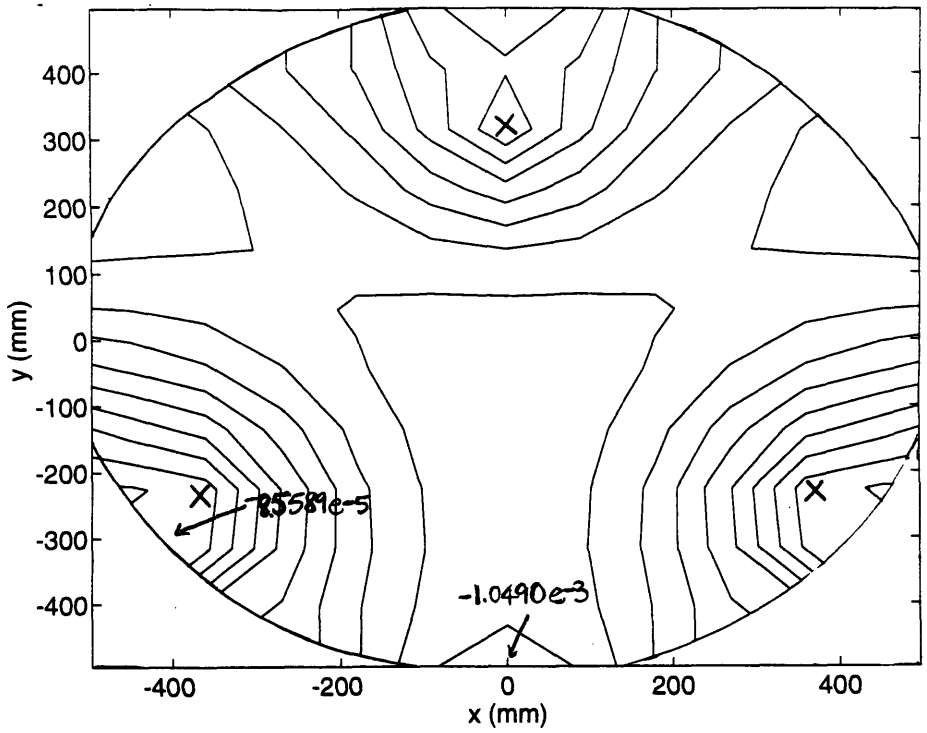

Figure 5-9 Least Squares SWD Correction for R=1e-9 (0.1μm contour spacing)

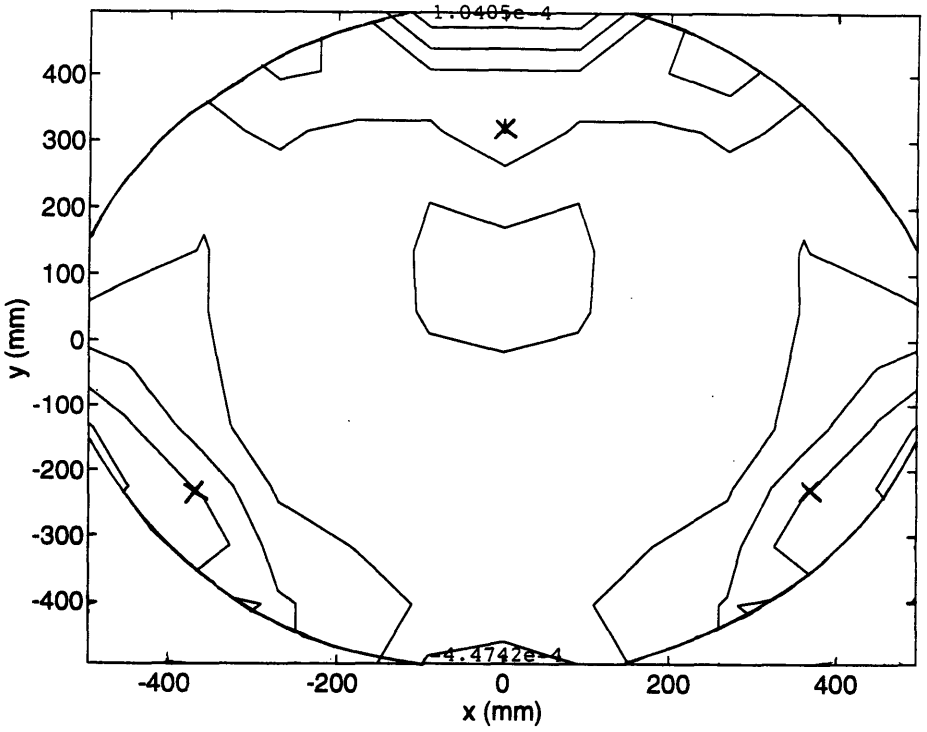

Figure 5-10 Least Squares SWD Correction for R=1e-10 (0.1μm contour spacing)

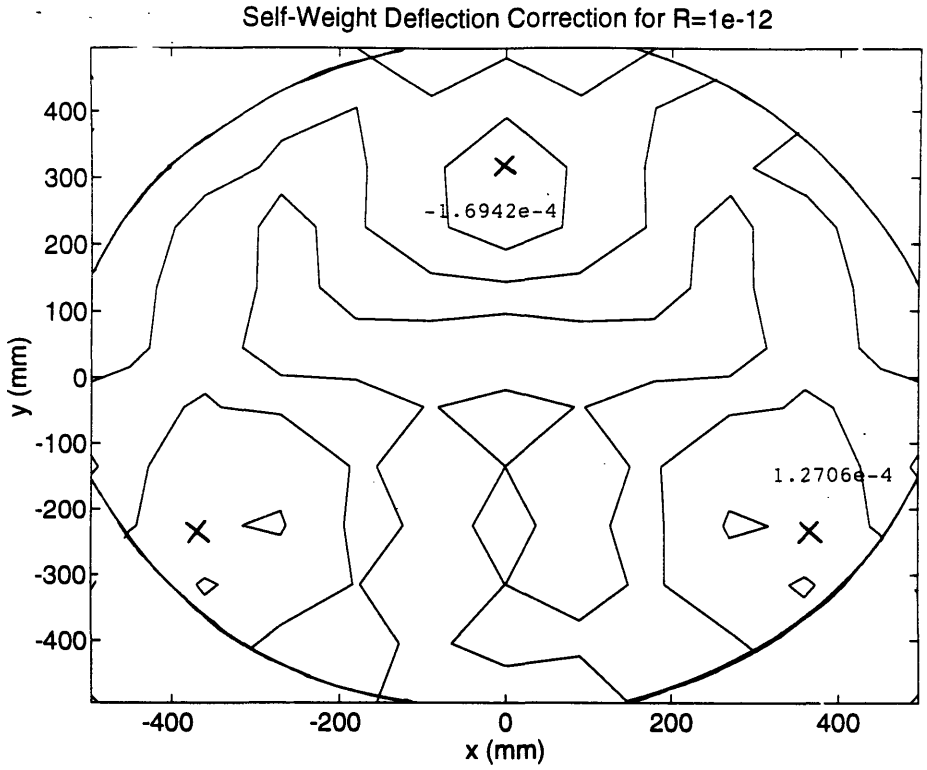

Figure 5-11 Least Squares SWD Correction for R=1e-12 (0.1μm contour spacing)

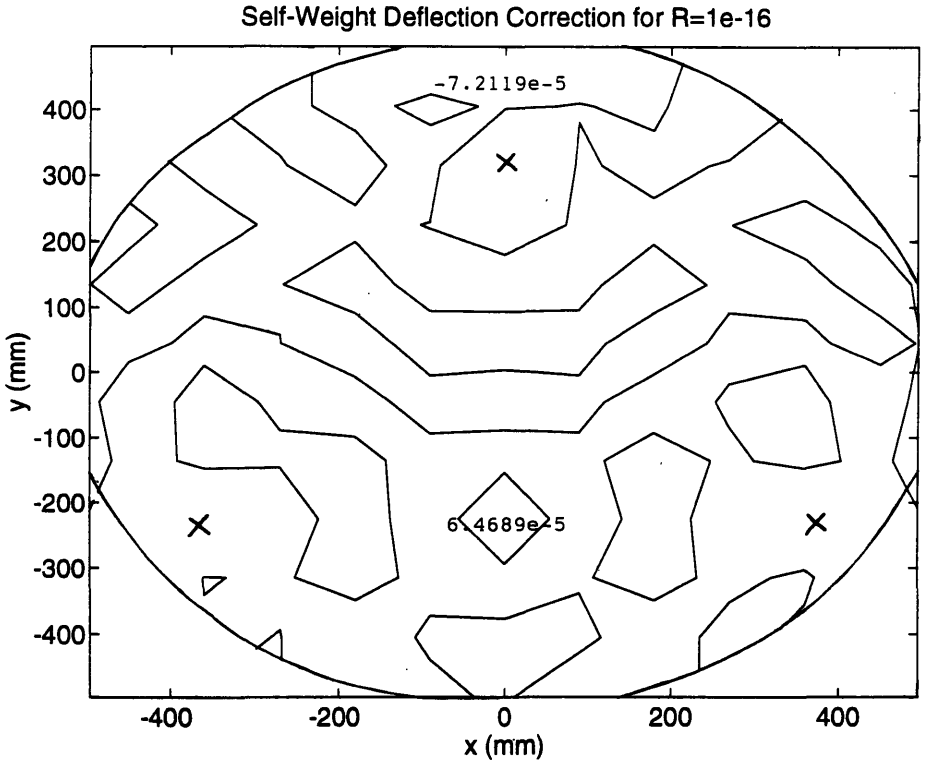

Figure 5-12 Least Squares SWD Correction for R=1e-16 (0.1μm contour spacing)

5.1.2 Thermal Deflection Correction

Similar correction levels are seen for thermal deflection correction. Although the deflected figure error starts out quite small due to the small temperature "load" and is, in fact, within quilting deflection levels, the correction study is still very relevant. Since linearity is assumed for temperature effects on both the mirror structure and the piezoceramic material, results from this analysis, including deflection characteristics and voltage values, can be linearly scaled to the appropriate temperature changes of the mirror. Therefore, to correct thermal deflection of a 10 Kelvin change, resulting in ten times the current deflection, would require ten times more applied field. Table 5-2 shows the deflection correction summary for a 1 Kelvin change using various cost factors.

Table 5-2 Least Squares Thermal Deflection Correction Summary

Cost Factor R	RMS Error (mm)	RMS Error Ratio	Highest Voltage |V|
0 (Full Control)	7.6944e -6	0.04870	2200
1e -16	8.0021e -6	0.05065	809
1e -15	8.5095e -6	0.05386	391
1e -14	1.0090e -5	0.06386	147
1e -13	1.2495e -5	0.07909	110
1e -12	1.9531e -5	0.12362	76
1e -11	3.1615e -5	0.20011	50
1e -10	5.9459e -5	0.37635	32
1e -9	1.2935e -4	0.81872	8.5
1e -8	1.5447e -4	0.97772	1.04
∞ (No Control)	1.5799e -4	1	1.07e -8

Graphing the maximum applied voltages and RMS surface errors show, once again, an exponential increase in error as voltages are constrained below 200V.

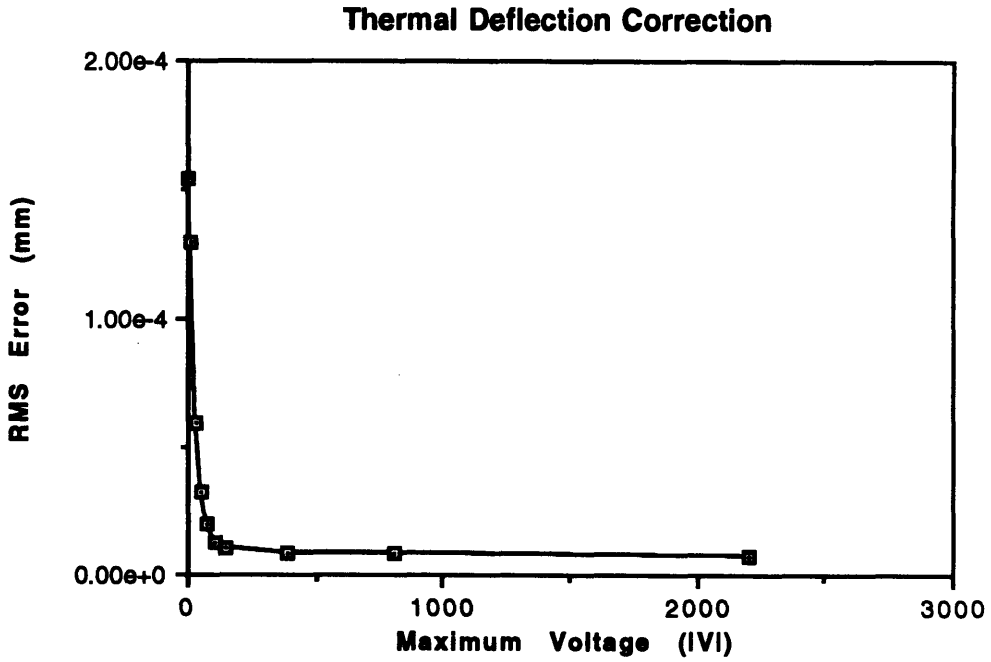

Figure 5-13 Maximum Voltage vs. RMS Error Given by Various Cost Factors for Thermal Deflection Correction

The results show that piezoceramics can be used to correct thermal deflection to the level of quilting deflection for temperature changes up to about 5 Kelvin. Of course, piezoceramics can be used to correct surfaces for less stringent deflection requirements as well. More detailed deflection characteristics are displayed in the following contour plots. Figures 5-14 through 5-18 feature deflection profiles for R= 1e-8, 1e-9, 1e-10, 1e-12, and 1e-16.

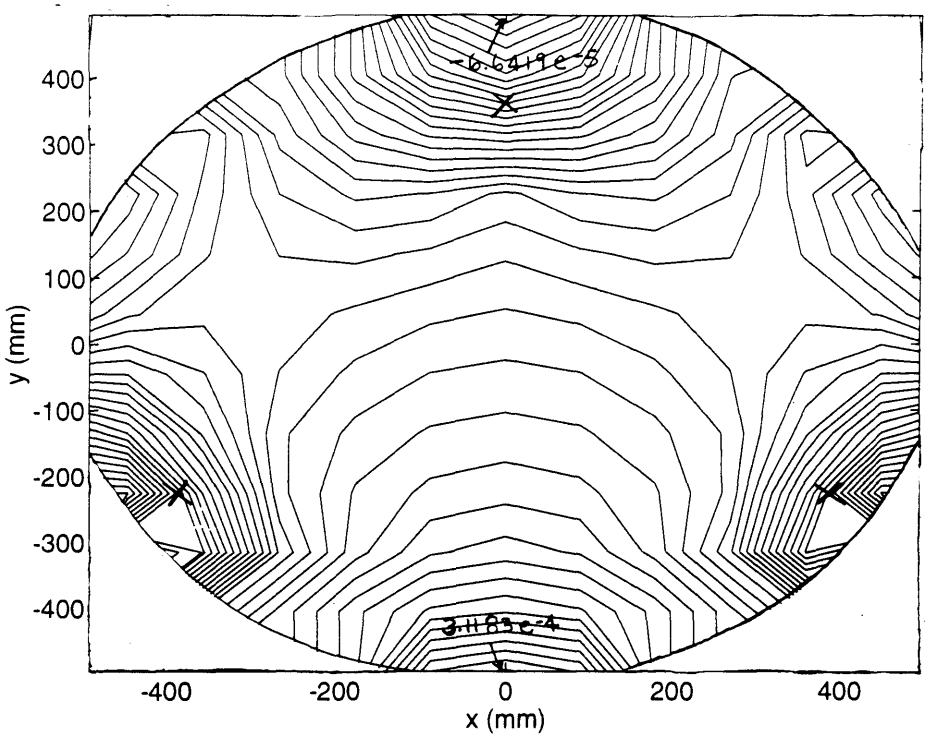

Figure 5-14 Least Squares Thermal Deflection Correction for R=1e-8 (0.01μm contour spacing)

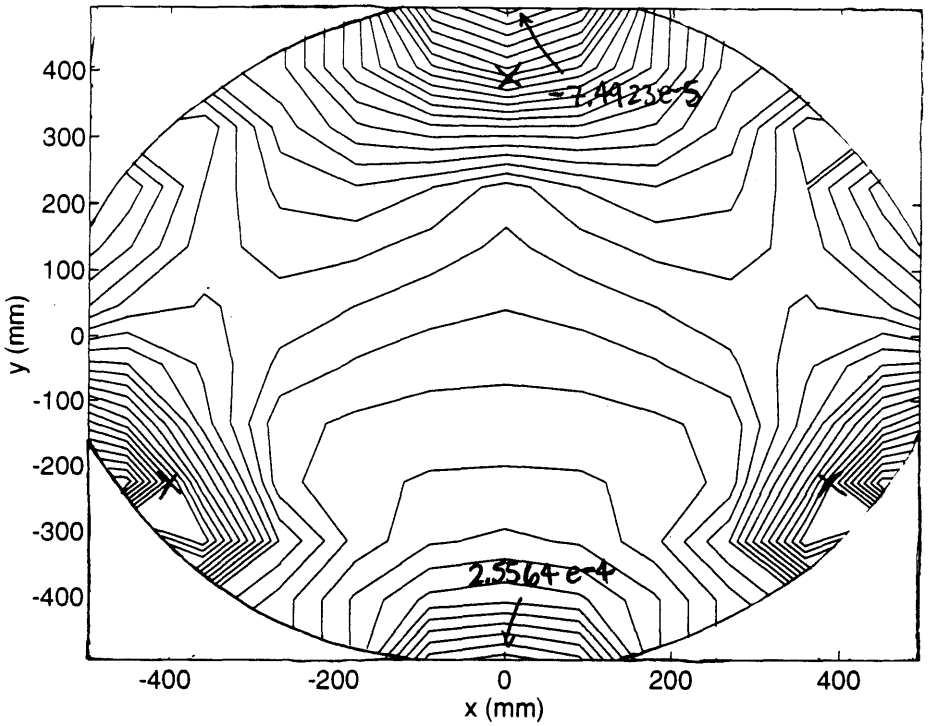

Figure 5-15 Least Squares Thermal Deflection Correction for R=1e-9 (0.01μm contour spacing)

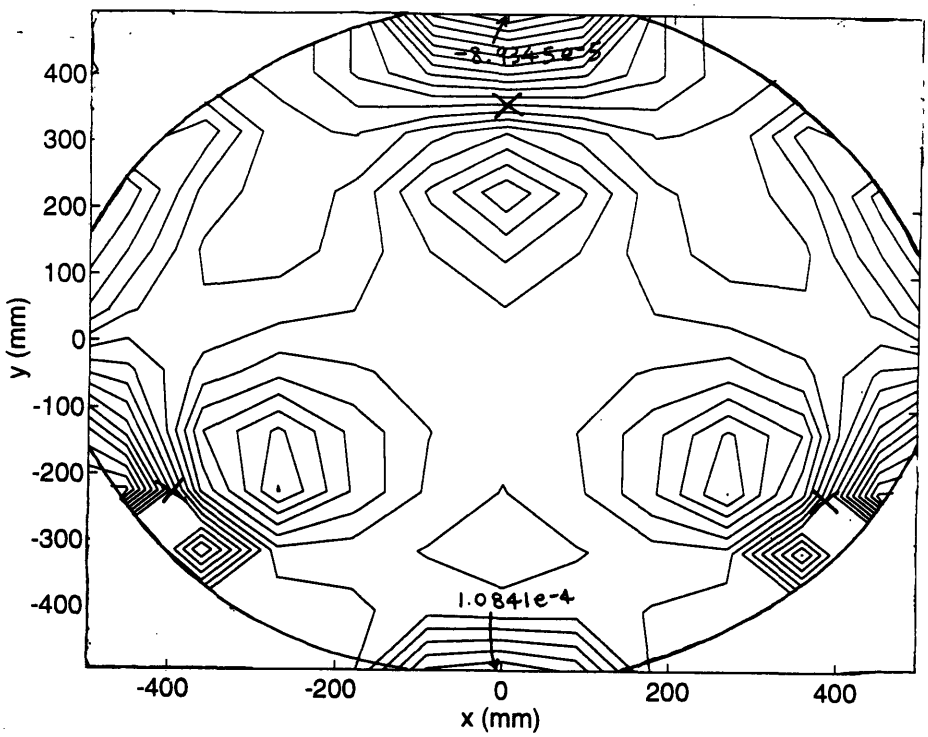

Figure 5-16 Least Squares Thermal Deflection Correction for R=1e-10 (0.01μm contour spacing)

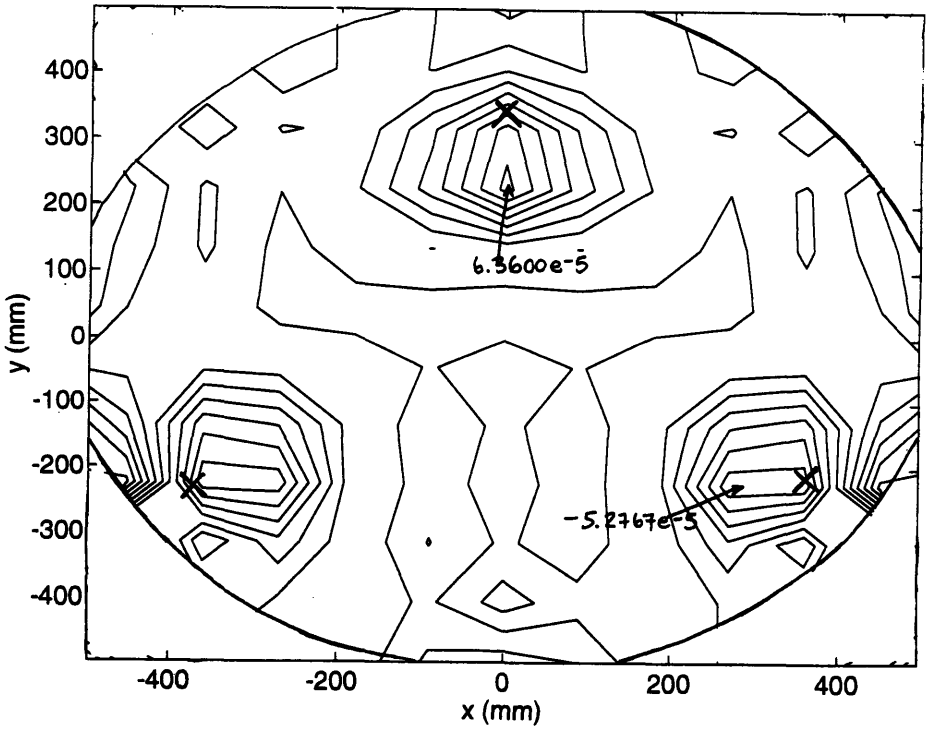

Figure 5-17 Least Squares Thermal Deflection Correction for R=1e-12 (0.01μm contour spacing)

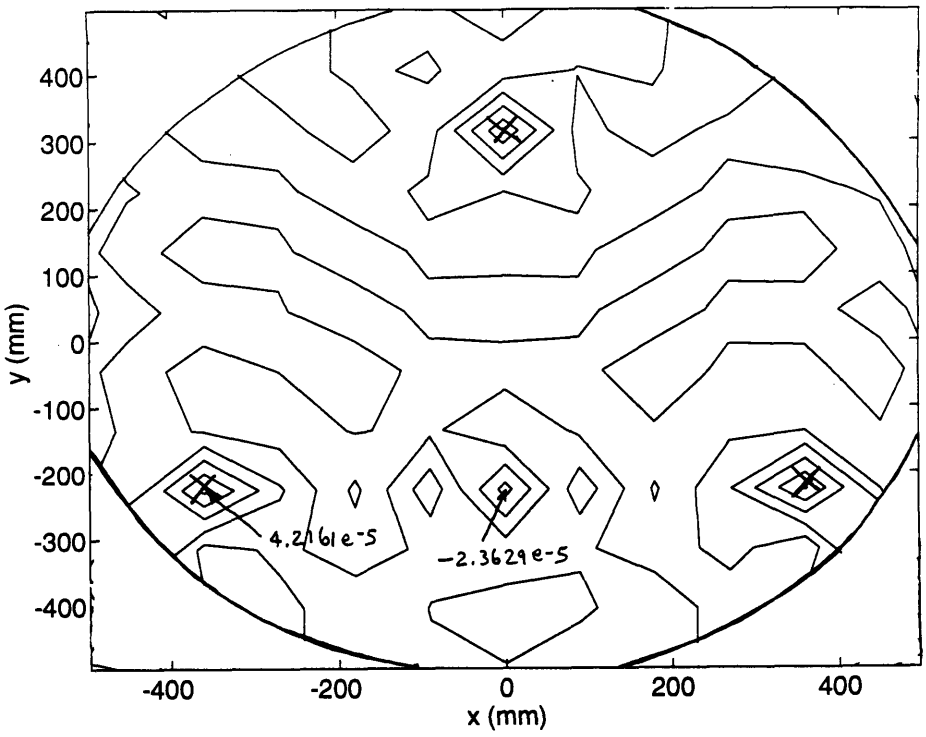

Figure 5-18 Least Squares Thermal Deflection Correction for R=1e-16 (0.01μm contour spacing)

Both of the least squares analyses show that piezoceramics have the capability to provide significant deflection improvements with low voltage levels. An order of magnitude improvement can be seen with a maximum voltage of only 269V in self-weight deflection correction, and 100V for thermal deflection correction. Thus, it can be deduced that an order of magnitude improvement in thermal deflection correction can be seen for temperature changes of up to about 5 Kelvin. These surface errors are all on the same order as the quilting deflection, which is definitely a vast improvement.

5.2 Optimization Problem Statement

Finding truly optimal locations and actuation voltages for this particular problem is almost impossible due to the large number of discrete piezoceramic locations. Integer optimization of such a problem would require a huge amount of calculations which do not meet the objective of an efficient mirror evaluation package. Instead, a routine using successive placement of piezoceramics is utilized (Ref.[6]).

Successive placement is an optimization scheme which finds the most effective actuation location and voltage for one piezoceramic at every step. A constraint on voltage can be built into the algorithm to keep voltages at each step below a specified field. The algorithm is outlined as follows:

(1) Find the voltage for each piezoceramic which minimizes the least squares error deflection W of the mirror.

$$V_i = - (a_{x,i}^T a_{x,i})^{-1} a_{x,i}^T W$$

This equation solves for the voltage of piezo location i with actuation profile a which contains the deflections at each nodal location x.

(2) Find the associated RMS surface error resulting from the mirror's deflection due to this particular piezo-actuation. Using MATLAB functions,

$$e_i = \text{norm}(W + a_i x V_i) / \text{sqrt}(136)$$

(3) Find the location of the piezoceramic giving the minimum RMS surface error.

(4) Check that the actuation voltage is not over some specified MAX VOLT.
If |V| > MAX VOLT, go to (6).

(5) If -MAX VOLT < V < MAX VOLT, add this influence function, multiplied by the

appropriate voltage, to the starting deflection to obtain a corrected profile.

$$W_n = W + a_i x V_i$$

Repeat from (1) using this new deflection with $W = W_n$.

(6) For |V| > MAX VOLT, find the deflection correction, or surface error, for |V| = MAX VOLT, where the sign of V depends on the sign of the original voltage.

(7) Compare this error at MAX VOLT with errors at all other locations.

(8) If there is another error less than this error, go to (3) and check characteristics for this new location.

(9) Given that this actuation location gives the lowest error even at |V| = MAX VOLT, add this influence function with MAX VOLT (with appropriate sign) to the starting deflection and repeat from (1) using $W = W_n$.

Each piezo location is allowed to be reevaluated as long as the combined voltages obtained from each step for that location does not exceed the specified maximum field. This implies that a voltage profile may change given new deflection characteristics. Thus, with added piezoceramics, an actuation voltage may increase or decrease depending on the successive placement of other piezoceramics.

Since each piezoceramic adds only a small fraction of a kilogram to the weight of the entire mirror and little stiffness, deflection profiles of the nominal lightweight mirror without attached piezoceramics can be used. More detailed studies would need to incorporate their weight as well as stiffness characteristics since a large number of piezoceramics would naturally affect mirror deflection, depending on their location.

The successive placement scheme is by no means the most optimal placement routine. Other algorithms are able to give near optimal solutions, but they require much more analyses. Successive placement, on the other hand, gives a very good first cut look which is sufficient for analyzing the feasibility of using a limited number of piezoceramics for deflection correction of this type of mirror. The next two sections contain discussions of the results from this optimization analysis.

5.3 Self-Weight Deflection Correction by Successive Placement

This section describes the results of self-weight deflection correction using the optimization scheme as outlined above. The algorithm was first used to find an optimal placement scheme with no voltage constraints in order to obtain the best error correction characteristics, and to insure the feasibility of using piezoceramics for self-weight deflection correction. Then, a voltage constraint of 510V (85% of coercive field for PZT-5H) was used to obtain a realistic placement profile.

Figure 5-19 illustrates the actuation sequence of optimal piezoceramic locations with no voltage constraint. Notice that the first four actuators went to the three support points, where piezo expansions induced an upward deflection in the mirror to correct the downward weight induced deflection. Conceptually, this is similar to the idea of placing actuators at the root of a cantilevered beam to provide maximum actuation effects. The actuators near the support tend to correct the large deflection which is seen at the edge of the mirror. The fifth actuator contracts in the center of the mirror. The merits of this can once again be derived from a beam example. For a pin-pinned beam, maximum deflection corrections can be realized by placing actuators between the pins. Similarly, an actuator in the center of the mirror can effectively correct the self-weight induced deflection at the center of the mirror. Further piezoceramic placements all seem to conglomerate around these points. They are either found near the support points or in between support points.

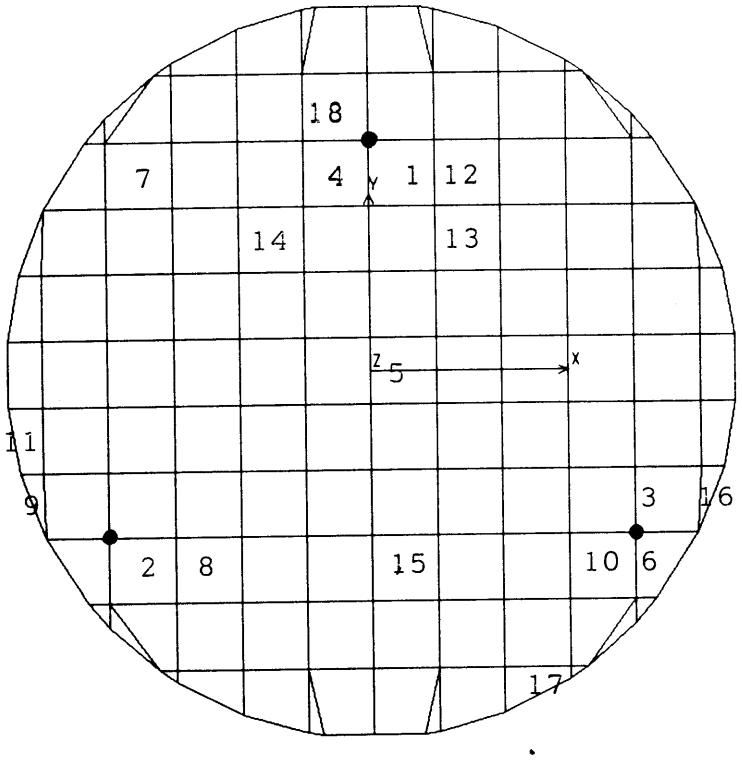

Figure 5-19 Actuation Sequence for Self-Weight Deflection Correction

Successive placement obtains the optimal actuation voltage for each chosen piezoceramic based on a fixed deflection characteristic. Once locations for some number of piezos are found, a least squares solution can be found based on those specified piezos. In this way, the actuation field of each piezo is not automatically constrained by the other piezos which were located before it. Figure 5-20 shows the RMS error due to successive placement and also due to finding least squares solutions at four various stages found from successive placement. The results show that, indeed, better deflection correction can be found by optimizing actuation voltages together.

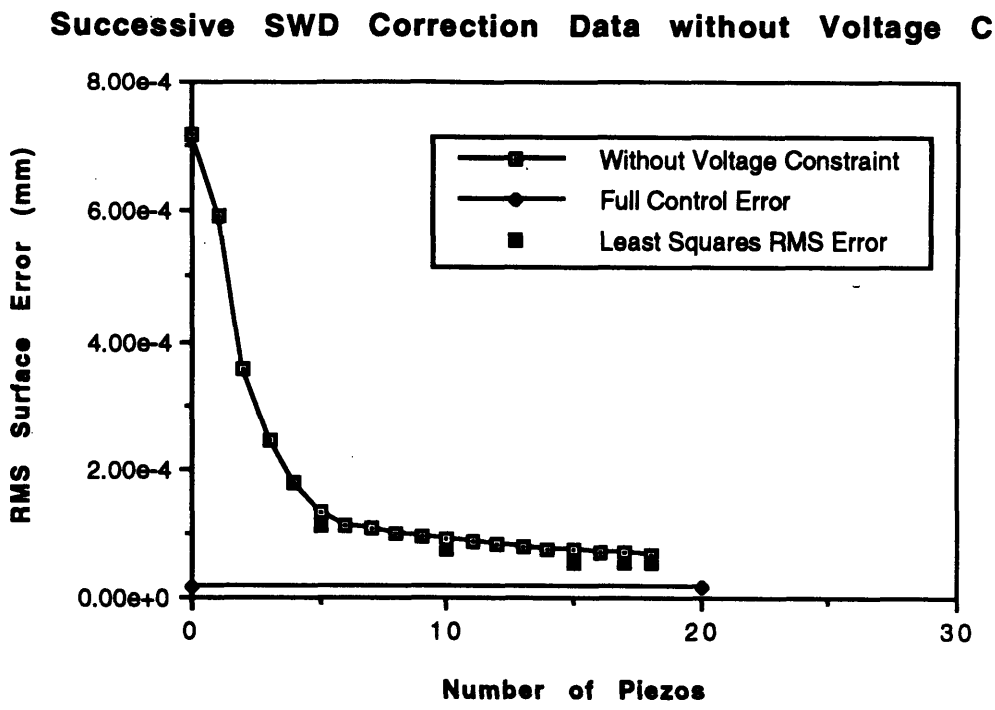

Figure 5-20 RMS Error vs. Number of Piezos in Correcting Self-Weight Deflection

More details are given in the following contour plots for the various discrete actuation points, at five, ten, fifteen, and eighteen piezos. The location profile also gives piezoceramic characteristics, where a positive sign stands for expansion (caused by a negative voltage, or an applied field in the opposing direction of piezo poling) and a negative sign is contraction (caused by a positive voltage). Maximum and minimum deflection values are given in the contour plots.

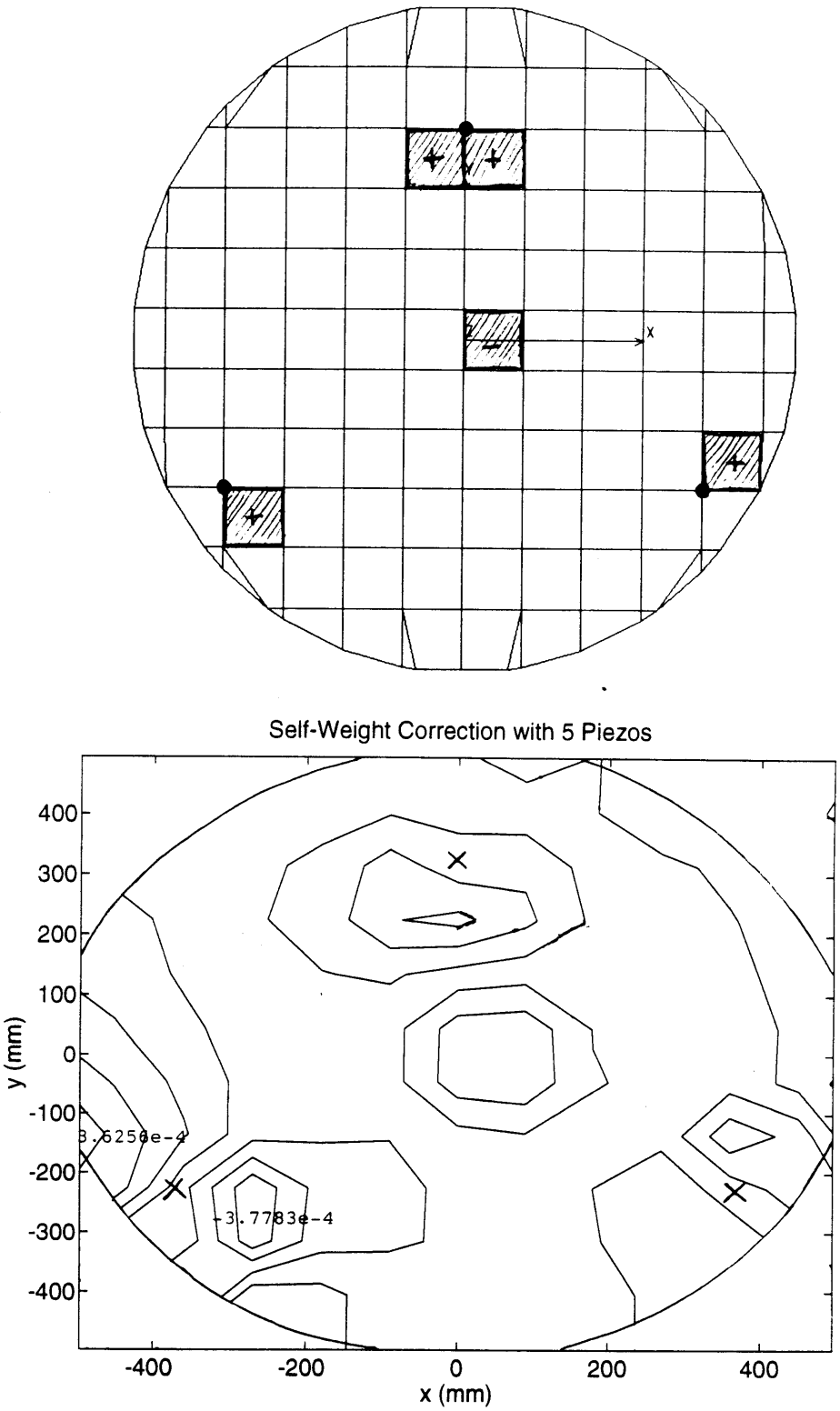

Figure 5-21 SWD Correction Using 5 PZTs with No Voltage Constraint: Location and Contour (0.1μm contour spacing)

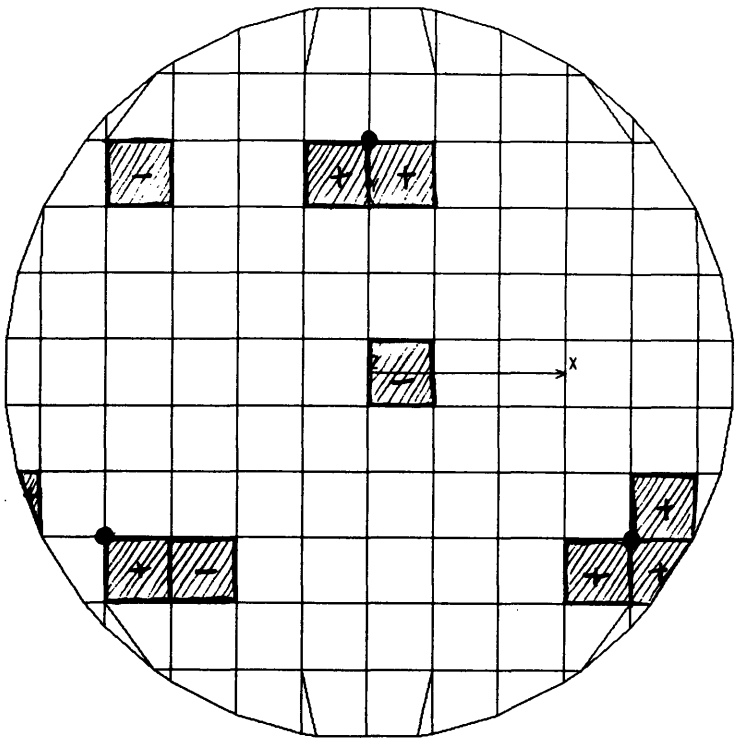

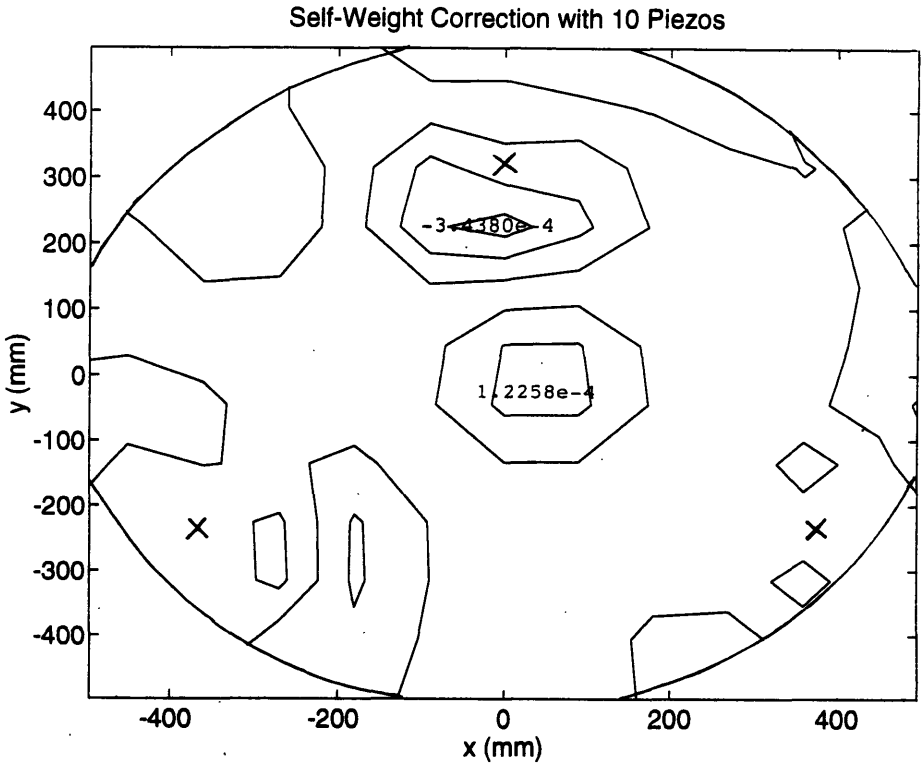

Figure 5-22 SWD Correction Using 10 PZTs with No Voltage Constraint: Location and Contour (0.1μm contour spacing)

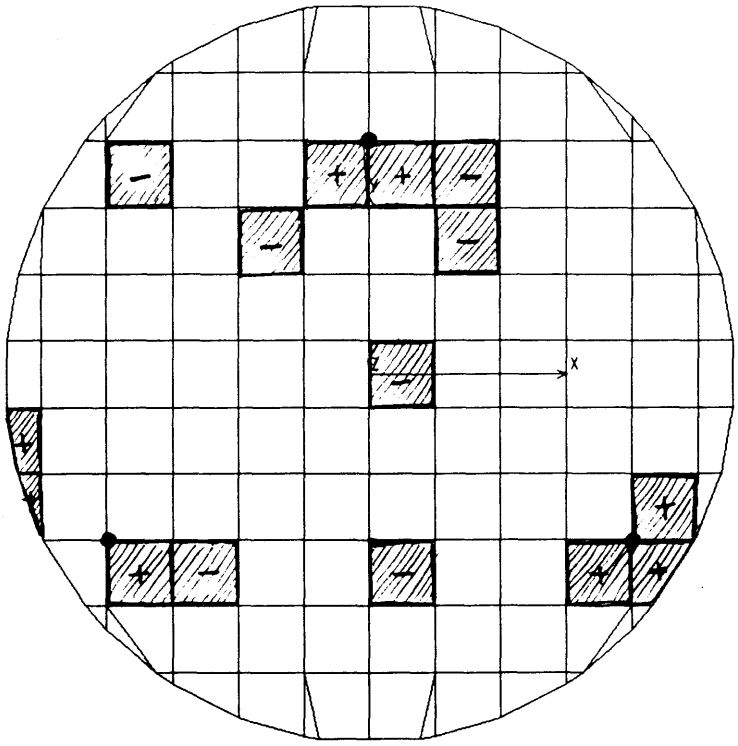

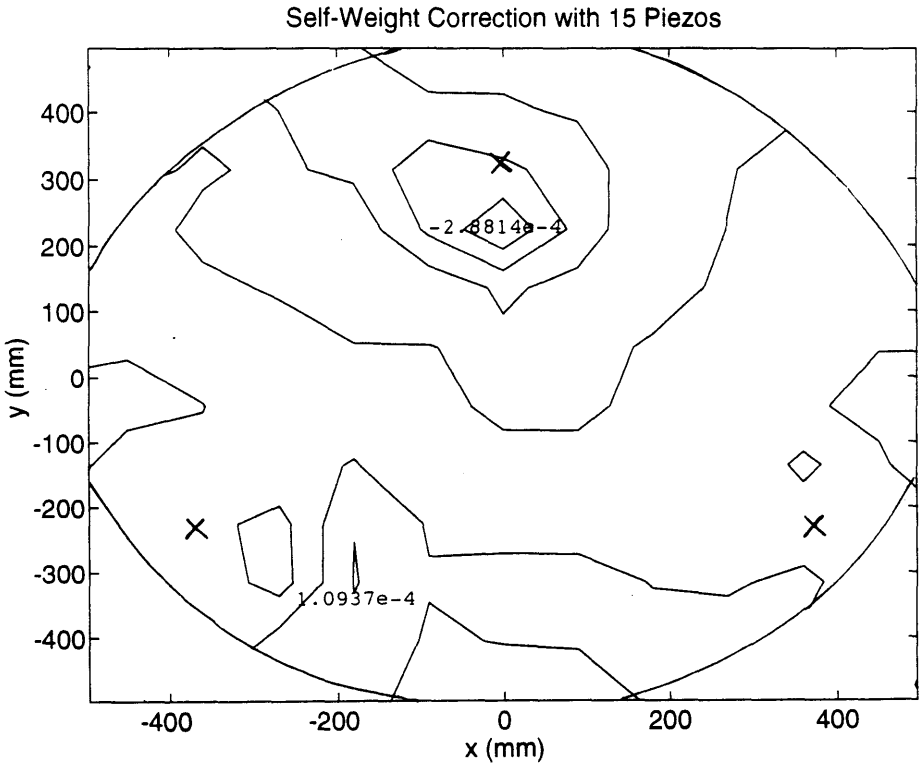

Figure 5-23 SWD Correction Using 15 PZTs with No Voltage Constraint: Location and Contour (0.1μm contour spacing)

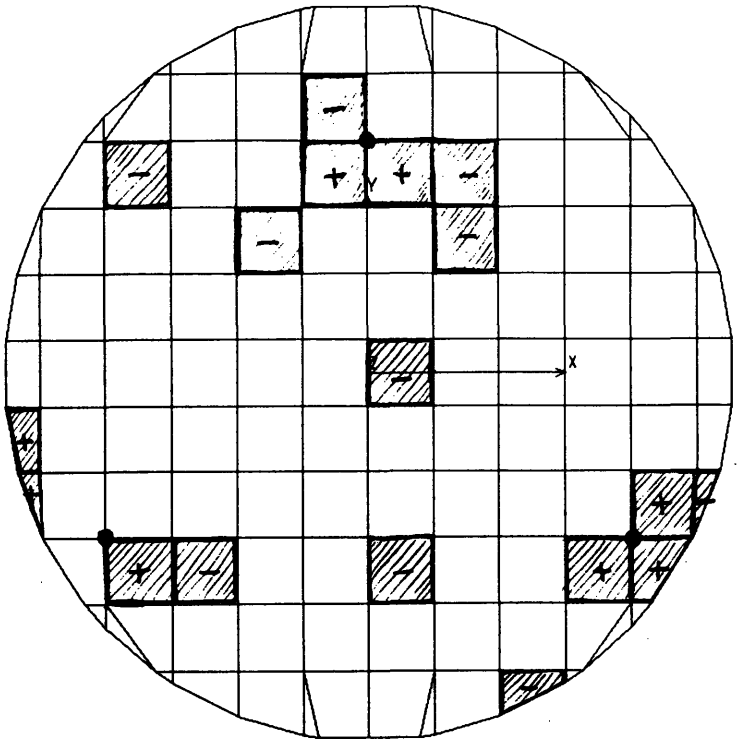

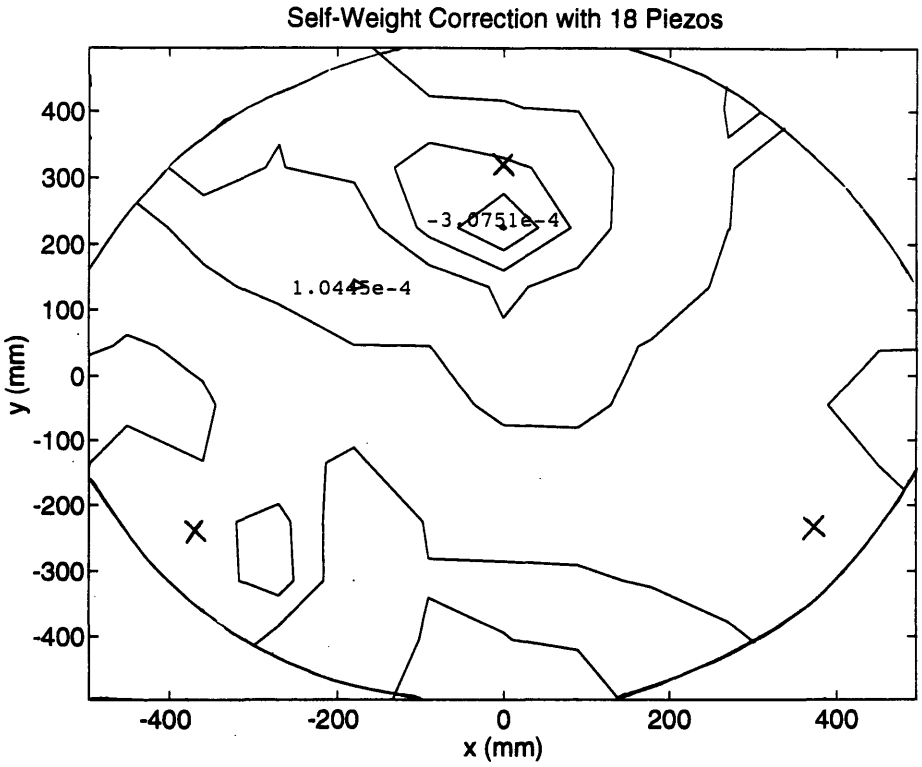

Figure 5-24 SWD Correction Using 18 PZTs with No Voltage Constraint: Location and Contour (0.1μm contour spacing)

These deflection profiles show that it is very feasible to use a limited number of piezoceramics to correct self-weight deflection, where RMS surface errors were corrected to a deflection level of quilting errors with maximum voltage exhibited by any single piezo to be only 604V. Now, more realistic voltage values may be obtained by limiting the maximum actuation voltage for each piezo to 510V.

Figure 5-25 illustrates the actuation sequence of optimal piezoceramic locations when maximum voltage is constrained, $|V| < 510V$.

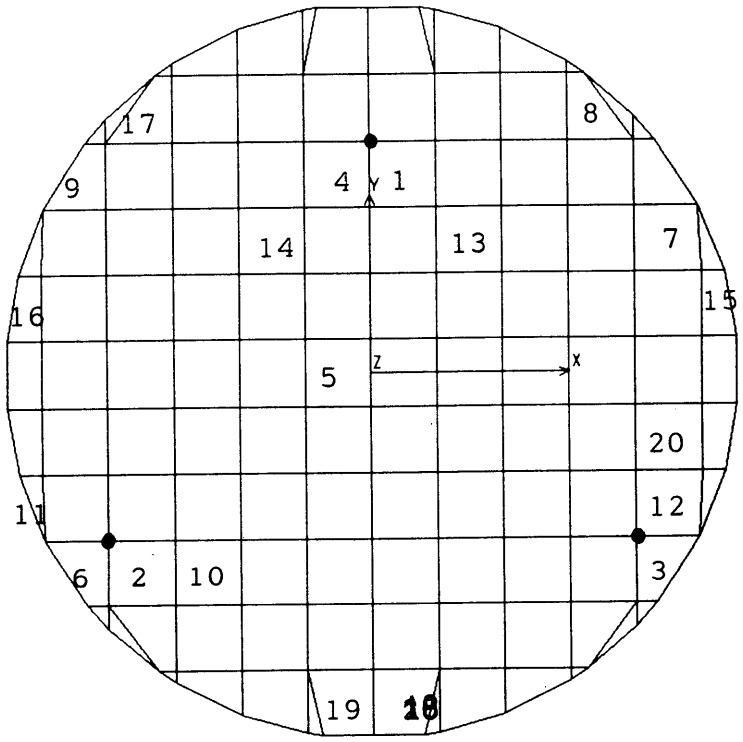

Figure 5-25 Actuation Sequence for Self-Weight Deflection Correction with Constrained Field

Notice that the actuator placement is quite different from that with unconstrained voltages. More actuators are concentrated at the edge of the mirror. The first five locations are similar,

where the first four actuators are placed near each of the three point supports and the fifth attaches in the center of the mirror. Again, the actuators at the supports expand to bring the downward edge deflections up, and the actuator at the center of the mirror contracts to bring the center deflection up. After these first five are in place, however, optimal locations differ from the first case considerably. There is still quite a large concentration of piezos at the support points, and the reason for that is quite clear, as explained before. Now, however, there is also a large concentration of edge actuation. This characteristic seem to agree with results concluded by Aspinwall and Karr in Ref.[9]. They found theoretically that lower figure errors can result by edge control alone as compared to the use of push-pull actuators in the interior of the mirror, and suggested that a hybrid system using both interior and edge actuation would probably be most effective. Graphing the number of piezos verses the RMS surface error, it can be seen that limiting the applied field to 510V does not degrade correction performance by very much.

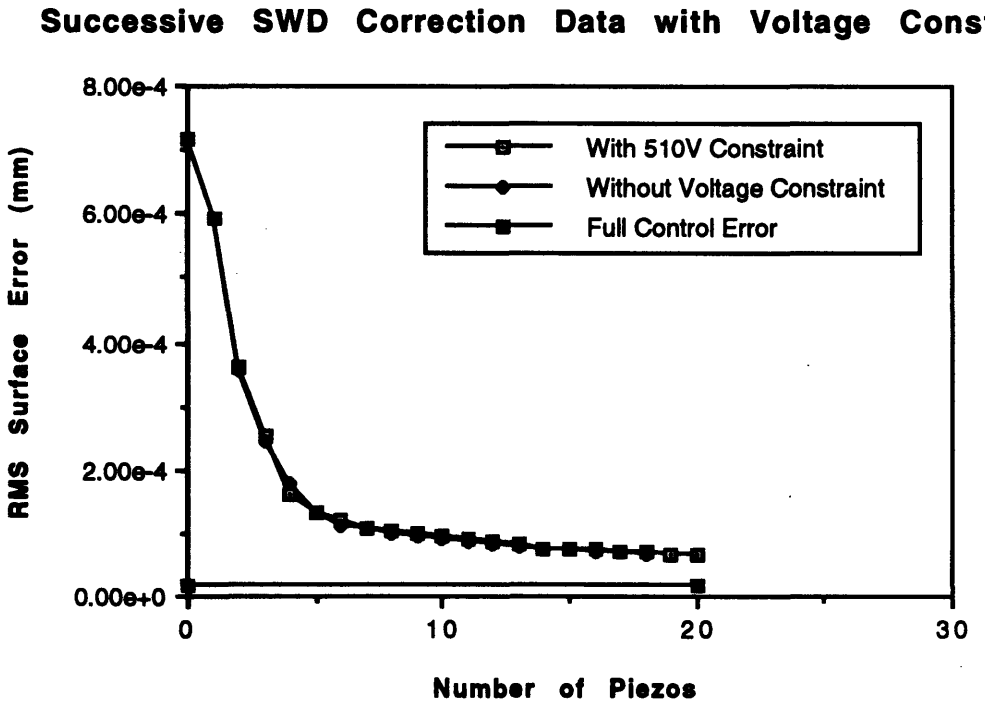

Figure 5-26 RMS Error vs. Number of Piezos in Correcting Self-Weight Deflection

In fact, the surface errors exhibited by the constrained case are essentially the same as those exhibited by the unconstrained case, since the maximum voltage allowed is not very much different.

Once again, the following contours give more detail to the deflection characteristics. Because voltages are constrained to 510V, separate least squares analyses at successive stages could not be performed because they would specify voltage characteristics greater than the 510V constraint. Therefore, contour plots illustrate the deflection profiles given straight from the successive placement sequence and voltages.

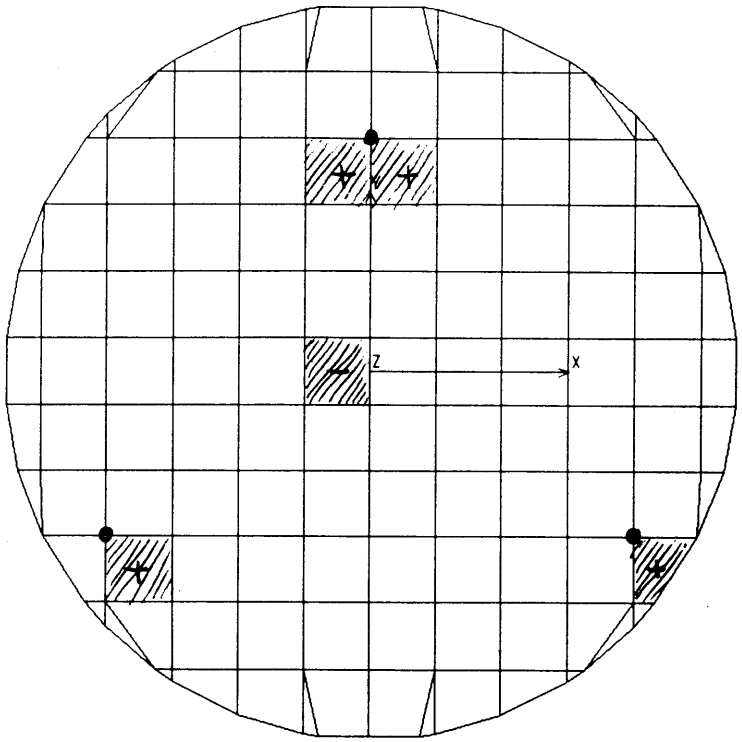

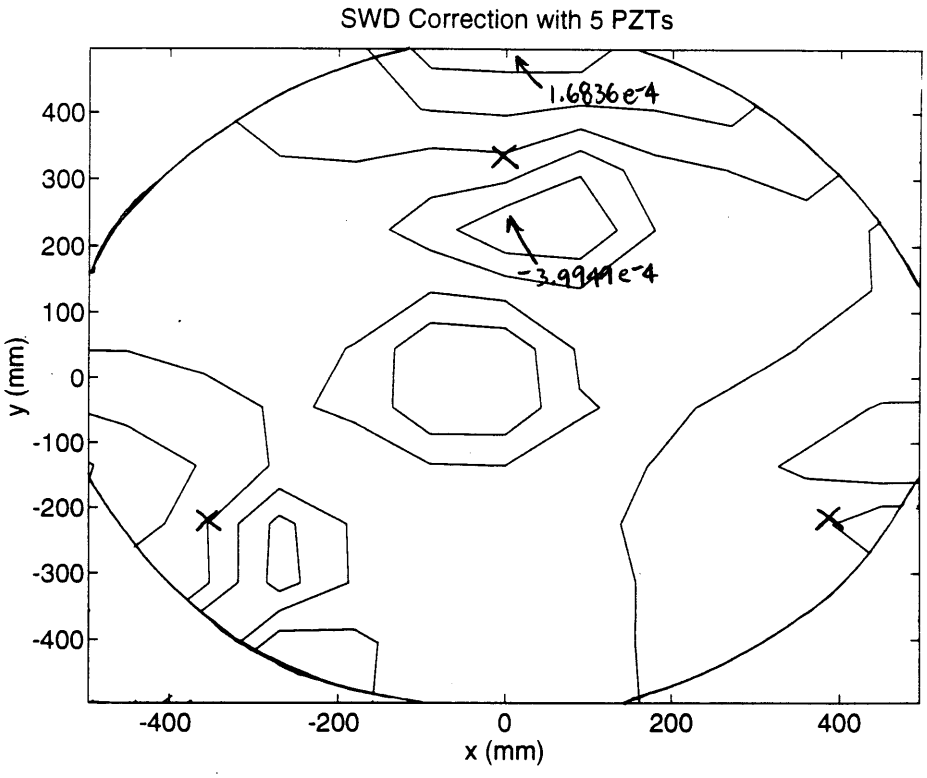

Figure 5-27 SWD Correction Using 5 PZTs with 510V Constraint: Location and Contour (0.1μm contour spacing)

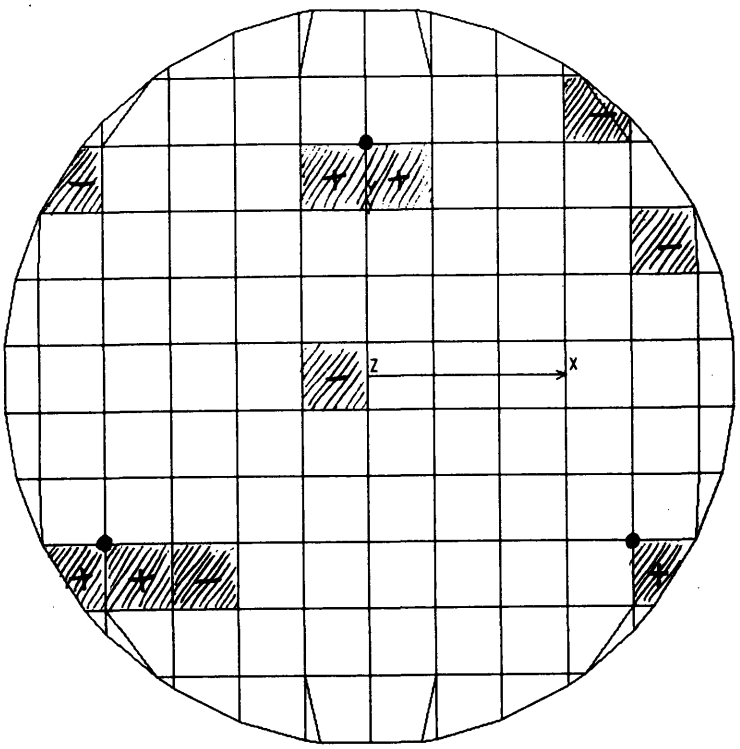

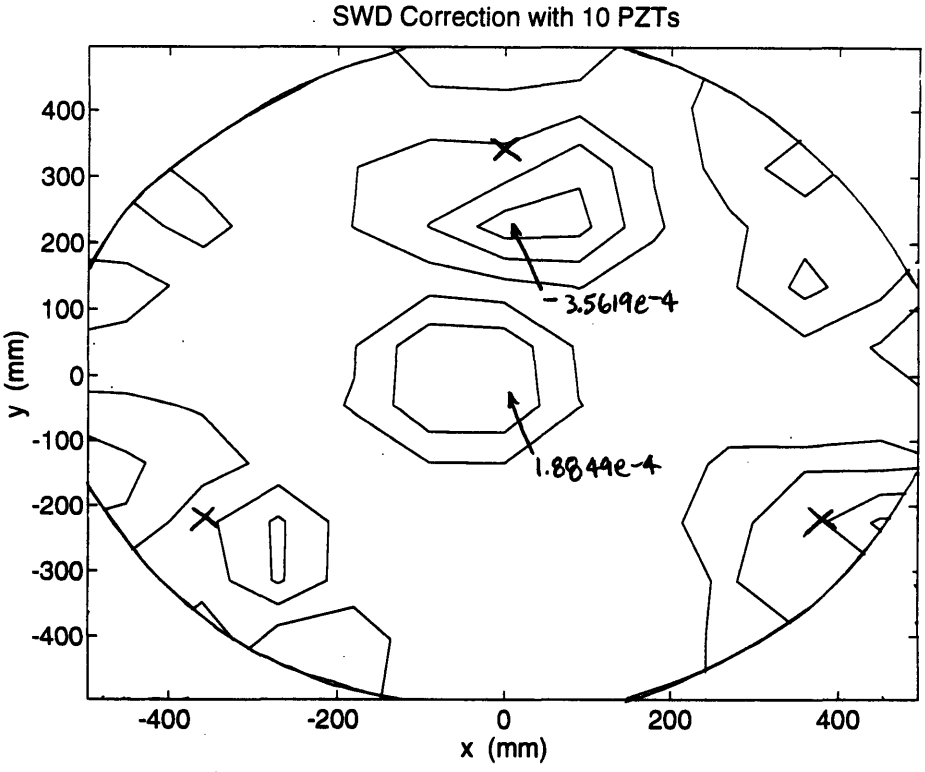

Figure 5-28 SWD Correction Using 10 PZTs with 510V Constraint: Location and Contour (0.1μm contour spacing)

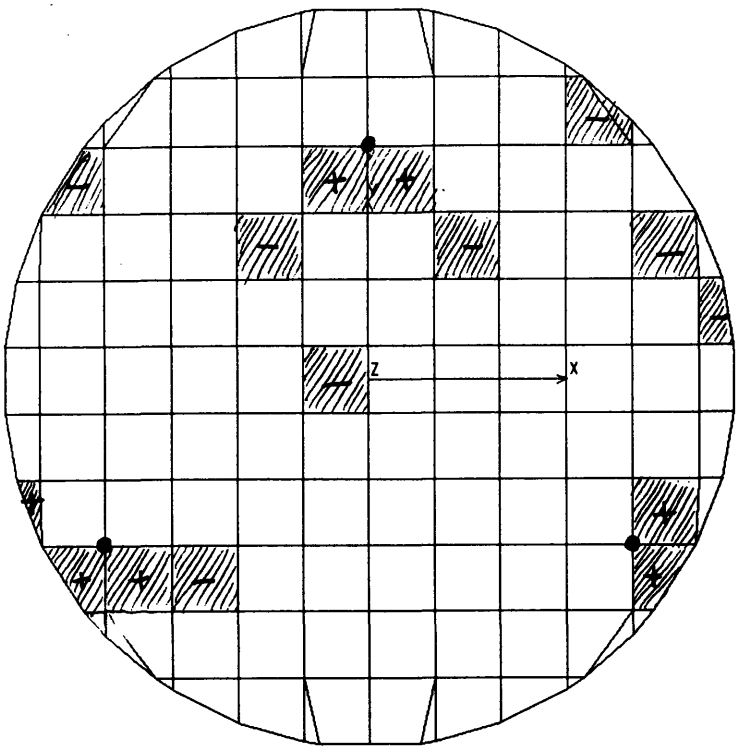

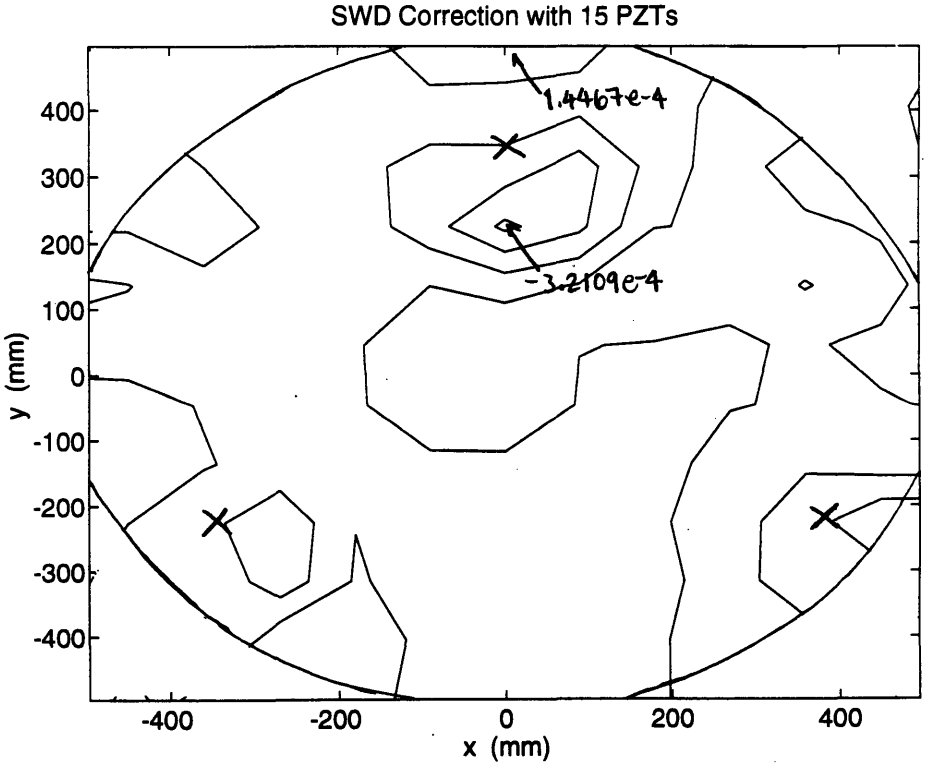

Figure 5-29 SWD Correction Using 15 PZTs with 510V Constraint: Location and Contour (0.1μm contour spacing)

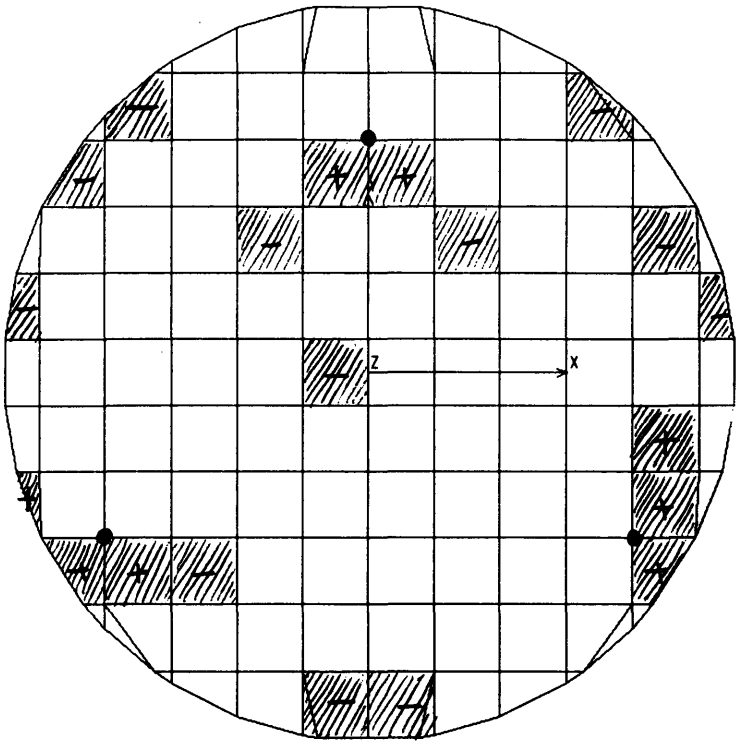

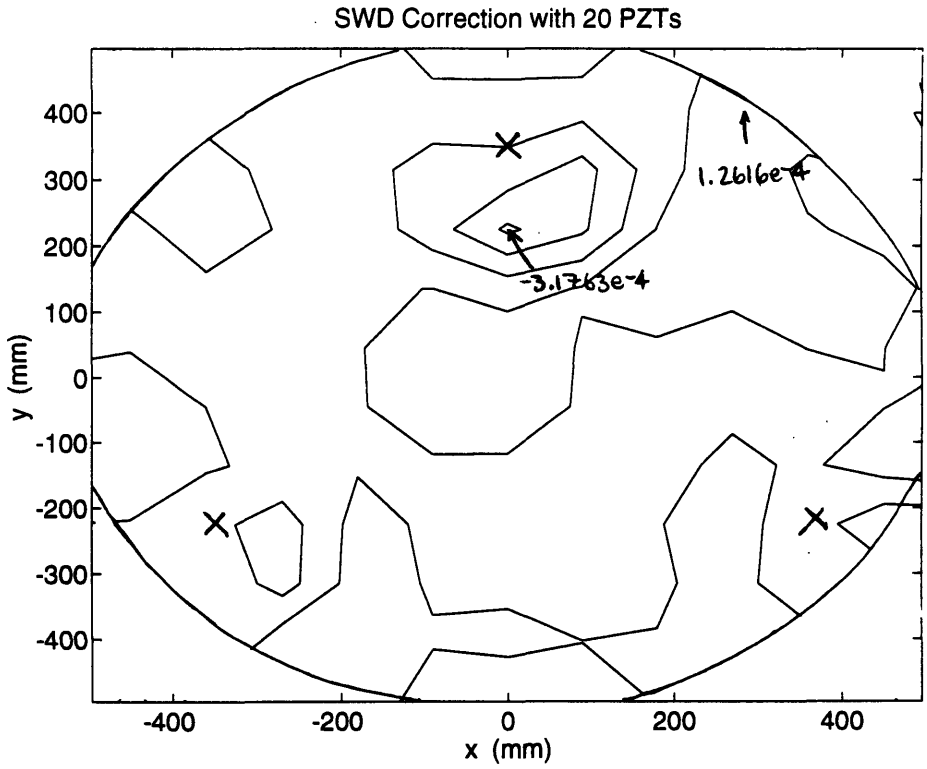

Figure 5-30 SWD Correction Using 20 PZTs with 510V Constraint: Location and Contour (0.1μm contour spacing)

This section concludes very interesting results for self-weight deflection correction using a limited number of piezoceramics. Under no voltage constraints, essentially all the optimal actuation locations are around the support points. This is because an unlimited amount of expansion can occur near the support locations where there is a high downward deflection gradient. Once voltage is constrained, however, a different avenue of optimal placement must be sought by the actuators. Such is accomplished with edge actuations. In general, voltage characteristics are such that actuation expansion is observed around the support points, and actuation contraction is seen elsewhere in the mirror.

5.4 Thermal Deflection Correction by Successive Placement

This section presents the thermal deflection correction results using the successive placement algorithm. Only constrained voltage case is studied because it was shown in the previous section that such a method has the potential to give good results. The 1 Kelvin temperature change is studied. Of course, higher temperature changes can be studied, and they can also be extrapolated from this study.

The first four successive placements of piezoceramics for thermal correction corresponds with that of self-weight deflection correction (see Figure 5-31), with each piezo going to the three location points and the center of the mirror. After that, piezo locations for thermal correction exhibit very different characteristics from that for self-weight correction. There appears to be an even mix of actuator locations, near the support points, on the edge, and in other areas. But in general, each area exhibits expansion characteristics to counter the upward deformation of the mirror. Around the support points, contraction is observed. Again, the merits of this action can be described by a cantilevered beam. Near the root of an upward deflection cantilevered beam, an actuator on the bottom of the beam needs to contract to correct the upward deflection.

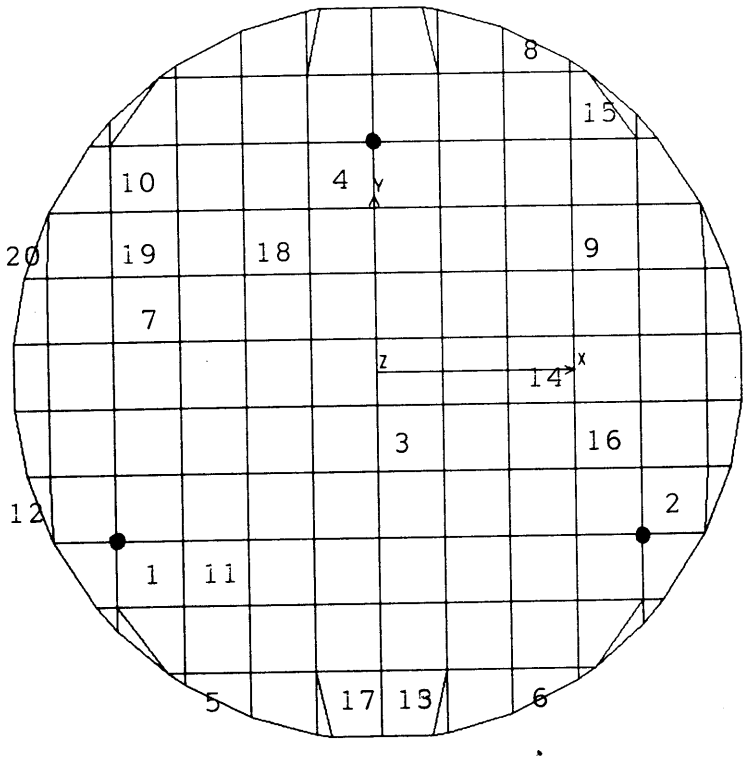

Figure 5-31 Actuation Sequence for Thermal Deflection Correction

Nowhere does actuation voltages exceed the 510V limit. Plotting the number of piezos verses the RMS surface error gives the following characteristics.

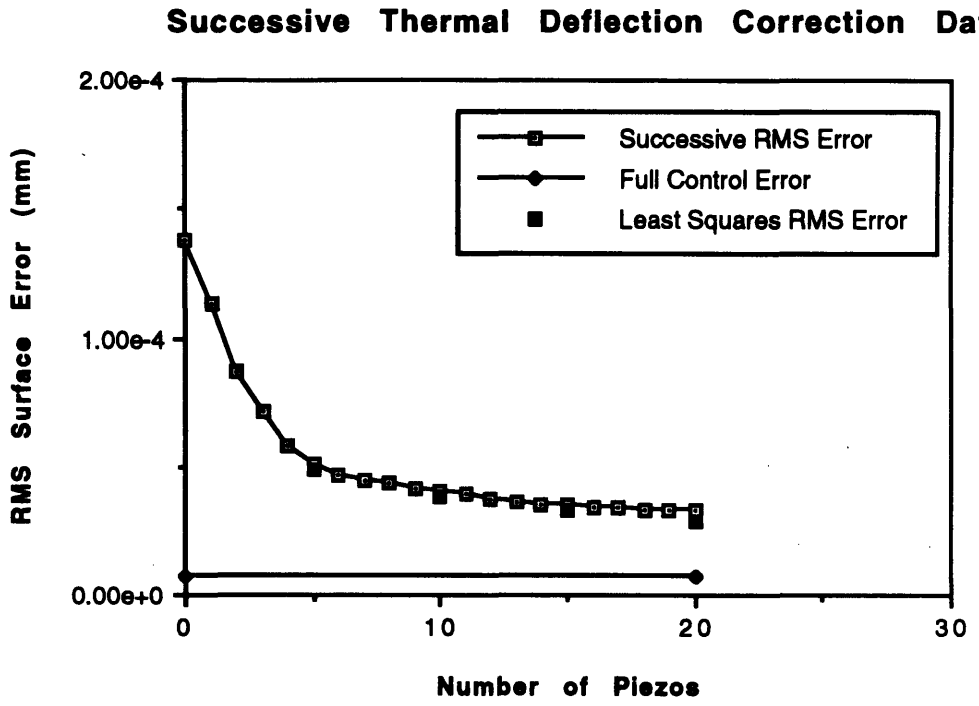

Figure 5-32 RMS Error vs. Number of Piezos for Thermal Deflection Correction

The following contour plots give more detail. Each contour spacing is only 0.1μm since deflections smaller than the quilting deflection really does not matter.

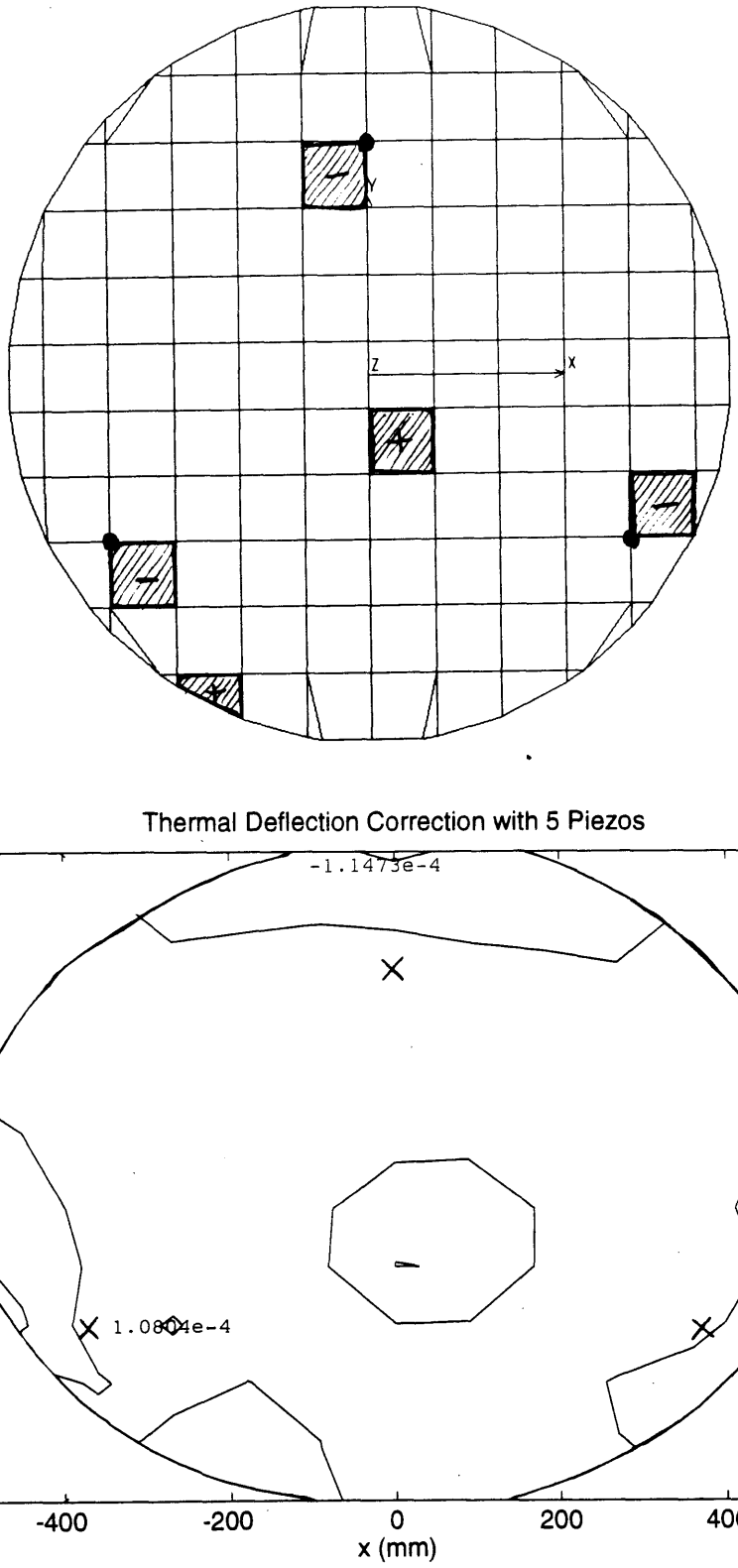

Figure 5-33 Thermal Deflection Correction Using 5 PZTs: Location and Contour (0.1μm contour spacing)

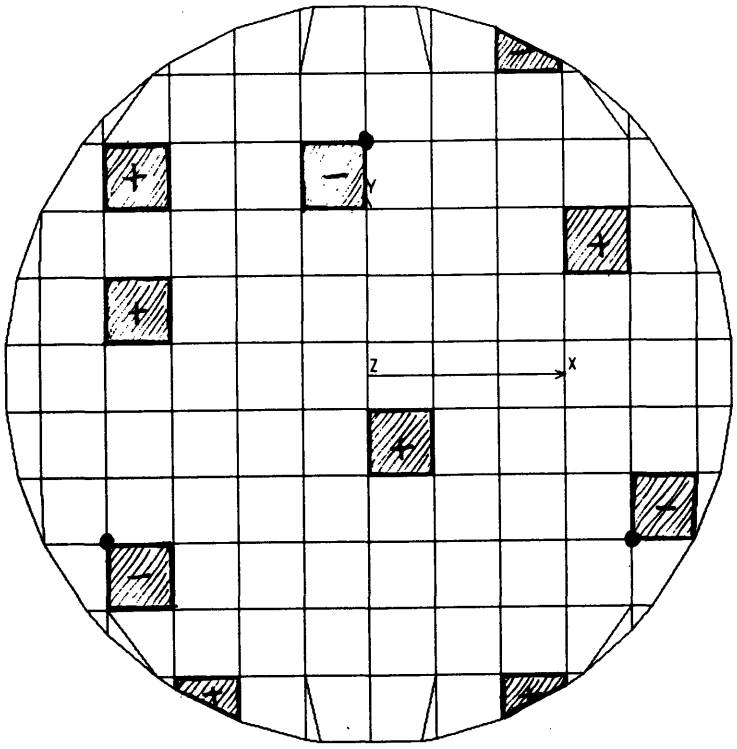

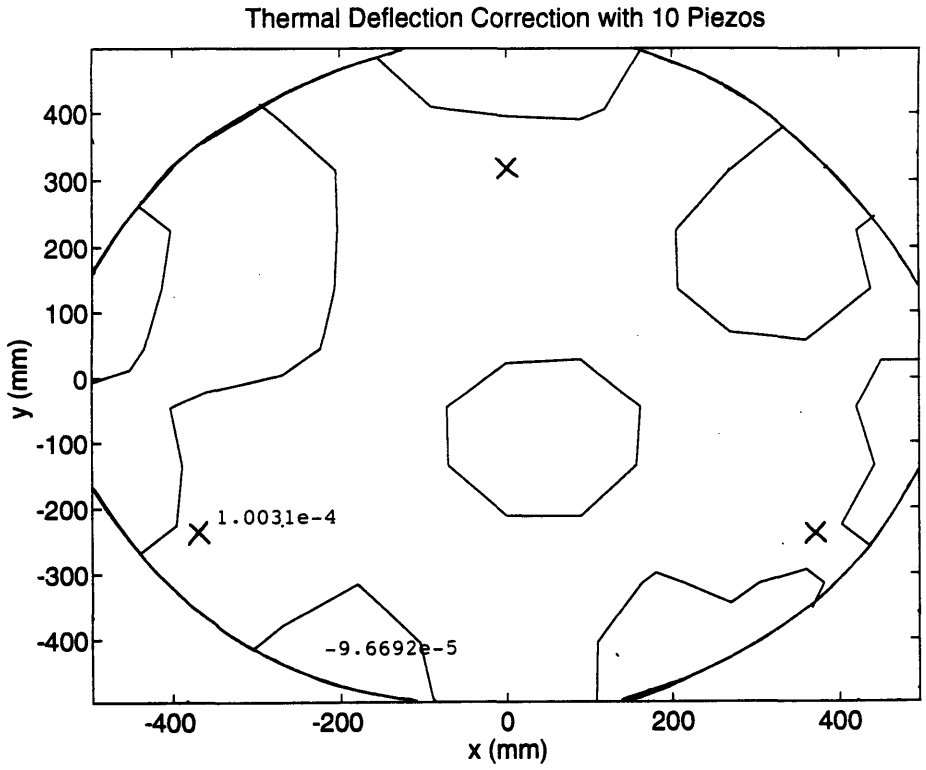

Figure 5-34 Thermal Deflection Correction Using 10 PZTs: Location and Contour (0.1μm contour spacing)

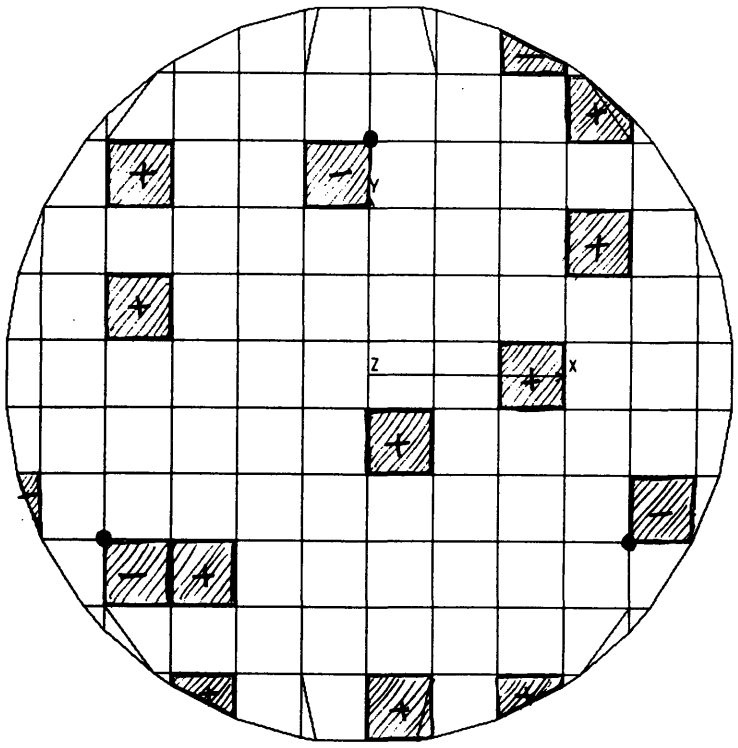

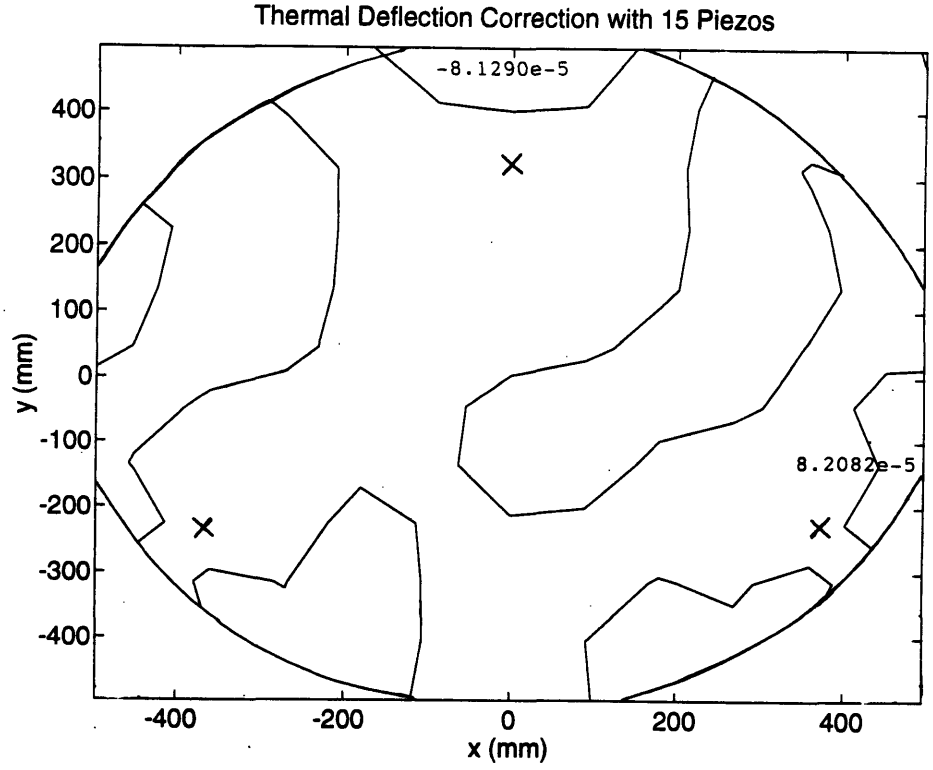

Figure 5-35 Thermal Deflection Correction Using 15 PZTs: Location and Contour (0.1μm contour spacing)

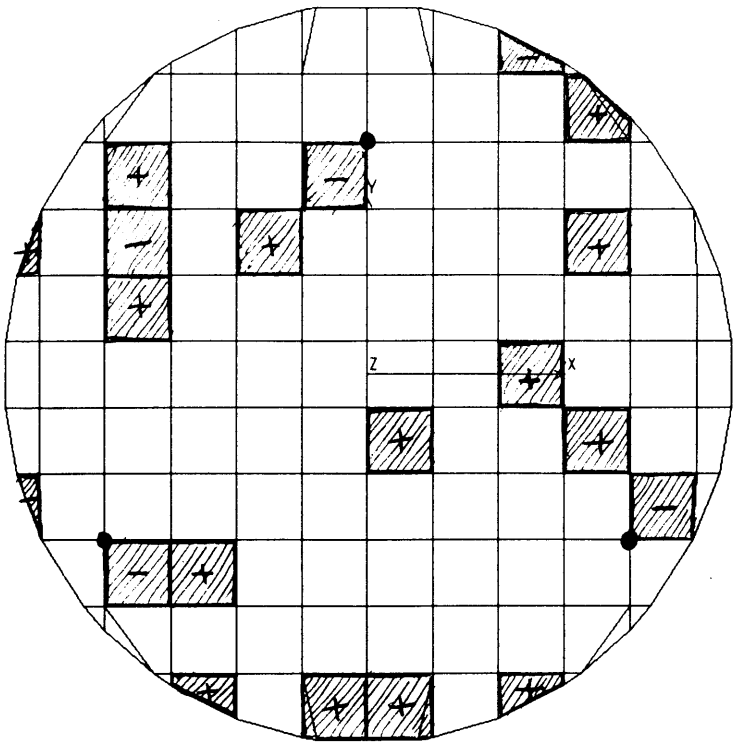

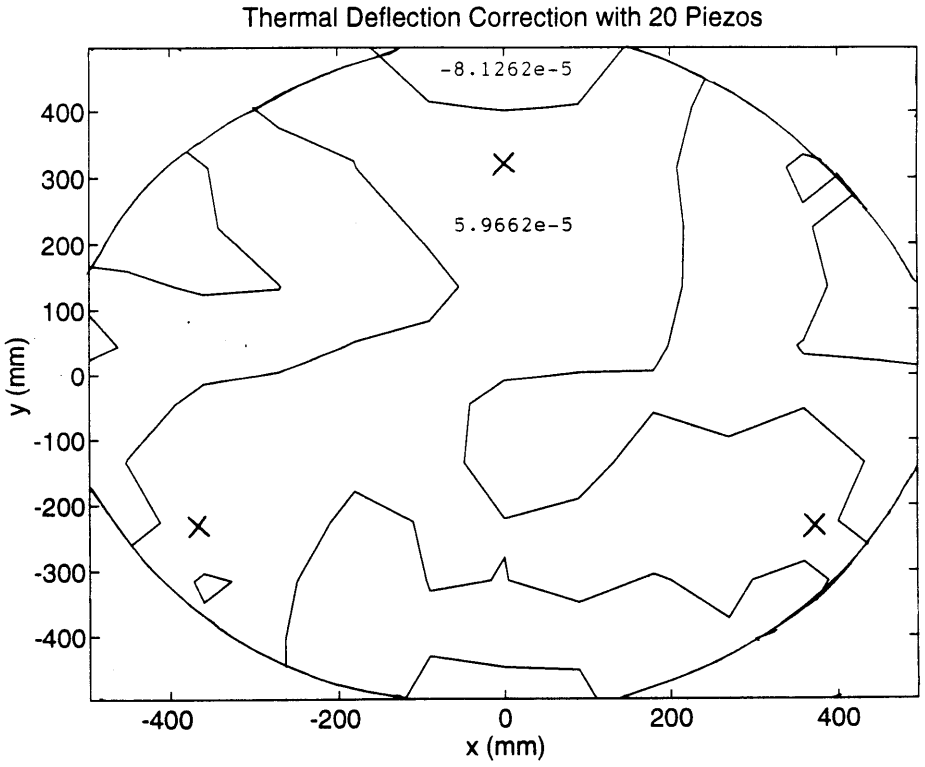

Figure 5-36 Thermal Deflection Correction Using 20 PZTs: Location and Contour (0.1μm contour spacing)

In conclusion, a vast improvement can be seen for both self-weight deflection and thermal deflection correction with a limited number of piezoceramics, where the greatest change in RMS surface error improvement occurs during the first five piezo placements. These first few locations lie around the support locations and the center of the mirror. Error improvement becomes incrementally less with an increased number of piezos. The first fifteen piezoceramics would correct the surface error down to a ratio of 8% of the uncorrected surface for self-weight deflection and 21% for thermal deflection, and this appears to be a good number of piezoceramics to use for either self-weight or thermal deflection correction.

5.5 Summary

Piezoceramics have been shown to be feasible for deflection correction of lightweight mirrors. A layer of piezoceramics on the backsheet of a mirror can correct self-weight deflection down to 2.94% of uncorrected deflection and thermal deflection down to 5.29% of uncorrected deflection using PZT-5H under a 510V field constraint.

Successive placement of optimal locations and actuations of piezoceramics also shows that a limited number of piezos can be used to successfully correct deformations in the mirror. Tables 5-2 and 5-3 summarizes the results under a 510V constraint.

Table 5-3 Summary of Self-Weight Deflection Correction Under 510V Constraint

Number of Piezos	Total Mass (kg)	RMS Error	RMS Error Ratio
116	28.9	2.7300e-5	2.94%
20	21.634	6.7398e-5	7.25%
15	21.255	7.4575e-5	8.03%
10	20.877	9.5610e-5	10.3%
5	20.498	1.3129e-4	14.13%

Figures 5-37 and 5-38 compares the trade-off between RMS surface error and mass of the total mirror system.

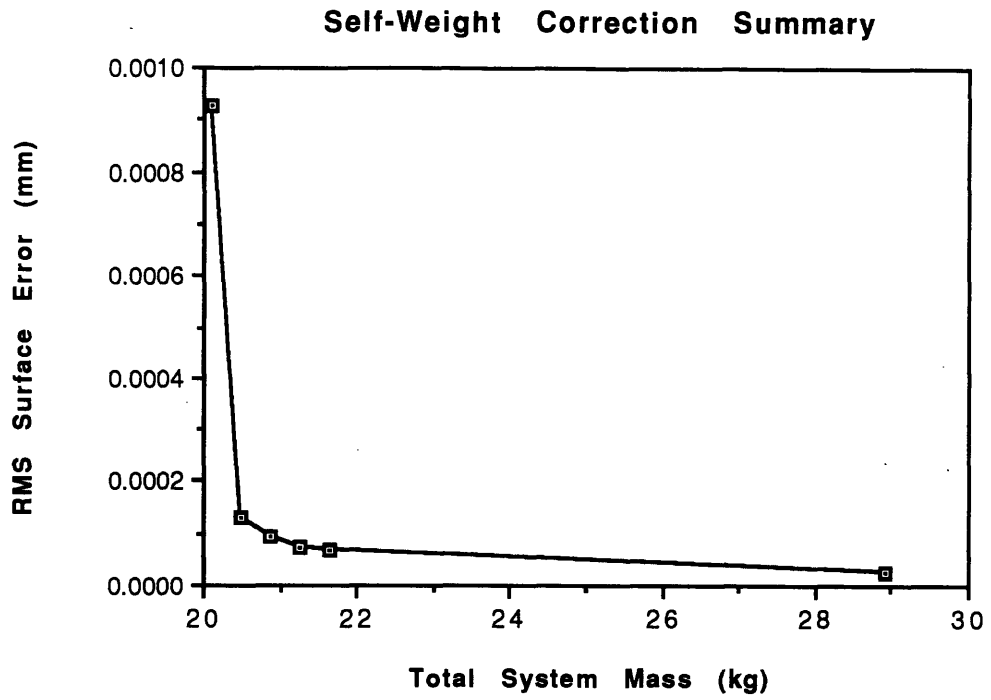

Figure 5-37 Summary of Total Mirror Mass vs. RMS Surface Error for Self-Weight Deflection Correction

From this graph, it can be seen that ten piezoceramics is sufficient for self-weight deflection correction by an order of magnitude.

Table 5-4 Summary of Thermal Deflection Correction Under 510V Constraint

Number of Piezos	Total Mass (kg)	RMS Error	RMS Error Ratio
116	28.9	8.3600e-6	5.29%
20	21.634	2.8628e-5	18.12%
15	21.255	3.3167e-5	20.99%
10	20.877	3.8546e-5	24.40%
5	20.498	4.9105e-5	31.08%

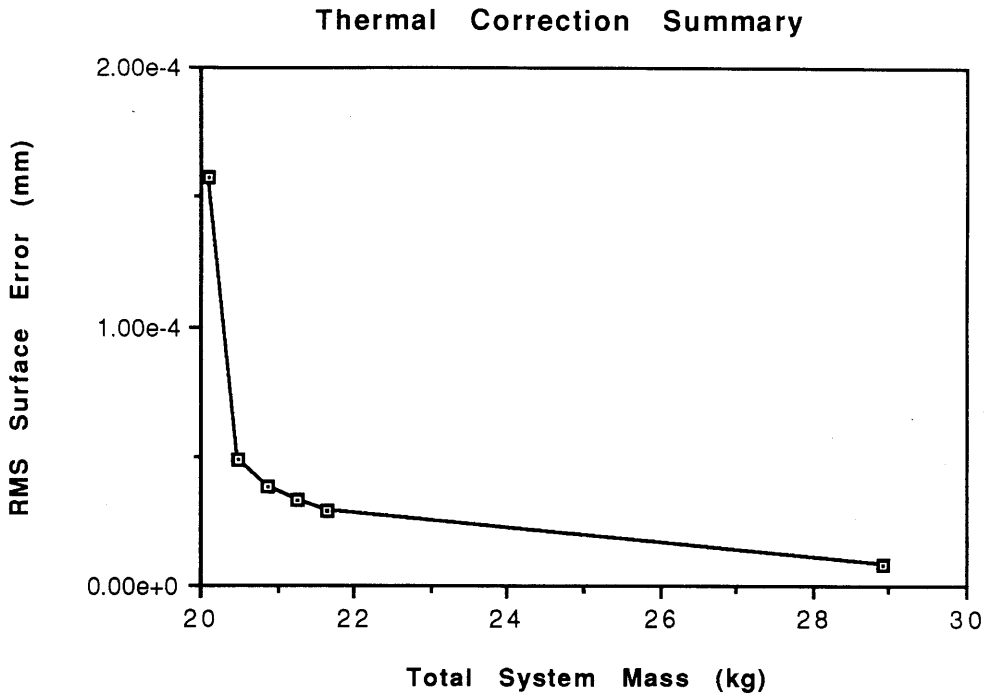

Figure 5-38 Summary of Total Mirror Mass vs. RMS Surface Error for Thermal Deflection Correction

These graphs show that deflection correction is significant even with a small number of piezoceramics. The effectiveness from an actuation to mass standpoint favors the use of a limited number of piezoceramics.

Chapter 6: Conclusions and Recommendations

This thesis has presented a methodology to improve the lightweight mirror design process through more efficient modeling and trade-offs, and to improve lightweight mirror performance through the use of adaptive structures. In this chapter, important results from this study are summarized, conclusions are drawn, and recommendations for future research are made.

The first part of this thesis focused on the development of a more efficient modeling technique for lightweight mirrors. Chapter 2 described an automated finite element mirror modeling and analysis routine developed to accelerate the mirror modeling process and eliminate user modeling errors. Verification of the routine began with a comparison of static deflection solutions for a uniformly loaded solid plate with analytical solutions. The results from a thin shell finite element analysis compared very well with analytical solutions. A similar comparison for a lightweight mirror, however, gave a wide discrepancy between finite element solutions and analytical solutions. This discrepancy is attributed to the fact that the analytical description of a cellular plate uses an equivalent uniform plate model which does not account for in-plane shear and compression of the ribs. These effects can be large near point supports, causing additional sag over the mirror surface. Thus, the finite element model which presents the exact ribbed structure of the mirror can be expected to yield better results. The approach as developed in this chapter met the first objective of this thesis. Finite element modeling of this type of mirrors was shown to give good approximations for self-weight deflection, and the Automatic Mirror Modeling and Analysis (AMMAP) routine made this process very efficient and practical. Future work may (1) further verify the automated finite element models by comparing analytical solutions to finite element models with increasingly small cells, thus making the localized effects less prominent and the mirror more like a continuum structure, to quantify convergence between the two solutions, and (2) develop

better analytical models which take local effects such as shearing and compression of the ribs into account.

Chapter 3 contained a discussion of adaptive material modeling, including the modeling limitations and nonlinear factors which affect modeling accuracy. Once assumptions were set, an analytical solution for a beam was found to verify the modeling accuracy of the piezoelectric ceramic actuators. The Uniform Strain model was used since the experimental beam was designed to have very thin actuators. Finite element analyses which incorporate piezoceramic properties through both a composite layering method and a rigid bars method show excellent correspondence with analytical solutions. They verify that, indeed, the chosen equivalent thermal expansion coefficient used to represent piezoelectric effects is accurate under the assumption of linear piezoelectricity. The composite layering method was then chosen for actuating the lightweight mirror due to its modeling simplicity. Future work should address the actual accuracy of this method when applied to plate and shell structures through experimental and analytical comparisons.

Chapter 4 described the process of lightweight mirror and adaptive lightweight mirror design, including discussions of the various trade-offs which are needed to meet design requirements. Typical design criteria were assumed for a one meter diameter circular mirror with square cells, and trades were made between having the lightest design and having a viable, practical design. A 110mm thick lightweight mirror with 90mm cell width, 5mm facesheet, 3mm backsheet, and 1.5mm rib thickness met all design requirements and was made adaptive with a layer of PZT-5H piezoceramics attached to the backsheet. This layer added considerable weight to the mirror, which translated into greater deflections in the mirror, from 0.98μm to 1.29μm. Analyses to arrive at an "optimal" design indicate that actuation capabilities afforded by thicker piezos outweigh the added deflection due to increased self-weight. The

limiting factor on the piezo thickness, then, is that the additional mass can reduce frequency below requirements and increase mass above requirements.

Finally, the potential deformation corrections offered by piezoceramic actuators bonded to the backsheet of a mirror were quantified. Chapter 5 presented results for actuation profiles derived from surface error minimization. A cost factor associated with the actuation voltage was built into the least squares method, limiting the value of applied field. From this analysis, it was shown that deformations could be reduced by over an order of magnitude while keeping the maximum voltage below the piezoceramic depoling voltage. Even though this method provides excellent correction characteristics, it adds over 8 kg of mass to the mirror. Thus, a trade-off of piezoceramic correction effect to mass was considered by restricting the number of actuators. An optimal placement routine was used, and both self-weight deflection correction and thermal deflection correction analyses gave RMS surface deflections of less than 20% of the uncorrected deflection. Thus, results from this chapter met the second goal of this thesis. Piezoelectric elements are feasible for correcting self-weight deflection and thermal deflection up to 5 Kelvin. This is assuming simply supported mirror mounts. Future work may consider the thermal deflection correction of mirrors on kinematic mounts.

Some general suggestions for more detailed mirror modeling and optimization analysis include the following. Mirrors are often designed with some specified curvature for beam steering purposes, and this makes deflections in the planar direction just as important as deflections in the z-direction. In order to apply the methods used in this thesis, a different set of coordinate axes must be defined. Afterall, piezoceramic expansions and contractions affect mirror deflections in all directions, and for a curved mirror such deformations affect the mirror's performance. One way to approach this problem may be to define a normal axis to the mirror's surface and relate displacements in all three directions to one displacement in

this direction. Then, the least squares approach and the successive placement scheme which find solutions based on one variable can be used.

Detailed mirror modeling may also benefit from accounting for the added mass and stiffness of each piezoceramic in the successive placement algorithm. This would also be important because piezoceramics may exhibit considerable thermal effects due to their high coefficient of thermal expansion. For this reason, other materials such as low CTE electrostrictives and low temperature magnetostrictives should also be studied.

Another change in the successive placement algorithm to obtain appropriate voltage and location profiles for large deflection corrections may be to incorporate a cost factor to limit the applied field. In this way, instead of truncating voltages over a specified limit, the cost factor can be used to directly limit voltages to below the specified limit throughout the optimization process.

As mentioned in Chapter 5, more extensive placement optimization routines are available for use, including ones developed originally for truss analysis. Such techniques may give near optimal solutions, depending on the depth in which analysis is conducted. Ref.[42] details and compares the algorithms for Worst-Out-Best-In (WOBI), Improved Simulated Annealing (ISA), and Exhaustive Single Point Substitution (ESPS). These algorithms should be considered should optimal placement be a major consideration in mirror design.

Finally, the accuracy of the mirror analysis as presented here may be compared to experimental results to insure that this first order study is applicable for detailed design and evaluations.

References:

[1] _____, *COSMOS/M Finite Element System User Guide*, 5th ed., version 1.65, Structural Research and Analysis Corporation, CA, July 1991.

[2] _____, *Guide to Modern Piezoelectric Ceramics*, Morgan Matroc Inc., Electro Ceramics Division, Bedford, OH, 1993.

[3] _____, *Isogrid Design Handbook*, McDonnell Douglas Astronautics Company, Huntington Bch, CA, 1973.

[4] _____, *Piezoelectric Technology Data for Designers*, Morgan Matroc Inc., Electro Ceramics Division, Bedford, OH, 1993.

[5] _____, *IEEE Standard on Piezoelectricity*, Institute of Electrical and Electronics Engineers, Inc., New York, NY, 1978.

[6] Anderson, Eric H., and Nesbitt W. Hagood, "The effect of modal error on actuator and damper placement for structural control", SPIE Paper No. 1917-65, presented at SPIE North American Conference of Smart Structures, Albuguerque, 1993.

[7] Apollonov, V.V., A.M. Prokhorov, S.N. Temnov, and S.A. Chetkin, "Adaptive deformable mirror with piezoelectric ceramic actuators", *Soviet J. Quantum Electron.*, Vol. 18, No. 12, December 1988. See 1989 American Institute of Physics, pp. 1621-1622.

[8] Apollonov, V.V., G.V. Vdovin, E.A. Ivanova, A.M. Prokhorov, and S.A. Chetkin, "Analytic model of an adaptive mirror in the form of a thin plate with discrete actuators", *Soviet J. Quantum Electron.*, Vol. 20, No. 11, November 1990. See *1991 American Institute of Physics*, pp. 1414-1418.

[9] Aspinwall, D.M., and T.J. Karr, "Improved Figure Control with Edge Application of Forces and Moments", SPIE, Vol. 228, Active Optical Devices and Applications, 1980.

[10] Backhaus, Brent J. and Steven Forman, "Active surface correction of metallic honeycomb sandwich mirrors", *Proc. SPIE*, Vol. 1303, pp. 20-32, 1990.

[11] Barnes, William P., Jr., "Optimal Design of Cored Mirror Structures", *Applied Optics*, Vol. 8, No. 6, 1969.

[12] Beckers, Jacques M., and Fritz Merkle, "A survey of present efforts in astronomical adaptive optics", *Proc. SPIE*, Vol. 1130, 1989.

[13] Cagan, Jonathan and Victor Genberg, "PLASHTRAN: An expert consultant on two-dimensional finite element modeling techniques", *Engineering with Computers*, 2, pp.199-208, 1987.

[14] Chiarappa, D.J., and C.R. Claysmith, "Deformable Mirror Surface Control Techniques", *J.of Guidance and Control*, Vol. 4, No.1, 1981.

[15] Cho, Myung K., Ralph M. Richard, and Daniel Vukobratovich, "Optimum mirror shapes and supports for light weight mirrors subjected to self-weight", *SPIE Proc.*,

Vol. 1167, pp. 2-19, Aug 1989.

[16] Crawley, E.F., and J. de Luis, "Use of Piezo-Ceramics as Distributed Actuators in Large Space Structures," AIAA SDM Conf., Paper No. 85-0626, pp. 126-133, 1985.

[17] Crawley, E.F., and E.H. Anderson, "Detailed Models of Piezoceramic Actuation of Beams", Journal of Intelligent Material Systems and Structures, Vol. 1, pp.4-25, 1990.

[18] Crowe, David A., "Ultra Lightweight Mirror Performance at 8 Degrees Kelvin", SPIE Vol. 509 *Cryogenic Optical Systems and Instruments*, 1984.

[19] Ealey, M.A., "Deformable Mirrors at Litton/ Itek: A Historical Perspective", *SPIE*, Vol. 1167, pp. 48-65, 1989.

[20] Ealey, Mark A., and John Wellman, "Fundamentals of Deformable Mirror Design and Analysis", *SPIE*, Vol. 1167, pp. 66-84, 1989.

[21] Everson, J.H., R.E. Aldrich, M. Cone, and J. Kenemuth, "Device parameters and optical performance of a stacked actuator deformable mirror", *Proc. SPIE*, Vol. 228, pp. 34-40, 1980.

[22] Hagood, Nesbitt W., Walter H. Chung, and Andreas von Flotow, "Modeling of Piezoelectric Actuator Dynamics for Active Structural Control", AIAA-90-1087-CP.

[23] Hagood, Nesbitt, and Andreas von Flotow, "Damping of Structural Vibrations with Piezoelectric Materials and Passive Electrical Networks", *Journal of Sound and Vibrations*, Vol. 146, pp. 243-268, 1991.

[24] Hall, E.K., "Modeling of Piezoceramic Actuators Bonded to Beam Structures", Aerospace Technical Memorandum 92(8187)-1, June 1992. Inter-Aerospace Corp. Distribution Only.

[25] Hall, E.K., conversation on May 18, 1993.

[26] Herring, Mark, James E. Duval, and Steven A. Macenka, "Development of the imaging spectrometer: technical challenges and solutions", *Proc. SPIE*, Vol. 810, pp. 100-111, 1987.

[27] ed. Hogan, Walter H., and Trevor S. Moss, Cryogenics and Infrared Detection, Boston Technical Publishers, Inc., Cambridge, MA, pp. 8-20, 1970.

[28] How, J.P., E. H. Anderson, D.W. Miller, and S.R. Hall, "High bandwidth control for low area density deformable mirrors", *1991 SPIE Aerospace Sensing Conference*, 1489-19.

[29] Jamieson, Thomas H., "Thermal effects in optical systems", *Optical Engineering*, Vol. 20, No. 2, pp. 156-160, March/April 1981.

[30] Khesin, G.L., S.V. Lyubarskii, E.M. Shvei, and A.L. Shchetinin, "Modeling and optimization of the parameters of light-weight mirrors of optical systems" *Soviet Journal of Optical Technology*, Vol. 55, No. 8, August 1988. See The Optical Society of America, pp. 496-499.

[31] Lazarus, Kenneth B., "Induced Strain Actuation of Composite Plates",Massachusetts Institute of Technology Master's Thesis, Department of Aeronautics and Astronautics, June 1989.

[32] Loboda, Gregory G., "Performance Enhancement of Segments Infrared Reflectors via Quasistatic Shape Control", Massachusetts Institute of Technology Master's Thesis, Department of Aeronautics and Astronautics, June 1992.

[33] Luu, K., "Ultra-Lightweight Optics Design Program", Unnumbered Aerospace Interoffice Correspondence, 3 Dec. 1990. Inter-Aerospace Corp. Distribution Only.

[34] Luu, K., conversations between July 1992 - December 1992.

[35] Mahajan, Virendra N., Jacques Govignon, and Ricky J. Morgan, "Adaptive optics without wavefront sensors", *Proc. SPIE*, Vol. 228, pp. 63-69, 1980.

[36] ed. Mattiat, O.E., Ultrasonic Transducer Materials, Plenum Press, New York, 1971. Chapter 2 Piezoelectric Crystals and Ceramics, contributed by Don Belincourt.

[37] Mehta, Pravin K., "Flexural rigidity characteristics of light-weighted mirrors", *Proc. SPIE*, Vol. 748, pp. 158-171, 1987.

[38] Mehta, Pravin K., "Moment actuator influence function for flat circular deformable mirrors", *Proc. SPIE*, Vol. 1303, pp. 2-19, 1990.

[39] Meyer, R.R., "Isogrid- A simple, efficient, stiffening concept", AIAA No. 73-365, *AIAA/ASME/SAE Conference*, March 20-22, 1973.

[40] Niemiec, "Structural analysis of an adaptive primary mirror", *AIAA/ASME/SAE Conference*, 1992.

[41] Ojalvo, I.U. "Will finite elements replace structural mechanics?", *Proc. SPIE*, Vol. 450, pp. 110-117, 1983.

[42] Onoda, Junjiro, and Yoji Hanawa, "Optimal locations of actuators for statistical static shape control of large space structures: a comparison of approaches", AIAA-92-2558, pp. 2788-2795.

[43] Orringer, Oscar, and Pin Tong, "Uses and abuses of the finite element method", *Proc. SPIE*, Vol. 450, pp. 2-33, 1983.

[44] Paimushin, V.N., I. Kh. Saitov, and V.D. Derevenskii, "The mathematics for a more precise calculation of the deformation of light-weight mirrors", *Soviet Journal of Optical Technology*, Vol. 50, No. 1, January 1983. See 1983 The Optical Society of America, pp. 11-13.

[45] Pepi, John W. "Analytical predictions for lightweight optics in a gravitational and thermal environment", *Poc. SPIE*, Vol. 748, pp. 172-179, 1987.

[46] Pepi, John W., and William P. Barnes, Jr., "Thermal Distortion of a Thin Low Expansion Fused Silica Mirror", AIAA/ASME/SAE Conference, 1992.

[47] Pollard, W., D. Vukobratovich, and R. Richard, "The structural analysis of a light-

weight aluminum foam core mirror", *SPIE*, Vol. 748, pp. 180-186, 1987.

[48] Robachevskaya, V.I., and G.V. Rodkevich, "A study of the stiffness of light-weight mirrors of various constructions", *Soviet Journal of Optical Technology*, Vol. 44, No. 1, January 1977. See 1977 The Optical Society of America, pp. 6-9.

[49] Sepulveda, A.E., I.M. Jin, and L.A. Schmit, Jr., "Optimal placement of active elements in control augmented structural synthesis", AIAA-92-2557, pp. 2768-2787.

[50] Strang, Gilbert, Introduction to Applied Mathematics, Wellesley-Cambridge Press, Wellesley, MA, 1986.

[51] Timoshenko, S., and S. Woinowsky-Krieger, Theory of Plates and Shells, 2nd ed., McGraw-Hill, New York, 1959.

[52] Valente, Tina M. and Daniel Vukobratovich, "A comparison of the merits of open-back, symmetric sandwich, and contoured back mirrors as light-weighted optics", *SPIE Proc.*, Vol. 1167, pp. 20-36, Aug 1989.

[53] Vukobratovich, Daniel, "Optimum shapes for lightweighted mirrors", *SPIE*, Vol. 332, *Advanced Technology Optical Telescopes*, 1982.

[54] Vukobratovich, Daniel, "Ultra-lightweight optics for laser communications", *SPIE*, Vol. 128, pp. 178-192, 1990.

[55] Williams, R., and H.F. Brinson, "Circular Plate on Multipoint Supports", *Journal of The Franklin Institute*, Vol. 297, No. 6, June 1974.

[56] Wong, Woon-Ying, "Thermal measurements and control of a lightweight mirror", McDonald Observatory, University of Texas, Austin.

[57] Yoder, Paul R. Jr., Opto-Mechanical Systems Design, Marcel Dekker, Inc., New York, 1986.

Appendix A Abridged Version of AMMAP

```
 * AMMAP.c *
 * Written by Celia H. Liu with consultation from Eric K. Hall *
 * This program reads an input file generated by the graphics routine "node_gen"
   and writes into an output file COSMOS/M commands that build a lightweight
   mirror finite element model */
 * It is able to accommodate: Circular, Rectangular, and Pseudoelliptical
   mirrors with either: Square, Triangular, or Hexagonal cell shapes *
 * Everything is in or converted to millimeters */

 * For this appendix, an abridged version which generates the Rectangular Cells
   is presented */

#include <stdio.h>
#include <math.h>

#define MAXPT 200       /* 500 */  /* These numbers describe the target constants */
#define MAXDIM 22       /* 50 */   /* which can make this program more versatile */
#define MAXSURF 1000    /* 5000 */ /* Currently this compiler will not accommodate */
#define NO_NODE -1                 /* these due to lack of disk space */
#define NO_ID   -1                 /* Workstations may accommodate more */

FILE *fopen(), *inputdata, *outputdata;
int surface[MAXSURF], sf;

struct node2   /* rearranged from structure node1 in function main */
{
        int no;          /* node # */
        int id;          /* status:      0= intersection of ribs
                                          1= intersection of rib w/ edge
                                          2= double points on boundary
                                          3= triple points on boundary  */
        float x,y,z;     /* coordinates of the points */
}       point2[MAXDIM][MAXDIM][6];

struct node2 temp1, temp2;
int r, rn, edge_band;

int start_back, start_rib, start_edge;
int no_front, no_back, no_rib, no_edge;

int rectangle_facesheet_generation (void);
int rectangle_rib_generation (int r);
int rectangle_edge_generation (int r);

void initialization (void);
void rec_swap(int a, int b);
void material_library (int material);
float curvature (float ptx, float pty);

float curv,K,A,B,C,D;
float x_offset, y_offset;   /* Offset from parent mirror */
float x_cell, y_cell;       /* Offset from cell center */

int main(void)
{
        extern FILE *fopen(), *inputdata, *outputdata;
        int mirror_dimension, mirror_type, material, rib_shape;
        extern int edge_band;
        float mirror_thickness, facesheet_thickness, backsheet_thickness;
        float rib_thickness, edge_thickness;
        char mirror_curvature, tol_change;
        float factor, tolerance;
        float ex, dens, nuxy;

        float distance, diagonal;
        float x0,y0,x02,y02;
```

```
        float x1,y1,x12,y12;

        int i,u,v,w,a,b,f,g;
        int p,q,s;
        int tot_sf, sfcount, count1, count2, count11;
        char junk[80];

        struct node1
        {                       /* reading in the input file */
                int no;         /* node # */
                int m,n;        /* coordinates of grid overlay */
                int id;         /* Same status as described in structure node2 */
                float x,y,z;    /* coordinates of the points */
        } point1[MAXPT];

        extern struct node2 point2[][][];
        extern struct node2 temp1, temp2;
        extern float curv,K,A,B,C,D;
        extern float x_offset,y_offset;
        extern float x_cell, y_cell;

/* Read in specifications from user */

        printf("How would you like to input mirror dimensions?\n");
        printf("Make sure this corresponds to dimensions from program NODE_GEN\n");
        printf("1  In millimeters\n");
        printf("2  In meters\n");
        printf("3  In inches\n");
        scanf("%d", &mirror_dimension);
        if (mirror_dimension == 2)
                factor = 1000.0;
        else if (mirror_dimension == 3)
                factor = 25.4;
        else factor = 1.0;

        printf("Input an integer for mirror type\n");
        printf("1  Open back mirror\n2  Close back mirror\n");
        scanf("%d", &mirror_type);

        printf("Input an integer for material type\n");
        printf("1  Silicon Carbide (SiC)\n2  Beryllium (Be)\n3  Fused Silica (SiO2)\n");
        printf("4  Aluminum (Al)\n5  Zerodur\n");
        scanf("%d", &material);

        printf("Input mirror thickness\n");
        scanf("%f", &mirror_thickness);
        mirror_thickness = factor * mirror_thickness;

        printf("Input face sheet thickness\n");
        scanf("%f", &facesheet_thickness);
        facesheet_thickness = factor * facesheet_thickness;

        if (mirror_type == 2)
        {
                printf("Input back sheet thickness\n");
                scanf("%f", &backsheet_thickness);
                backsheet_thickness = factor * backsheet_thickness;


        }

        printf("Input an integer for rib support shape\n");
        printf("1  Rectangular\n2  Triangular\n3  Hexagonal\n");
        scanf("%d", &rib_shape);

        printf("Input rib support thickness\n");
```

```
scanf("%f", &rib_thickness);
rib_thickness = factor * rib_thickness;

printf("Is there an edge band around the mirror?\n");
printf("1  No edge band\n2  Edge band\n");
scanf("%d", &edge_band);
if (edge_band == 2)
{
        printf("Input edge band thickness\n");
        scanf("%f", &edge_thickness);
        edge_thickness = factor * edge_thickness;
}

printf("Does the mirror have curvature?  (y or n)");
scanf("%s", &mirror_curvature);
if (mirror_curvature =='y')
{
        printf("Input mirror parameters as given directly from Code 5\n");
        printf("No conversion is needed\n");
        printf("CURV?\t");
        scanf("%f", &curv);
        printf("K?\t");
        scanf("%f", &K);
        printf("A?\t");
        scanf("%f", &A);
        printf("B?\t");
        scanf("%f", &B);
        printf("C?\t");
        scanf("%f", &C);
        printf("D?\t");
        scanf("%f", &D);

        printf("Input mirror center offset from parent mirror\n");
        printf("x offset?\t");
        scanf("%f", &x_offset);
        x_offset = factor * x_offset;

        printf("y offset?\t");
        scanf("%f", &y_offset);
        y_offset = factor * y_offset;
}
else
{
        curv = 0.0;
        K = 0.0;
        A = 0.0;
        B = 0.0;
        C = 0.0;
        D = 0.0;
        x_offset = 0.0;
        y_offset = 0.0;
}

printf("Input mirror center offset from cell center\n");
printf("(This is the same as the one for graphics routine)\n");
printf("x cell offset?\t");
scanf("%f", &x_cell);
x_cell = factor * (0 - x_cell);

printf("y cell offset?\t");
scanf("%f", &y_cell);
y_cell = factor * (0 - y_cell);

printf("Default tolerance for merging COSMOS/M nodal points is 0.0001\n");
printf("Would you like to change it?  (y or n)\n");
scanf("%s", &tol_change);
```

```
        if (tol_change == 'y')
        {
                printf("Please specify desired tolerance\n");
                scanf("%f", &tolerance);
        }
        else if (tol_change == 'n')
                tolerance = 0.0001;

* Read input points from input file */
* And rearrange input data into workable sequence */

        inputdata = fopen("node.dat","r");
        if (inputdata == NULL)
        {
            printf("Can't open input file\n");
            return 0;
        }
        else printf("Input Process Started\n");

        initialization();
        fgets(junk,80,inputdata);
        i = 1;
        while (fscanf(inputdata,"%d%d%d%d%f%f", &point1[i].no,
                  &point1[i].m, &point1[i].n, &point1[i].id,
                  &point1[i].x, &point1[i].y) == 6)
                {
                  point1[i].x = factor * point1[i].x;
                  point1[i].y = factor * point1[i].y;
                  point1[i].z = 0 - curvature(point1[i].x, point1[i].y);

                  p = point1[i].m;
                  q = point1[i].n;

                  if (point2[p][q][1].no != NO_NODE)
                  {
                        point2[p][q][2].no = point1[i].no;
                        point2[p][q][2].id = point1[i].id;
                        point2[p][q][2].x = point1[i].x;
                        point2[p][q][2].y = point1[i].y;
                        point2[p][q][2].z = point1[i].z;
                  }
                  else if (point2[p][q][0].no != NO_NODE)
                  {
                        point2[p][q][1].no = point1[i].no;
                        point2[p][q][1].id = point1[i].id;
                        point2[p][q][1].x = point1[i].x;
                        point2[p][q][1].y = point1[i].y;
                        point2[p][q][1].z = point1[i].z;
                  }
                  else
                  {
                        point2[p][q][0].no = point1[i].no;
                        point2[p][q][0].id = point1[i].id;
                        point2[p][q][0].x = point1[i].x;
                        point2[p][q][0].y = point1[i].y;
                        point2[p][q][0].z = point1[i].z;
                  }
                  i++;
                }
        fclose(inputdata);


/* Rearrange status 2 and above nodes into specific order */

/* For double points of rectangular ribs, the point further from the center
   of the x dimension is labeled in the [1] array */
```

```
    if (rib_shape == 1)
    {
        for (b=0; b< MAXDIM; b++)
            for (a=0; a< MAXDIM; a++)
                if (point2[a][b][0].no != NO_NODE && point2[a][b][1].no != NO_NODE)
                        rec_swap(a,b);
    }


/* Print mirror specifications into outputfile */

        outputdata = fopen("fem.out","w");
        if (outputdata == NULL)
        {
                printf("Can't open output file\n");
                return 0;
        }
        else printf("Model Generation Output Process    rted\n");


/* Rename the points in increasing m and n order */
/* Generate COSMOS/M points of mirror facesheet */

        s=1;
        for (u=0; u< MAXDIM; u++)
            for (v=0; v< MAXDIM; v++)
                for (w=0; w< 3; w++)
                        if (point2[u][v][w].no != NO_NODE)
                        {
                                point2[u][v][w].no = s;
                                fprintf(outputdata,"PT,%d,%.6f,%.6f,%.6f\n",
                                        point2[u][v][w].no, point2[u][v][w].x,
                                        point2[u][v][w].y, point2[u][v][w].z);
                                s++;
                        }
        fprintf(outputdata,"SCALE,0\n");


/* Generate points on mirror backsheet */

        for (f=0; f< MAXDIM; f++)
            for (g=0; g< MAXDIM; g++)
            {
                if (point2[f][g][0].no != NO_NODE)
                {
                        point2[f][g][3].no = s;
                        point2[f][g][3].id = point2[f][g][0].id;
                        point2[f][g][3].x = point2[f][g][0].x;
                        point2[f][g][3].y = point2[f][g][0].y;
                        point2[f][g][3].z = point2[f][g][0].z - mirror_thickness;
                        fprintf(outputdata, "PT,%d,%.6f,%.6f,%.6f\n",
                                point2[f][g][3].no, point2[f][g][3].x,
                                point2[f][g][3].y, point2[f][g][3].z);
                        s++;
                }
                if (point2[f][g][1].no != NO_NODE)
                {
                        point2[f][g][4].no = s;
                        point2[f][g][4].id = point2[f][g][1].id;
                        point2[f][g][4].x = point2[f][g][1].x;
                        point2[f][g][4].y = point2[f][g][1].y;
                        point2[f][g][4].z = point2[f][g][1].z - mirror_thickness;
                        fprintf(outputdata, "PT,%d,%.6f,%.6f,%.6f\n",
                                point2[f][g][4].no, point2[f][g][4].x,
                                point2[f][g][4].y, point2[f][g][4].z);
```

```
                        s++;
                }
                if (point2[f][g][2].no != NO_NODE)
                {
                        point2[f][g][5].no = s;
                        point2[f][g][5].id = point2[f][g][2].id;
                        point2[f][g][5].x = point2[f][g][2].x;
                        point2[f][g][5].y = point2[f][g][2].y;
                        point2[f][g][5].z = point2[f][g][2].z - mirror_thickness;
                        fprintf(outputdata, "PT,%d,%.6f,%.6f,%.6f\n",
                                point2[f][g][5].no, point2[f][g][5].x,
                                point2[f][g][5].y, point2[f][g][5].z);
                        s++;
                }
        }


/* Generate COSMOS/M surfaces */

        printf("Generating surfaces\n");

if (rib_shape == 1)                     /* Generate rectangular surfaces */
 {
        no_front = rectangle_facesheet_generation();
          start_rib = no_front + 1;
          fprintf(outputdata,"C*\t There are %d front surfaces\n", no_front);

        no_rib = rectangle_rib_generation (start_rib);
          start_edge = no_rib + 1;
          fprintf(outputdata,"C*\nC*\tSurfaces %d through %d make up Rib Supports\nC*\n"!
                                start_rib, no_rib);
        tot_sf = no_rib;

        if (edge_band == 2)
        {
          no_edge = rectangle_edge_generation (start_edge);
          tot_sf = no_edge;
          fprintf(outputdata,"C*\nC*\tSurfaces %d through %d make up Edge Band\nC*\n",
                                start_edge, no_edge);
        }
 }


/* Define material properties */

        fprintf(outputdata,"EGROUP,1,SHELL4T,1,0,0,0,0,0,0,\n");
        material_library (material);

/* Mesh facesheet surface */

        count1 = 0;
        fprintf(outputdata,"RCONST,1,1,,1,%.3f\n", facesheet_thickness);
        for (sf=1; sf<= no_front; sf++)
        {
            if (surface[sf] == 4)
            {
                fprintf(outputdata,"M_SF,%d,%d,1,4,1,1,1,1,\n", sf, sf);
                count1++;
            }
        }
        fprintf(outputdata,"ECOMPRESS;\n");

        fprintf(outputdata,"EGROUP,2,SHELL3T,1,0,0,0,0,0,0,\n");
        fprintf(outputdata,"RCONST,2,2,,1,%.3f\n", facesheet_thickness);
        count2 = 0;
```

```
        for (sf=1; sf<= no_front; sf++)
        {
            if (surface[sf] == 3)
            {
                fprintf(outputdata,"M_SF,%d,%d,1,3,1,1,1,1,\n", sf, sf);
                count2++;
            }
        }

        fprintf(outputdata,"ECOMPRESS;\n");
        sfcount = count1 + count2;


/* Generate and mesh backsheet surfaces */
 if (mirror_type == 2)
    {
        mirror_thickness = 0 - mirror_thickness;
        fprintf(outputdata,"ACTSET,EG,1,\n");
        fprintf(outputdata,"RCONST,1,3,,1,%.3f\n", backsheet_thickness);
        fprintf(outputdata,"ELGEN,1,1,%d,1,0,0,0,%.3f\n", count1, mirror_thickness);
      if (count2 != 0)
      {
        count11 = count1 + 1;
        fprintf(outputdata,"ACTSET,EG,2,\n");
        fprintf(outputdata,"RCONST,2,4,,1,%.3f\n", backsheet_thickness);
        fprintf(outputdata,"ELGEN,1,%d,%d,1,0,0,0,%.3f\n", count11, sfcount, mirror_thic!
kness);
      }
    }


/* Mesh rib support surfaces */

        fprintf(outputdata,"ACTSET,EG,1,\n");
        fprintf(outputdata,"RCONST,1,5,,1,%.3f\n", rib_thickness);
        fprintf(outputdata,"M_SF,%d,%d,1,4,1,1,1,1,\n", start_rib, no_rib);

/* Mesh edge band surfaces */

        fprintf(outputdata,"ACTSET,EG,1,\n");
        fprintf(outputdata,"RCONST,1,6,,1,%.3f\n", edge_thickness);
        fprintf(outputdata,"M_SF,%d,%d,1,4,1,1,1,1,\n", start_edge, tot_sf);
        fprintf(outputdata,"NMERGE,1,,1,%f;\n", tolerance);
        fprintf(outputdata,"NCOMPRESS;\n");

        fclose(outputdata);
        return 0;
}


void initialization (void)
{
 int j,k,l;

 for (l=0; l< 6; l++)
  for (k=0; k< MAXDIM; k++)
   for (j=0; j< MAXDIM; j++)
   {
        point2[j][k][l].no = NO_NODE;
        point2[j][k][l].id = NO_ID;
   }
}


void rec_swap(int a, int b)
{
```

```
        if (point2[a][b][1].x > 0)
                if (point2[a][b][1].x < point2[a][b][0].x)
                {
                        temp1 = point2[a][b][1];
                        point2[a][b][1] = point2[a][b][0];
                        point2[a][b][0] = temp1;
                }
                else;
        else if (point2[a][b][1].x < 0)
                if (point2[a][b][1].x > point2[a][b][0].x)
                {
                        temp1 = point2[a][b][1];
                        point2[a][b][1] = point2[a][b][0];
                        point2[a][b][0] = temp1;
                }
                else;
}


int rectangle_facesheet_generation (void)
{
 extern FILE *outputdata;
 extern struct node2 point2[][][][];
 int r;
 int c,d;
 int nc,nd,cn;
 float distance, diagonal;
 float x0,y0,x02,y02;
 float x1,y1,x12,y12;

 r=1;
 for (c=0; c< MAXDIM; c++)
    for (d=0; d< MAXDIM; d++)
    {
        nc = c+1;
        nd = d+1;
        cn = c-1;
        if (point2[c][d][0].no != NO_NODE)
        {
            if (point2[c][nd][0].no != NO_NODE)
            {
                if (point2[nc][nd][0].no != NO_NODE)
                {
                    if (point2[nc][d][0].no != NO_NODE)
                    {
                        if (point2[c][d][1].id == 2 && point2[c][nd][0].id == 1)
                        {
                            fprintf(outputdata,"SF4PT,%d,%d,%d,%d,%d,0\n",
                                    r, point2[c][d][1].no, point2[c][nd][0].no,
                                    point2[nc][nd][0].no, point2[nc][d][0].no);
                            surface[r] = 4;
                            r++;
                        }
                        else if (point2[nc][nd][0].id == 1 && point2[nc][d][1].id == 2)
                        {
                            fprintf(outputdata,"SF4PT,%d,%d,%d,%d,%d,0\n",
                                    r, point2[c][d][0].no, point2[c][nd][0].no,
                                    point2[nc][nd][0].no, point2[nc][d][1].no);
                            surface[r] = 4;
                            r++;
                        }
                        else if (point2[nc][nd][1].id == 2 && point2[nc][d][0].id == 1)
                        {
                            fprintf(outputdata,"SF4PT,%d,%d,%d,%d,%d,0\n",
                                    r, point2[c][d][0].no, point2[c][nd][0].no,
                                    point2[nc][nd][1].no, point2[nc][d][0].no);
```

```
        surface[r] = 4;
        r++;
    }
    else if (point2[c][d][0].id == 1 && point2[c][nd][1].id == 2)
    {
        fprintf(outputdata,"SF4PT,%d,%d,%d,%d,%d,0\n",
                r, point2[c][d][0].no, point2[c][nd][1].no,
                point2[nc][nd][0].no, point2[nc][d][0].no);
        surface[r] = 4;
        r++;
    }
    else
    {
     fprintf(outputdata,"SF4PT,%d,%d,%d,%d,%d,0\n",
            r, point2[c][d][0].no, point2[c][nd][0].no,
            point2[nc][nd][0].no, point2[nc][d][0].no);
     surface[r] = 4;
     r++;
     if (point2[c][d][0].x < 0 && point2[c][d][0].y < 0)
        if (point2[c][d][0].id == 1 && point2[cn][nd][1].no != NO_NO!
DE)
        {
            fprintf(outputdata,"SF3PT,%d,%d,%d,%d,0\n",
                    r, point2[c][d][0].no,
                    point2[c][nd][0].no,
                    point2[cn][nd][1].no);
            surface[r] = 3;
            r++;
        }
    }
    if (point2[c][nd][1].no != NO_NODE)     {
            x0 = point2[c][d][0].x - point2[nc][nd][0].x;
            y0 = point2[c][d][0].y - point2[nc][nd][0].y;
            x02 = x0*x0;
            y02 = y0*y0;
            diagonal = x02 + y02;

            x1 = point2[nc][d][0].x - point2[c][nd][1].x;
            y1 = point2[nc][d][0].y - point2[c][nd][1].y;
            x12 = x1*x1;
            y12 = y1*y1;
            distance = x12 + y12;

            if (distance < diagonal)
            {
               fprintf(outputdata,"SF3PT,%d,%d,%d,%d,0\n",
                    r, point2[c][nd][0].no,
                    point2[c][nd][1].no,
                    point2[nc][nd][0].no);
               surface[r] = 3;
               r++;
            }
                                                    }

    else if (point2[nc][nd][1].no != NO_NODE)       {
            x0 = point2[nc][d][0].x - point2[c][nd][0].x;
            y0 = point2[nc][d][0].y - point2[c][nd][0].y;
            x02 = x0*x0;
            y02 = y0*y0;
            diagonal = x02 + y02;

            x1 = point2[c][d][0].x - point2[nc][nd][1].x;
            y1 = point2[c][d][0].y - point2[nc][nd][1].y;
            x12 = x1*x1;
            y12 = y1*y1;
            distance = x12 + y12;
```

```
                    if (distance < diagonal)
                    {
                       fprintf(outputdata,"SF3PT,%d,%d,%d,%d,0\n",
                            r, point2[nc][nd][1].no,
                            point2[nc][nd][0].no,
                            point2[c][nd][0].no);
                       surface[r] = 3;
                       r++;
                    }
                                                                    }

            else if (point2[nc][d][1].no != NO_NODE)                {
                    x0 = point2[c][d][0].x - point2[nc][nd][0].x;
                    y0 = point2[c][d][0].y - point2[nc][nd][0].y;
                    x02 = x0*x0;
                    y02 = y0*y0;
                    diagonal = x02 + y02;

                    x1 = point2[nc][d][1].x - point2[c][nd][0].x;
                    y1 = point2[nc][d][1].y - point2[c][nd][0].y;
                    x12 = x1*x1;
                    y12 = y1*y1;
                    distance = x12 + y12;

                    if (distance < diagonal)
                    {
                       fprintf(outputdata,"SF3PT,%d,%d,%d,%d,0\n",
                            r, point2[nc][d][0].no,
                            point2[nc][d][1].no,
                            point2[c][d][0].no);
                       surface[r] = 3;
                       r++;
                    }
                                                                    }
        }
        else if (point2[nc][nd][0].id != 2)
            {
                    fprintf(outputdata,"SF3PT,%d,%d,%d,%d,0\n",
                            r, point2[c][d][0].no,
                            point2[c][nd][0].no,
                            point2[nc][nd][0].no);
                    surface[r] = 3;
                    r++;
             }
        else if (point2[nc][nd][0].id == 2)
             {
                    fprintf(outputdata,"SF3PT,%d,%d,%d,%d,0\n",
                            r, point2[c][d][0].no,
                            point2[c][nd][0].no,
                            point2[nc][nd][1].no);
                    surface[r] = 3;
                    r++;
             }
}
else
{
     if (point2[nc][d][0].no != NO_NODE && point2[nc][d][0].id != 2)
     {
        fprintf(outputdata,"SF3PT,%d,%d,%d,%d,0\n",
                r, point2[c][d][0].no,
                point2[c][nd][0].no,
                point2[nc][d][0].no);
        surface[r] = 3;
        r++;
     }
```

```
                else if (point2[nc][d][0].no != NO_NODE && point2[nc][d][0].id == 2
)
                {
                    fprintf(outputdata,"SF3PT,%d,%d,%d,%d,0\n",
                            r, point2[c][d][0].no,
                            point2[c][nd][0].no,
                            point2[nc][d][1].no);
                    surface[r] = 3;
                    r++;
                }
            }

        }
        else if (point2[nc][d][0].no != NO_NODE)
        {
                if (point2[nc][nd][0].no != NO_NODE && point2[c][d][1].id == 2)
                {
                    fprintf(outputdata,"SF3PT,%d,%d,%d,%d,0\n",
                            r, point2[c][d][1].no,
                            point2[nc][d][0].no,
                            point2[nc][nd][0].no);
                    surface[r] = 3;
                    r++;
                }

                else if (point2[nc][nd][0].no != NO_NODE && point2[nc][nd][0].id !=2
)
                {
                    fprintf(outputdata,"SF3PT,%d,%d,%d,%d,0\n",
                            r, point2[c][d][0].no,
                            point2[nc][nd][0].no,
                            point2[nc][d][0].no);
                    surface[r] = 3;
                    r++;
                }
                else if (point2[nc][nd][0].no != NO_NODE && point2[nc][nd][0].id == !
2)
                {
                    fprintf(outputdata,"SF3PT,%d,%d,%d,%d,0\n",
                            r, point2[c][d][0].no,
                            point2[nc][nd][0].no,
                            point2[nc][d][0].no);
                    surface[r] = 3;
                    r++;
                }
        }

    }

    if (point2[c][d][1].no != NO_NODE && point2[c][d][1].x < 0)
    {
         if (point2[nc][d][0].no != NO_NODE && point2[nc][d][0].y < 0)
         {
            x0 = point2[nc][d][0].x - point2[c][nd][0].x;
            y0 = point2[nc][d][0].y - point2[c][nd][0].y;
            x02 = x0*x0;
            y02 = y0*y0;
            diagonal = x02 + y02;

            x1 = point2[c][d][1].x - point2[nc][nd][0].x;
            y1 = point2[c][d][1].y - point2[nc][nd][0].y;
            x12 = x1*x1;
            y12 = y1*y1;
            distance = x12 + y12;

            if (distance < diagonal)
```

```
                {
                   fprintf(outputdata,"SF3PT,%d,%d,%d,%d,0\n",
                        r, point2[c][d][1].no,
                        point2[nc][d][0].no,
                        point2[c][d][0].no);
                   surface[r] = 3;
                   r++;
                }
                if (point2[cn][nd][1].no != NO_NODE && point2[cn][d][0].no == NO_NODE)
                {
                     fprintf(outputdata,"SF3PT,%d,%d,%d,%d,0\n",
                             r, point2[c][d][0].no,
                             point2[cn][nd][1].no,
                             point2[c][nd][0].no);
                     surface[r] = 3;
                     r++;
                }
                else if (point2[cn][nd][0].no != NO_NODE && point2[cn][d][0].no == NO_NO!
DE)
                {
                     fprintf(outputdata,"SF3PT,%d,%d,%d,%d,0\n",
                             r, point2[c][d][0].no,
                             point2[cn][nd][0].no,
                             point2[c][nd][0].no);
                     surface[r] = 3;
                     r++;
                }
              }
          }
    }
    return (r-1);
}


int rectangle_rib_generation (int r)
{
 extern FILE *outputdata;
 extern struct node2 point2[][][];
 int c,d,cc,dd;
 int nd,ncc;

 printf("Generating horizontal rib supports\n");
 for (c=0; c< MAXDIM; c++)              /* Generate horizontal rib surfaces */
    for (d=0; d< MAXDIM; d++)
    {
        nd = d+1;
        if (point2[c][d][0].no != NO_NODE)
        {
            if (point2[c][nd][0].no != NO_NODE)
            {
                if (point2[c][d][0].id == 1 && point2[c][nd][0].id == 1)
                ;
                else if (point2[c][d][0].id == 1 && point2[c][nd][0].id == 2)
                ;
                else if (point2[c][d][0].id == 2 && point2[c][nd][0].id == 1)
                ;
                else {
                        fprintf(outputdata,"SF4PT,%d,%d,%d,%d,%d,0\n",
                                r, point2[c][d][0].no, point2[c][nd][0].no,
                                point2[c][nd][3].no, point2[c][d][3].no);
                        surface[r] = 4;
                        r++;
                     }
            }
        }
    }
```

```
printf("Generating vertical rib supports\n");
for (cc=0; cc< MAXDIM; cc++)            /* Generate vertical rib surfaces */
    for (dd=0; dd< MAXDIM; dd++)
    {
        ncc = cc+1;
        if (point2[cc][dd][1].no != NO_NODE)
        {
            if (point2[ncc][dd][0].no != NO_NODE && point2[ncc][dd][0].id != 1)
            {
                fprintf(outputdata,"SF4PT,%d,%d,%d,%d,%d,0\n",
                        r, point2[cc][dd][1].no, point2[ncc][dd][0].no,
                        point2[ncc][dd][3].no, point2[cc][dd][4].no);
                surface[r] = 4;
                r++;
            }
        }
        else if (point2[cc][dd][0].no != NO_NODE)
        {
            if (point2[ncc][dd][1].no != NO_NODE)
            {
                if (point2[cc][dd][0].id == 1 && point2[ncc][dd][1].id == 2)
                ;
                else {
                        fprintf(outputdata,"SF4PT,%d,%d,%d,%d,%d,0\n",
                                r, point2[cc][dd][0].no, point2[ncc][dd][1].no,
                                point2[ncc][dd][4].no, point2[cc][dd][3].no);
                        surface[r] = 4;
                        r++;
                    }
            }
            else if (point2[ncc][dd][0].no != NO_NODE)
            {
                if (point2[cc][dd][0].id == 1 && point2[ncc][dd][0].id == 1)
                ;
                else {
                        fprintf(outputdata,"SF4PT,%d,%d,%d,%d,%d,0\n",
                                r, point2[cc][dd][0].no, point2[ncc][dd][0].no,
                                point2[ncc][dd][3].no, point2[cc][dd][3].no);
                        surface[r] = 4;
                        r++;
                    }
            }
        }
    }
    return (r-1);
}


int rectangle_edge_generation (int r)
{
 extern FILE *outputdata;
 extern struct node2 point2[][][];
 int c,d,cc,dd,ccc,ddd,ff,gg;
 int nc,nd,ncc,ndd,cn,ccn,ddn,nnd,nccc,nddd,nff,ffn,ngg,ggn;
 float distance, diagonal;
 float x0,y0,x02,y02;
 float x1,y1,x12,y12;

    printf("Generating edge band\n");
    for (ff=0; ff< MAXDIM; ff++)
        for (gg=0; gg< MAXDIM; gg++)
        {
            nff = ff+1;
            ngg = gg+1;
```

```
ffn = ff-1;
ggn = gg-1;
if (point2[ff][gg][0].id == 1)
{
    if (point2[ff][ngg][0].id == 1)
    {
        fprintf(outputdata,"SF4PT,%d,%d,%d,%d,%d,0\n",
                r, point2[ff][gg][0].no, point2[ff][ngg][0].no,
                point2[ff][ngg][3].no, point2[ff][gg][3].no);
        surface[r] = 4;
        r++;
    }
    else if (point2[nff][gg][0].id == 1)
    {
        fprintf(outputdata,"SF4PT,%d,%d,%d,%d,%d,0\n",
                r, point2[ff][gg][0].no, point2[nff][gg][0].no,
                point2[nff][gg][3].no, point2[ff][gg][3].no);
        surface[r] = 4;
        r++;
    }
    if (point2[nff][ngg][1].id == 2)
    {
        fprintf(outputdata,"SF4PT,%d,%d,%d,%d,%d,0\n",
                r, point2[ff][gg][0].no, point2[nff][ngg][1].no,
                point2[nff][ngg][4].no, point2[ff][gg][3].no);
        surface[r] = 4;
        r++;
    }
    else if (point2[nff][gg][0].id == 2)
    {
        fprintf(outputdata,"SF4PT,%d,%d,%d,%d,%d,0\n",
                r, point2[ff][gg][0].no, point2[nff][gg][0].no,
                point2[nff][gg][3].no, point2[ff][gg][3].no);
        surface[r] = 4;
        r++;
    }
}
else if (point2[ff][gg][1].id == 2)
{
    if (point2[ff][ngg][0].id == 1)
    {
            fprintf(outputdata,"SF4PT,%d,%d,%d,%d,%d,0\n",
                    r, point2[ff][gg][1].no, point2[ff][ngg][0].no,
                    point2[ff][ngg][3].no, point2[ff][gg][4].no);
            surface[r] = 4;
            r++;
    }
    else if (point2[nff][ngg][0].id == 2)
    {
            fprintf(outputdata,"SF4PT,%d,%d,%d,%d,%d,0\n",
                    r, point2[ff][gg][1].no, point2[nff][ngg][0].no,
                    point2[nff][ngg][3].no, point2[ff][gg][4].no);
            surface[r] = 4;
            r++;
    }
    else if (point2[nff][ngg][0].id == 1)
    {
            fprintf(outputdata,"SF4PT,%d,%d,%d,%d,%d,0\n",
                    r, point2[ff][gg][1].no, point2[nff][ngg][0].no,
                    point2[nff][ngg][3].no, point2[ff][gg][4].no);
            surface[r] = 4;
            r++;
    }
    else if (point2[ff][gg][0].id == 2)
    {
            fprintf(outputdata,"SF4PT,%d,%d,%d,%d,%d,0\n",
```

```
                r, point2[ff][gg][1].no, point2[ff][gg][0].no,
                point2[ff][gg][3].no, point2[ff][gg][4].no);
        surface[r] = 4;
        r++;
    }
    else if (point2[ffn][ggn][0].id == 2)
    {
        fprintf(outputdata,"SF4PT,%d,%d,%d,%d,%d,0\n",
                r, point2[ff][gg][1].no, point2[ffn][ggn][0].no,
                point2[ffn][ggn][3].no, point2[ff][gg][4].no);
        surface[r] = 4;
        r++;
    }
    else if (point2[ffn][ggn][0].id == 1)
    {
        fprintf(outputdata,"SF4PT,%d,%d,%d,%d,%d,0\n",
                r, point2[ff][gg][1].no, point2[ffn][ggn][0].no,
                point2[ffn][ggn][3].no, point2[ff][gg][4].no);
        surface[r] = 4;
        r++;
    }
}
else if (point2[ff][gg][0].id == 2)
{
    if (point2[nff][ngg][0].id == 1)
    {
        fprintf(outputdata,"SF4PT,%d,%d,%d,%d,%d,0\n",
                r, point2[ff][gg][0].no, point2[ff][gg][0].no,
                point2[ff][gg][3].no, point2[ff][gg][3].no);
        surface[r] = 4;
        r++;
    }
    else if (point2[nff][ngg][1].id == 2)
    {
        fprintf(outputdata,"SF4PT,%d,%d,%d,%d,%d,0\n",
                r, point2[ff][gg][0].no, point2[ff][gg][1].no,
                point2[ff][gg][4].no, point2[ff][gg][3].no);
        surface[r] = 4;
        r++;
    }
    else if (point2[nff][gg][0].id == 1)
    {
        fprintf(outputdata,"SF4PT,%d,%d,%d,%d,%d,0\n",
                r, point2[ff][gg][0].no, point2[nff][gg][0].no,
                point2[nff][gg][3].no, point2[ff][gg][3].no);
        surface[r] = 4;
        r++;
    }
}
else if (point2[ff][ngg][0].id == 1)
{
    if (point2[nff][gg][0].id == 1)
    {
        fprintf(outputdata,"SF4PT,%d,%d,%d,%d,%d,0\n",
                r, point2[ff][ngg][0].no, point2[nff][gg][0].no,
                point2[nff][gg][3].no, point2[ff][ngg][3].no);
        surface[r] = 4;
        r++;
    }
    else if (point2[nff][gg][1].id == 2)
    {
        fprintf(outputdata,"SF4PT,%d,%d,%d,%d,%d,0\n",
                r, point2[ff][ngg][0].no, point2[nff][gg][1].no,
                point2[nff][gg][4].no, point2[ff][ngg][3].no);
        surface[r] = 4;
        r++;
```

```
                }
            }
            else if (point2[ff][ngg][0].id == 2)
            {
                if (point2[nff][gg][0].id == 1)
                {
                        fprintf(outputdata,"SF4PT,%d,%d,%d,%d,%d,0\n",
                                r, point2[ff][ngg][0].no, point2[nff][gg][0].no,
                                point2[nff][gg][3].no, point2[ff][ngg][3].no);
                        surface[r] = 4;
                        r++;
                }
                else if (point2[nff][gg][1].id == 2)
                {
                        fprintf(outputdata,"SF4PT,%d,%d,%d,%d,%d,0\n",
                                r, point2[ff][ngg][0].no, point2[nff][gg][1].no,
                                point2[nff][gg][4].no, point2[ff][ngg][3].no);
                        surface[r] = 4;
                        r++;
                }
            }
        }
        return (r-1);
}


/* NOTE: curvature parameters are given in inches, so here x and y are
converted to inches before the z equation is calculated.  Then, z is
converted back to meters */

float curvature(float ptx, float pty)
{
 float Y2,Y4,Y6,Y8,Y10;
 float C1,C2,C3,C4;
 float numerator,denominator,root,number;
 float x,y,z;

 x = 0.03937 * (ptx - x_offset);        /* 0.03937 is the conversion factor */
 y = 0.03937 * (pty - y_offset);        /* from millimeters to inches */
 Y2 = x*x + y*y;
 Y4 = Y2*Y2;
 Y6 = Y2*Y2*Y2;
 Y8 = Y2*Y2*Y2*Y2;
 Y10 = Y2*Y2*Y2*Y2*Y2;

 C1 = A*Y4;
 C2 = B*Y6;
 C3 = C*Y8;
 C4 = D*Y10;

 number = 1 - ((1+K) * curv * curv * Y2);
 root = sqrt(number);
 denominator = 1 + root;
 numerator = curv * Y2;

 z = 25.4 * (numerator/denominator + C1 + C2 + C3 + C4);
                                /* 25.4 convertes inches back to millimeters */
 return z;
}


void material_library (int material)
{
 if (material == 1)     /* Silicon Carbide */
 {
        fprintf(outputdata,"MPROP,1,EX,3.7921E8,\n");
```

```
        fprintf(outputdata,"MPROP,1,DENS,3.100149E-6,\n");
        fprintf(outputdata,"MPROP,1,NUXY,0.20,\n");

    }
    if (material == 2)      /* Beryllium */
    {
        fprintf(outputdata,"MPROP,1,EX,3.03369E8,\n");
        fprintf(outputdata,"MPROP,1,DENS,1.849017E-6,\n");
        fprintf(outputdata,"MPROP,1,NUXY,0.025,\n");

    }
    if (material == 3)      /* Fused Silica */
    {
        fprintf(outputdata,"MPROP,1,EX,7.30844E7,\n");
        fprintf(outputdata,"MPROP,1,DENS,2.20332E-6,\n");
        fprintf(outputdata,"MPROP,1,NUXY,0.167,\n");
    }
    if (material == 4)      /* Aluminum */
    {
        fprintf(outputdata,"MPROP,1,EX,6.89476E7,\n");
        fprintf(outputdata,"MPROP,1,DENS,2.70986E-6,\n");
        fprintf(outputdata,"MPROP,1,NUXY,0.334,\n");
    }
    if (material == 5)      /* Zerodur */
    {
        fprintf(outputdata,"MPROP,1,EX,9.170024E7,\n");
        fprintf(outputdata,"MPROP,1,DENS,2.49949E-6,\n");
        fprintf(outputdata,"MPROP,1,NUXY,0.252,\n");
    }
}
```

Appendix B Voltage Profiles for Deflection Correction Studies

This appendix is a supplement to Chapter 5. The following results are the voltage profiles obtained for each deflection correction study, including the least squares case, least squares with various cost factors, and successive optimization. Unless otherwise indicated, the voltages are given in order from the first piezo to the 116th piezo.

Self-Weight Deflection Correction Profile for R = 0

voltswd =

-4.3517e+03	-3.9207e+02	-7.3852e+02
2.2749e+03	-5.0201e+02	2.1636e+01
-1.4935e+01	9.2721e+02	3.8627e+02
-2.2724e+02	-1.3955e+03	-1.0201e+03
1.4338e+02	5.2404e+02	-1.6564e+02
1.7706e+02	2.2107e+03	5.0313e+02
-3.2046e+03	-1.2304e+03	-1.2349e+02
5.5320e+03	3.1090e+01	-1.0573e+03
-3.2208e+03	9.2901e+01	1.3620e+03
5.4047e+02	-1.0002e+03	-1.3687e+03
-2.0238e+02	1.1007e+03	1.0581e+03
-9.4306e+02	-5.1477e+02	-1.8974e+02
1.3994e+03	1.9101e+02	-4.0145e+02
-1.2831e+03	7.7973e+02	-5.9464e+02
9.3008e+02	-1.1300e+03	-3.6942e+03
2.5929e+02	1.4764e+03	2.7326e+03
-7.7313e+02	-2.1263e+03	2.3376e+01
-1.2024e+03	-5.8956e+02	-2.3866e+02
8.0836e+02	9.7497e+02	2.9932e+02
6.0501e+01	3.1153e+02	-2.6750e+02
-4.2993e+02	-4.9955e+02	-1.5611e+03
1.3637e+03	1.3665e+03	5.3301e+03
-1.6911e+03	-1.5299e+03	
1.5308e+03	9.1568e+02	
-1.2104e+03	-5.5193e+02	
3.4528e+02	-2.2247e+02	
-9.4475e+01	6.6837e+02	
-1.1689e+03	-1.1185e+03	
2.0294e+03	4.8163e+02	
-1.1587e+03	1.2166e+03	
-3.9966e+02	1.3299e+02	
3.4747e+02	-1.3379e+03	
-1.2763e+03	1.4820e+03	
1.4135e+03	-2.5038e+03	
-9.7874e+02	2.5645e+03	
6.8522e+02	-1.9983e+03	
3.4449e+02	1.6991e+03	
-8.2197e+02	-8.6887e+02	
1.2442e+03	5.6219e+02	
-2.5345e+03	-1.0418e+02	
-1.1744e+03	-4.1057e+02	
1.1432e+03	1.0183e+03	
2.1430e+02	3.8375e+02	
-3.9130e+02	-5.6014e+02	
1.2054e+03	1.4850e+03	
-1.3205e+03	-1.8870e+03	
8.3924e+02	8.8319e+02	

Self-Weight Deflection Correction Profile for R = 1e-5

vswd =

2.2271e-05	1.5304e-04	-6.4146e-03
3.3534e-04	-1.1177e-04	-6.4162e-03
5.2871e-04	-3.8574e-04	-1.6707e-03
8.7014e-04	-9.4529e-04	-6.3255e-04
8.1294e-04	-4.2636e-04	3.9600e-04
5.0323e-04	2.3184e-04	5.9419e-04
3.3051e-04	3.1636e-04	5.1374e-05
2.0306e-05	1.8579e-04	4.6890e-04
-7.4688e-05	-1.5300e-04	-5.5532e-04
-7.0027e-04	-1.0009e-04	-1.5785e-03
7.6875e-05	-7.6694e-05	-5.0308e-03
2.5040e-04	-7.8342e-05	-5.0325e-03
5.9676e-04	-7.6662e-05	-1.5789e-03
6.3673e-04	-7.2956e-05	-5.5573e-04
3.0719e-04	-9.6747e-05	4.6857e-04
1.1057e-04	-1.5182e-04	5.1323e-05
-4.5178e-04	1.8402e-04	1.0871e-05
-1.0966e-04	3.1444e-04	-2.1411e-04
-3.3544e-03	3.2840e-04	-7.1780e-04
-4.4004e-03	6.4183e-04	-1.7229e-03
-9.1680e-04	3.1106e-04	-1.7229e-03
-2.1375e-04	3.2238e-06	-7.1793e-04
3.8317e-04	-3.9621e-04	-2.1431e-04
4.0452e-04	-8.6485e-04	1.0860e-05
-1.8842e-04	-8.6407e-04	
-8.7748e-04	-3.9441e-04	
-4.3566e-03	4.8744e-06	
-3.4087e-03	3.1145e-04	
-1.5829e-04	6.4052e-04	
-2.9025e-03	3.2740e-04	
-4.9417e-03	1.5571e-04	
-1.1171e-03	7.9442e-04	
-3.1498e-04	3.6722e-04	
2.4067e-04	-2.3881e-04	
2.4828e-04	-7.2051e-04	
-2.9806e-04	-1.7748e-03	
-1.1016e-03	-1.7747e-03	
-4.9374e-03	-7.1982e-04	
-2.9082e-03	-2.3817e-04	
-1.5616e-04	3.6713e-04	
2.3513e-04	7.9346e-04	
-4.2267e-04	1.5551e-04	
-9.4669e-04	5.9475e-04	
-3.9184e-04	3.9646e-04	
-1.1963e-04	-6.3250e-04	
1.4953e-04	-1.6706e-03	

Self-Weight Deflection Correction Profile for R= 1e-9

v9 =

1.8641e-01	2.4987e+00	-4.7728e+01
2.8524e+00	1.2736e-01	-4.7751e+01
4.5757e+00	-2.4466e+00	-1.1443e+01
7.5277e+00	-7.4268e+00	-3.7242e+00
6.9936e+00	-3.2415e+00	3.8001e+00
4.3748e+00	1.9524e+00	4.9456e+00
2.8335e+00	2.6380e+00	4.0567e-01
1.6930e-01	1.7847e+00	3.9538e+00
-6.1665e-01	-6.5792e-01	-3.5178e+00
-5.7591e+00	1.5898e-01	-1.0935e+01
8.4345e-01	7.5207e-01	-3.6527e+01
2.4325e+00	9.9063e-01	-3.6550e+01
5.3614e+00	1.0028e+00	-1.0939e+01
5.6821e+00	7.7824e-01	-3.5199e+00
2.8905e+00	1.8044e-01	3.9539e+00
1.1401e+00	-6.5452e-01	4.0550e-01
-3.6839e+00	1.7666e+00	7.8715e-02
-9.1102e-01	2.6221e+00	-1.4743e+00
-2.7585e+01	2.7219e+00	-5.0505e+00
-3.6976e+01	5.5268e+00	-1.2631e+01
-7.2927e+00	3.2408e+00	-1.2631e+01
-1.2737e+00	1.2288e+00	-5.0501e+00
3.7726e+00	-1.4988e+00	-1.4756e+00
3.9459e+00	-4.8952e+00	7.8690e-02
-1.0773e+00	-4.8899e+00	
-6.9795e+00	-1.4865e+00	
-3.6632e+01	1.2397e+00	
-2.8055e+01	3.2421e+00	
-1.2927e+00	5.5163e+00	
-2.3516e+01	2.7142e+00	
-4.1306e+01	1.2633e+00	
-8.7974e+00	6.6710e+00	
-1.8781e+00	3.7150e+00	
2.8670e+00	-5.9953e-01	
2.9264e+00	-4.0204e+00	
-1.7482e+00	-1.1934e+01	
-8.6836e+00	-1.1935e+01	
-4.1304e+01	-4.0163e+00	
-2.3585e+01	-5.9502e-01	
-1.2757e+00	3.7148e+00	
1.9801e+00	6.6656e+00	
-3.2033e+00	1.2621e+00	
-7.4262e+00	4.9477e+00	
-2.4869e+00	3.8016e+00	
6.9958e-02	-3.7238e+00	
2.4724e+00	-1.1439e+01	

Self-Weight Deflection Correction Profile for R = 1e-14

vswd =

-2.7273e+01	9.2104e+01	2.4635e+02
-3.9892e+01	-1.2251e+02	-1.3734e+02
1.4489e+01	3.2271e+02	2.0478e+02
-1.3730e+01	-1.0812e+02	-5.4044e+01
5.3734e+01	-1.9818e+02	-7.3792e+01
-1.2591e+02	1.6656e+02	7.7571e+01
-1.2677e+02	3.1623e+01	-1.2755e+02
-2.3832e+01	-1.8822e+02	3.7568e+01
-3.5619e+01	1.7079e+01	4.2049e-01
9.3397e+01	-3.8923e+01	3.7444e+01
-7.7942e+01	1.3579e+02	-3.0436e-02
3.6322e+01	1.7508e+02	-9.1249e+01
-1.1119e+01	-3.1727e+01	5.3138e+01
-2.7327e+00	9.8238e+00	-8.1034e+01
1.2352e+02	-1.9371e+02	7.5911e+01
-1.0637e+02	5.3434e+01	3.1870e+02
-6.8473e+01	8.9271e+01	-8.8909e+01
-1.6449e+02	3.7810e+00	-8.3788e+00
5.9348e+01	-2.1157e+01	-6.7213e+00
-2.3785e+02	1.4123e+02	-7.1292e+01
9.9427e+01	1.8761e+01	2.9307e+02
-4.2302e+01	5.8043e+01	8.1840e+01
-1.0269e+01	-1.9659e+02	
8.6642e+00	-2.1489e+02	
-1.5204e+02	5.5007e+01	
2.0211e+02	3.1140e+01	
-2.0622e+02	1.3862e+02	
-9.4417e+01	-3.0415e+01	
2.1250e+02	-3.4171e+01	
5.2061e+01	1.7133e+02	
-5.6452e+02	8.3320e+01	
2.3774e+02	-1.5262e+02	
-1.9495e+02	5.7890e+01	
1.4726e+02	-1.7576e+02	
9.7899e+01	2.4939e+02	
-4.7854e+01	2.2353e+02	
9.2128e+01	-1.3809e+02	
-4.6922e+02	2.1075e+01	
3.0731e+01	-1.1122e+02	
7.6682e+01	3.9842e+01	
-9.7333e+01	1.8123e+02	
-6.9566e+01	-4.2302e+01	
3.1452e+02	2.1289e+02	
-1.5814e+02	-1.3938e+02	
1.0309e+02	2.4736e+02	
-1.0360e+02	-5.2111e+02	
-1.5161e+02	-5.1033e+02	

Self-Weight Deflection Correction Profile for R = 1e-15

vswd =

-1.9478e+02	-1.2130e+02	-7.8841e+01
1.7172e+02	5.2151e+02	-1.3621e+02
7.8534e+00	4.7450e+02	4.7154e+02
-5.3839e+01	-7.5601e+02	7.0501e+01
3.8094e+01	4.4125e+02	-4.1420e+02
-9.7293e+01	-4.6467e+02	2.8653e+02
-3.5032e+02	3.4211e+02	-4.2878e+02
5.7517e+01	3.2842e+01	3.3442e+02
-1.1811e+02	-9.2550e+01	1.7599e+02
1.0146e+02	1.9787e+02	-2.5112e+02
-8.2271e+01	-5.8915e+02	1.6355e+02
-4.9801e+01	8.0450e+01	-2.6134e+02
1.2795e+02	3.9274e+01	-1.3138e+01
-8.3936e+01	-9.2184e+01	5.0966e+02
1.7193e+02	-1.0110e+02	5.1654e+01
-8.9961e+01	5.7436e+02	3.5320e+02
-1.0129e+02	-4.4486e+02	-2.1321e+02
-6.8336e+02	4.1141e+02	3.4187e+02
1.1108e+02	-2.7702e+02	-5.1187e+02
-9.8184e+01	-1.5751e+02	-4.9320e+02
-3.4210e+01	2.5764e+02	3.3961e+02
1.3959e+02	-3.5264e+02	-2.5232e+02
-1.7637e+02	5.5419e+02	
7.6161e+01	-2.0918e+02	
-1.4036e+02	-2.0742e+02	
1.2022e+02	2.7509e+02	
-9.3720e+01	5.6806e+01	
-1.5408e+02	-4.7566e+02	
3.8419e+02	3.0433e+02	
4.9123e+01	-3.4106e+02	
3.5716e+02	2.4836e+02	
-5.4502e+01	2.3619e+02	
-2.7444e+02	-2.8400e+02	
1.1616e+02	3.2383e+02	
-2.2029e+02	-5.0329e+02	
2.1433e+01	1.7581e+02	
4.7677e+00	3.9242e+01	
-9.7393e+00	-9.2673e+01	
9.2209e+00	7.4253e-01	
-1.3768e+02	4.1181e+02	
5.6694e+01	-2.5156e+02	
-3.3636e+02	3.2698e+02	
3.3663e+02	-2.9184e+02	
7.4920e+02	-2.5730e+02	
-1.5583e+02	2.7276e+02	
2.5780e+01	-2.3819e+02	
4.3382e+01	4.0056e+02	

Self-Weight Deflection Correction Profile for R = 1e-16

vswd =

-1.4070e+03	1.4578e+02	1.4376e+02
7.3387e+02	-4.5791e+02	-2.4265e+02
1.4482e+01	6.9633e+02	4.0955e+02
-1.0218e+02	-4.8003e+02	-2.6252e+02
6.1087e+01	-6.6734e+01	-2.7557e+02
-2.2453e+01	6.4194e+02	1.8518e+02
-1.0788e+03	-1.7974e+02	-2.5354e+02
1.3090e+03	-4.8847e+02	-1.8378e+02
-7.3592e+02	3.5974e+02	2.7984e+02
1.7574e+02	-6.0310e+02	-3.1130e+02
-7.5679e+01	5.0427e+02	2.3174e+02
-3.3587e+02	5.2512e+01	-1.4651e+02
5.1249e+02	-2.3835e+02	-4.5506e+01
-4.3220e+02	5.2596e+02	-4.6763e+02
3.9543e+02	-7.2868e+02	-1.6795e+02
-2.8910e+01	4.8854e+02	1.2812e+03
-2.3080e+02	-4.5370e+02	-1.5707e+02
-1.2672e+03	-1.6330e+02	-1.4772e+01
2.8852e+02	1.8449e+02	1.0831e+02
-2.2556e+01	4.9943e+02	-1.5140e+02
-1.5695e+02	-3.8290e+02	9.8992e+01
4.8207e+02	6.3903e+02	1.7073e+03
-5.7841e+02	-6.0299e+02	
4.3172e+02	5.0048e+00	
-3.6355e+02	1.5534e+02	
1.1763e+02	-3.3358e+02	
-4.9518e+01	5.4409e+02	
-3.9392e+02	-3.2575e+02	
7.1634e+02	-2.4971e+00	
-2.0304e+02	6.2486e+02	
-7.5429e+02	9.0653e+01	
4.9140e+02	-6.9506e+02	
-7.5518e+02	5.7882e+02	
6.7324e+02	-9.2306e+02	
-2.4678e+02	8.2885e+02	
8.1571e+01	-3.0460e+02	
2.6696e+02	1.2891e+02	
-6.6036e+02	6.1638e+00	
3.2265e+02	-1.3837e+02	
-5.4188e+02	-3.8971e+01	
-2.7070e+02	3.6770e+02	
1.3663e+02	2.8062e+02	
5.9981e+02	3.9354e+02	
-5.3051e+02	-2.5833e+02	
7.0871e+02	5.7207e+02	
-5.9579e+02	-7.7982e+02	
1.0126e+02	-2.0295e+02	

Thermal Deflection Correction Profile for R = 0

volttherm =

8.6932e+02	7.3207e+01	2.6495e+02
-7.0902e+02	2.8248e+02	9.4115e+00
1.8874e+01	-4.3586e+02	-1.1680e+02
8.0428e+01	6.3928e+02	3.6914e+02
-4.6318e+01	-4.4112e+02	1.3913e+02
-9.2826e+01	-7.5541e+02	-1.8445e+02
1.2714e+03	4.8018e+02	3.2848e+01
-2.1481e+03	4.6797e+01	4.4620e+02
1.9451e+03	-7.5202e+01	-5.6061e+02
-1.2241e+02	3.9788e+02	4.6583e+02
9.4025e+01	-3.8363e+02	-3.3592e+02
3.0766e+02	1.6451e+02	1.9256e+01
-4.3621e+02	1.1854e+01	1.7437e+02
4.2364e+02	-3.9107e+02	2.1020e+02
-2.4999e+02	5.2027e+02	9.9604e+02
-1.8411e+02	-6.5554e+02	-1.0117e+03
3.9828e+02	1.0746e+03	-6.1999e+01
4.3338e+02	1.4162e+02	1.2474e+02
-2.3952e+02	-3.6004e+02	-8.1263e+01
-1.7270e+02	-1.6249e+02	3.8221e+01
2.0807e+02	2.3595e+02	6.8315e+02
-5.4679e+02	-5.3645e+02	-2.1995e+03
6.5537e+02	5.5257e+02	
-5.9490e+02	-3.1495e+02	
4.6297e+02	1.3035e+02	
-1.4224e+02	1.9068e+02	
-1.5060e+01	-3.3328e+02	
4.8264e+02	5.3345e+02	
-6.0002e+02	-4.3313e+02	
4.9380e+02	-3.5139e+02	
5.6863e+01	-4.7590e+01	
-9.8767e+01	5.6694e+02	
4.1825e+02	-6.0305e+02	
-4.3845e+02	9.8663e+02	
2.9411e+02	-9.7590e+02	
-1.5037e+02	7.3812e+02	
-2.4887e+02	-5.8884e+02	
3.4410e+02	2.6392e+02	
-6.4712e+02	-1.5426e+02	
1.4525e+03	-1.1747e+01	
4.4381e+02	4.2510e+02	
-4.4259e+02	-4.4245e+02	
-1.4070e+02	-1.1644e+02	
1.8382e+02	2.0938e+02	
-4.6483e+02	-5.6965e+02	
4.7049e+02	6.2703e+02	
-2.7835e+02	-4.1717e+02	

Thermal Deflection Correction Profile for R = 1e-9

vtherm =

-4.2590e-02	-3.6034e-01	4.9179e+00
-6.0953e-01	1.2287e-01	4.9188e+00
-9.2179e-01	6.4096e-01	9.0484e-01
-1.5161e+00	1.6176e+00	4.7503e-02
-1.4166e+00	7.0463e-01	-8.4124e-01
-8.7671e-01	-3.3064e-01	-9.0799e-01
-6.0683e-01	-4.5104e-01	-7.0184e-02
-4.1626e-02	-2.0073e-01	-7.5217e-01
1.2955e-01	2.6586e-01	8.1167e-02
1.3181e+00	5.8120e-02	8.7657e-01
-8.4719e-02	-1.7258e-01	3.2651e+00
-3.1574e-01	-3.2297e-01	3.2662e+00
-9.0925e-01	-3.2620e-01	8.7704e-01
-9.9290e-01	-1.7966e-01	8.2107e-02
-4.3708e-01	5.1760e-02	-7.5106e-01
-1.4147e-01	2.6295e-01	-7.0045e-02
8.6651e-01	-1.9798e-01	-7.4149e-03
1.9753e-01	-4.4742e-01	1.3547e-01
5.5122e+00	-4.7624e-01	4.6165e-01
8.0099e+00	-9.3528e-01	1.3717e+00
1.6747e+00	-5.4635e-01	1.3719e+00
4.9566e-01	-3.4131e-01	4.6214e-01
-5.0188e-01	-1.0720e-01	1.3584e-01
-5.4434e-01	2.0146e-01	-7.3895e-03
4.4675e-01	1.9997e-01	
1.6069e+00	-1.1053e-01	
7.9263e+00	-3.4423e-01	
5.5966e+00	-5.4700e-01	
2.7537e-01	-9.3262e-01	
4.3577e+00	-4.7420e-01	
8.5481e+00	-2.2032e-01	
1.9403e+00	-1.1916e+00	
6.0849e-01	-7.4466e-01	
-3.1984e-01	-2.4942e-01	
-3.3475e-01	9.8069e-02	
5.7668e-01	9.1629e-01	
1.9122e+00	9.1579e-01	
8.5337e+00	9.6710e-02	
4.3630e+00	-2.5041e-01	
2.7133e-01	-7.4413e-01	
-3.3648e-01	-1.1892e+00	
7.0016e-01	-2.1982e-01	
1.6225e+00	-9.0951e-01	
6.5278e-01	-8.4262e-01	
1.3785e-01	4.7290e-02	
-3.5355e-01	9.0496e-01	

Thermal Deflection Correction Profile for R = 1e-14

vtherm =

-2.8108e+01	-3.7389e+01	-1.0056e+02
3.6127e+01	7.4735e+01	6.5428e+01
-1.5050e+00	-1.1962e+02	-2.9056e+01
2.1048e+01	4.1791e+01	-3.2933e+01
9.8374e+00	2.8976e+00	3.0441e+01
1.8680e+01	-4.4590e+01	-4.9014e+01
5.1122e+01	1.5973e+01	1.5549e+01
-2.7418e+01	6.0697e+01	4.4838e+01
2.4483e+01	-1.3656e+01	-6.8138e+01
1.3149e+01	1.9879e+01	-7.0313e+01
1.6493e+01	-4.9440e+01	4.8455e+01
-1.6406e+00	-5.6621e+01	9.4170e+00
-4.0963e+00	1.9293e+01	-4.7322e+01
-8.3146e+00	-1.4059e+01	3.4757e+01
-1.4944e+01	5.8969e+01	-3.7592e+01
2.4034e+01	6.6302e+00	-1.0209e+02
3.1633e+01	-2.9188e+01	-2.7435e+01
9.8222e+01	-2.5133e+01	4.6248e+01
-3.6849e+00	-7.6294e+00	4.5671e+01
4.4189e+01	-3.4859e+01	-3.1277e+01
-5.2602e+01	1.7385e+01	-9.1722e+01
3.8961e+01	-2.3570e+01	-4.0396e+01
9.7668e+00	7.8541e+01	
1.7335e+01	8.2082e+01	
4.7604e+01	-2.3610e+01	
-6.1257e+01	1.6281e+01	
3.4604e+01	-3.1248e+01	
3.6282e+01	-1.6674e+00	
8.8746e+01	-1.5346e+01	
-7.0313e+01	-6.5203e+01	
1.4738e+02	-1.8164e+01	
-1.0235e+02	6.8079e+01	
6.6304e+01	-4.6052e+01	
-5.0245e+01	8.5453e+01	
-3.9193e+01	-1.0648e+02	
3.9220e+01	-1.0069e+02	
-7.6061e+01	7.7305e+01	
1.2518e+02	-3.8768e+01	
-7.1269e+01	5.4903e+01	
1.0819e+02	-1.0848e+01	
-1.7880e+01	-7.2239e+01	
2.8759e+01	-4.2470e+01	
-1.2120e+02	-2.7599e+01	
8.0157e+01	5.8266e+01	
-3.8983e+01	-9.4308e+01	
5.3958e+01	1.1908e+02	
6.1843e+01	1.2355e+02	

Thermal Deflection Correction Profile for R = 1e-15

vtherm =

-7.4641e+01	-1.4048e+02	-1.5639e+02
4.4657e+01	1.9201e+02	1.2310e+02
-1.2472e+01	-2.3088e+02	-8.6055e+01
2.6999e+01	1.0794e+02	-2.9478e+01
5.0742e+00	-2.6390e+01	1.3176e+02
1.0328e+01	-8.6662e+00	-5.1241e+01
1.6969e+02	-1.7431e+01	3.7661e+01
-1.3228e+02	1.9705e+02	6.2675e+01
1.8129e+02	-1.5079e+02	-6.9782e+01
5.2477e+01	1.5760e+02	-4.8925e+01
-8.1570e+00	-9.2109e+01	5.4993e+01
4.1738e+01	-9.4030e+01	1.4845e+01
-4.0473e+01	1.5108e+02	-4.3376e+01
2.4460e+01	-1.6776e+02	1.6575e+02
-2.4920e+01	1.9978e+02	-1.7145e+02
8.0787e+00	-6.7348e+01	-2.3793e+02
7.0494e+01	5.8627e+01	-8.5382e+00
3.9077e+02	-4.5789e+01	3.0462e+01
2.2699e+00	6.5711e+00	2.5118e+01
-3.0287e+01	-1.5996e+02	-2.1497e+01
5.8080e+00	1.4398e+02	-1.4989e+02
-3.3707e+01	-1.5160e+02	-2.1947e+02
5.0282e+01	1.1498e+02	
8.5324e+00	1.0825e+02	
1.3278e+01	-1.4274e+02	
-1.0855e+01	1.4989e+02	
-3.2219e+01	-1.5056e+02	
9.1390e+01	4.2025e+01	
1.2983e+02	-2.7979e+01	
-7.0130e+01	-1.0675e+02	
2.2222e+02	-1.8141e+01	
-1.8439e+02	1.7460e+02	
1.6829e+02	-1.4685e+02	
-1.0506e+02	1.9834e+02	
-3.3992e+01	-1.3969e+02	
8.4704e+01	-9.1654e+01	
-1.3347e+02	1.4757e+02	
1.7168e+02	-1.1604e+02	
-9.6197e+01	1.1860e+02	
2.0215e+02	1.4783e+00	
-4.9750e+01	-1.4001e+02	
6.0990e+01	-8.1451e+01	
-2.4341e+02	-7.3014e+01	
2.0600e+02	8.4997e+01	
-1.7257e+02	-1.3643e+02	
1.0756e+02	1.0972e+02	
8.1068e+01	1.2260e+02	

Thermal Deflection Correction Profile for R = 1e-16

vtherm =

9.2641e+01	-1.2033e+02	-8.3003e+01
-1.2236e+02	2.4897e+02	1.1705e+02
-9.5672e+00	-3.2154e+02	-1.2346e+02
3.7910e+01	2.4693e+02	6.8172e+01
-1.0840e+01	-1.3678e+02	1.4426e+02
-1.1916e+01	-1.0457e+02	-5.9854e+01
4.4365e+02	5.4120e+01	5.7421e+01
-6.2163e+02	2.4256e+02	1.3122e+02
7.1529e+02	-1.8919e+02	-1.6192e+02
3.3378e+01	2.5838e+02	6.8091e+01
4.0301e+00	-1.7149e+02	-2.9953e+01
1.2151e+02	-4.2049e+01	1.8285e+01
-1.4524e+02	1.6108e+02	1.7101e+01
1.3435e+02	-2.7285e+02	2.1174e+02
-8.6805e+01	3.3516e+02	-1.6965e+02
-3.1244e+01	-2.3464e+02	-4.3234e+02
1.5176e+02	3.4224e+02	-2.6771e+00
5.7769e+02	-6.6915e+01	4.1283e+01
-5.3311e+01	-3.6856e+01	-4.7488e+00
-9.7021e+01	-2.3301e+02	-4.7846e+00
7.3253e+01	2.0716e+02	2.4323e+01
-1.7779e+02	-2.7207e+02	-8.0942e+02
2.0225e+02	2.1534e+02	
-1.3825e+02	2.2843e+01	
1.0715e+02	-1.2437e+02	
-2.6737e+01	2.1206e+02	
-5.2313e+01	-2.5422e+02	
1.8782e+02	1.8759e+02	
1.5937e+01	-1.6772e+02	
5.6334e+01	-8.4447e+01	
2.2429e+02	-4.1959e+01	
-1.9496e+02	3.1142e+02	
2.5985e+02	-2.6515e+02	
-1.9948e+02	3.8540e+02	
5.0271e+01	-3.1600e+02	
4.1276e+01	8.6802e+01	
-1.7529e+02	1.2624e+01	
2.2939e+02	-6.5564e+01	
-2.1942e+02	1.0039e+02	
5.2638e+02	-1.5740e+01	
2.6074e+01	2.9432e+01	
-2.6940e+01	-1.5854e+02	
-2.8489e+02	-1.0596e+02	
2.4866e+02	9.7117e+01	
-2.8508e+02	-2.1762e+02	
2.0822e+02	1.9943e+02	
-3.3187e+00	1.0986e+01	

Self-Weight Deflection Correction Profile
Under No Voltage Constraints
(least squares solution taken at successive stages)

5 Piezos

94	-3.0402e2
20	-6.7325e2
39	-5.9587e2
93	-3.4845e2
59	3.1775e2

10 Piezos

94	-2.8622e2
20	-6.0888e2
39	-3.7522e2
93	-3.9441e2
59	2.3691e2
28	-5.7057e1
90	1.9042e2
21	2.5010e2
29	-6.2758e2
27	-1.6734e2

15 Piezos

94	-3.6628e2
20	-6.1570e2
39	-3.2554e2
93	-3.9504e2
59	8.9715e1
28	-1.4564e2
90	6.3532e1
21	2.3948e2
29	-6.3363e2
27	-1.1337e2
41	-9.4880e1
95	1.4747e2
84	6.9512e1
81	1.8010e2
14	6.4367e1

18 Piezos

v18 =

94	-3.7552e+02
20	-6.1411e+02
39	-3.2610e+02
93	-4.3402e+02
59	7.3081e+01
28	-9.0155e+01
90	4.4760e+01
21	2.3183e+02
29	-5.5850e+02
27	-1.5709e+02
41	-1.3537e+02
95	1.4724e+02
84	6.9091e+01
81	1.8625e+02
14	4.9668e+01
40	2.1312e+02
7	9.4327e+01
103	5.2207e+01

Self-Weight Deflection Correction Profile
Under 510V Constraint (specified successive placement voltages)

5 Piezos

94	-440.61
20	-510
28	-466.43
93	-208.16
58	326.71

10 Piezos

94	-440.61
20	-510
28	-466.43
93	-208.16
58	326.71
19	-98.374
87	277.91
107	231.56
89	214.46
21	63.314

15 Piezos

94	-440.61
20	-510
28	-466.43
93	-232.188
58	202.788
19	-98.374
87	200.81
107	231.56
89	214.46
21	110.211
29	-418.76
39	-34.14
84	118.442
81	49.304
76	174.18

20 Piezos

94	-440.61
20	-510
28	-466.43
93	-232.188
58	161.24
19	-98.374
87	139.419
107	231.56
89	214.46
21	145.23
29	-418.76
39	-34.14
84	118.442
81	49.304
76	174.18
65	148.12
100	80.284
5	48.529
4	44.056
51	-40.137

Thermal Deflection Correction Profile
Under 510V Constraint (least squares solution taken at successive stages)

5 Piezos

vtherm =

20	1.1258e+02
39	1.3574e+02
47	-1.8413e+02
93	5.3075e+01
2	-3.5575e+02

10 Piezos

vtherm =

20	8.3020e+01
39	1.0995e+02
47	-1.2042e+02
93	5.3019e+01
2	-4.9876e+02
7	-3.3323e+02
67	-5.5972e+01
115	4.2787e+01
86	-6.6231e+01
90	-7.4760e+01

15 Piezos

vtherm =

20	1.0799e+02
39	1.1728e+02
47	-7.8079e+01
93	4.9389e+01
2	-3.5365e+02
7	-2.8128e+02
67	-4.8767e+01
115	4.0322e+01
86	-3.6426e+01
90	-6.2769e+01
21	-9.2426e+01
29	2.8592e+02
5	-2.6276e+01
61	-5.2988e+01
107	-4.8577e+01

20 Piezos

vtherm =

20	1.0105e+02
39	1.2397e+02
47	-5.1599e+01
93	5.7557e+01
2	-2.8601e+02
7	-2.7824e+02
67	-6.2142e+01
115	3.2744e+01
86	-3.3703e+01
90	-9.2318e+01
21	-8.6464e+01
29	2.6279e+02
5	-4.8160e+01
61	-2.5342e+01
107	-5.2625e+01
50	-3.8718e+01
4	-5.8802e+01
81	-7.1528e+01
79	8.5036e+01
77	-1.6946e+02